Geophysical Characterization of Subsurface Biofuel Contamination and Biodegradation

By

Yves Robert Personna

A Dissertation submitted to the
Graduate-School Newark
Rutgers, The State University of New Jersey
in partial fulfillment of the requirements
for the degree of
Doctor of Philosophy
Graduate Program in
Environmental Sciences
written under the direction of
Professor Lee D. Slater
and approved by

_____

_____

_____

_____

Newark, New Jersey
May 2013

ABSTRACT OF THE DISSERTATION

Geophysical Characterization of Subsurface Biofuel Contamination and Biodegradation

By Yves Robert Personna

Dissertation Director:

Professor Lee D. Slater

In the last two decades, the production of ethanol (EtOH), one of the most common biofuels in the USA, has substantially increased due to regulations aiming at reducing air pollution and providing a supplement to petroleum. Scenarios of large spills of EtOH during production, transportation and at storage facilities are likely. Accidental release of EtOH and its persistence in the subsurface pose threats to human health and the environment, including the deterioration of municipal water supplies. Thus, there is a need to develop adequate monitoring tools to help with the remediation efforts of subsurface EtOH contamination. Ethanol presence, interaction and biodegradation could substantially alter the electrical properties of geologic materials, thereby potentially leading to distinctive geophysical responses. This dissertation demonstrates the potential application of non-invasive and cost effective complex resistivity (CR) technique for the characterization of biofuel contamination and biodegradation in the subsurface.

The first research topic examined the electrical geophysical signatures arising from groundwater contamination by EtOH. Conductivity measurements were performed at the laboratory scale on EtOH-water mixtures (0 to 0.97 v/v EtOH) and EtOH-salt solution mixtures (0 to 0.99 v/v EtOH) with and without a sand matrix. A mixing model was used to simulate electrical conductivity as a function of EtOH concentration in the mixture. It was found that increasing EtOH concentration resulted in a decrease in measured conductivity magnitude ($|\sigma|$), which reflected changes in relative strength of the types of interactions occurring in EtOH-water mixtures.

The second research topic explored the electrical properties associated with EtOH-clay interactions using CR measurements on laboratory columns of varying ethanol (EtOH) concentration (0% to 30% v/v) in a sand-clay (bentonite) matrix. A Debye Decomposition approach was applied to fit the CR data. Overall, the results showed a significant suppression ($P \leq 0.001$) of the clay driven polarization with increasing EtOH concentration. The suppression effects are associated with alterations in the electrical double layer (EDL) at the clay-fluid interface due to strong EtOH adsorption on clay and complex intermolecular EtOH-water interactions. The persistent EtOH adsorption on clay also indicated strong hysteresis effects in the electrical response.

The third research topic investigated changes in electrical properties during EtOH biodegradation processes in sand matrix using CR measurements in conjunction with

geochemical data analysis on microbial stimulated (inoculation of bacterial cells) and control (without bacteria inoculation) columns. A Debye Decomposition approach was applied to fit the CR data. Overall, the results showed a clear distinction between the bio-stimulated and control columns in terms of real (σ') and imaginary (σ'') conductivity, phase (ϕ) and apparent formation factor (F_{app}). Temporal geochemical changes and high resolution scanning electron microscopy imaging corroborated the CR findings, thus indicating the sensitivity of CR measurements to EtOH biodegradation processes.

Dedication

Johanne, Jade and Sarie.

Acknowledgements

First and foremost, I thank God Almighty for preserving my life and guiding my road. May God be always present in my life.

I gratefully acknowledge the continuous support of my advisor, Professor Lee Slater. I really appreciate your help, encouragement, valuable guidance and critical reviews of my work from the beginning until the achievement of my thesis. I am also grateful to my thesis committee members, Dimitrios Ntarlagiannis (Rutgers), Dale Werkema (USEPA) and Zoltan Szabo (Rutgers/USGS), for providing valuable critiques at different stages of my research and publications. It was a great privilege for me to collaborate with this team.

I also like to thank the faculty and staff at the Department of Earth and Environmental Sciences, especially Drs Kristina Keating, Evert Jan Elzinga, Adam Kustka, and Alexander Gates for sharing their knowledge and experiences, and providing me the opportunities to substantially improve my skills on various aspects of geosciences. My appreciation goes to Liz Morrin for her support in all administrative aspects regarding class enrollment, ordering products and materials for my research. I thank Drs Angelo Lampousis and Markus Wehrer for their assistance and Sweeta Chauhan for her encouragement and friendship.

I am thankful to my fellow graduate students and friends at the Department for their support, encouragement and the opportunities to learn from their experiences and skills. My thanks goes especially to Chi Zhang, Judy Robinson, Kisa Mwakanyamale, Dawn

Semple, Simla Sahin, Ashley Samuel, Jessica Halsey, Jianqiong Zhan, Ying Zhu, Jeff Heenan, Andrew Parsekian, Jay Nolan, Neil Terry, Samuel Falzone, Zhongjie Yu, Sundeep Sharma, Gordon Osterman, Mehrez Elwaseif, Michael Kalczynski, Rafael Jusino-Atresino and Joshua Lefkowitz.

I am appreciative of Andrea Ustra for the productive discussions on the matlab code used for the Debye Decomposition model. I thank Jacob Gibbs (USGS, Trenton) and Martin Briggs (USGS, OGW, Branch of Geophysics, Storrs, CT) for providing valuable review comments on some of my manuscripts.

My thanks go also to the students Mark Perlmutter and Maribel Granja for their help with the lab work.

I would also like to acknowledge the financial support of the United States Environmental Protection Agency through its Office of Research and Development under contract # EP10D000751 to Yves Robert Personna.

Finally, I am indebted to my parents, family and family in-law for their support during this journey. I like to especially thank my wife, Johanne and my daughters, Jade and Sarie, for their support, love, understanding and sacrifices during PhD work. You are just incredible!

Table of Contents

List of illustrations

List of Tables

CHAPTER 1. INTRODUCTION

1.1. Background and overview

Ethanol (EtOH) production, the most common biofuel in the USA, has significantly increased during the last two decades (Figure 1.1). Its production was stimulated by a series of government promotions and regulations that aimed at reducing air pollution and providing an alternative to petroleum. For instance, the Clean Air Act Amendments of 1990 required the use of oxygenated or reformulated gasoline (RFG). In 2005, the Energy Policy Act (P.L. 109-58) established a renewable fuels standard (RFS), which mandated the use of ethanol and other renewable fuels in gasoline. This act was recently amended by the Energy Independence and Security Act of 2007 that focused on increasing the production of clean renewable fuels and reducing consumption of gasoline.

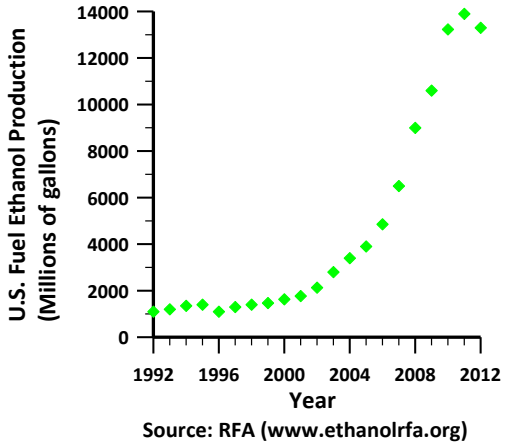

Figure 1.1: Statistics of ethanol production in the USA (1992-2012)

As EtOH production increases, scenarios of large spills of EtOH have become more likely. Ethanol is currently treated as an emerging contaminant [*Gomez and Alvarez*, 2010] that poses potential risks to water resources [*Powers et al.*, 2001a] when accidental

releases of large volumes occur during transportation [*Spalding et al.*, 2011] or from storage facilities (McDowell et al., 2003). Ethanol contamination could persist for years in soil, capillary zone and shallow groundwater as reported by *Spalding et al.* [2011] for spills of large volume of E95 (95% EtOH, 5% gasoline) following train derailment in Balaton and Cambria, Minnesota and South Hutchinson, Kansas in 2004, 2006 and 2005, respectively. Numerous recent studies have documented potential adverse effects associated with subsurface EtOH contamination including , (1) toxicity to indigenous microorganisms [*Nelson et al.*, 2010] involved in the degradation or transformation of existing contaminants, (2) increase in aqueous phase BTEX (benzene, toluene, ethyl-benzene and xylene) compounds contained in gasoline (Powers et al., 2001b) due to cosolvency effects [*Powers et al.*, 2001b; *Da Silva et al.*, 2002; *Corseuil et al.*, 2004; *Stafford et al.*, 2009], (3) slower natural degradation of BTEX compounds [*Corseuil et al.*, 1998; *Powers et al.*, 2001b; *Ruiz-Aguilar et al.*, 2003; *Mackay et al.*, 2006; *Gomez and Alvarez*, 2009 & 2010; *Freitas et al.*, 2011] attributed to the preferential biodegradation of EtOH and associated rapid depletion of dissolved oxygen and other electron acceptors, and (4) methane production associated with anaerobic degradation of EtOH reaching the explosive limit level [*Nelson et al.*, 2010; *Freitas et al.*, 2010, *Spalding et al.*, 2011].

The potential risks associated with subsurface EtOH contamination call for the preparation of adequate remediation responses. Yet, the design and application of relevant remediation actions depend upon a) a comprehensive understanding of EtOH-water and EtOH-mineral interactions, and EtOH biodegradation processes, and b) the

availability of cost-effective tools to characterize and monitor the spatial and temporal evolution of EtOH in the subsurface. The potential EtOH interactions and degradation processes could conceivably induce changes in physical, chemical and, subsequently, electrical properties of geologic media. Therefore, non-invasive geophysical methods, particularly complex resistivity method, appear as attractive monitoring tools for tracking subsurface EtOH contamination.

1.2. Overall Objectives and organization of the thesis

This thesis is directed at providing a comprehensive understanding of the electrical properties associated with EtOH-water interactions, EtOH-mineral interactions and EtOH biodegradation processes in porous media. The availability of non-invasive and cost-effective geophysical methods for characterizing and monitoring the spatial and temporal evolution of EtOH in the near surface can help design and apply relevant remediation actions in biofuels contaminated sites.

The specific objectives are regrouped under three research topics.

Research topic 1: Electrical signatures of ethanol-liquid mixtures: implications for monitoring biofuels migration in the subsurface.

Objective 1.1: Determine the low-frequency electrical properties of EtOH in water and a porous medium.

Research topic 2: Complex resistivity signatures of ethanol in sand-clay mixtures.

Objective 2.1: Determine the electrical properties of EtOH in a sand-clay medium;

Objective 2.2: Determine if clay-organic reactions associated with EtOH enhance or suppress the CR response;

Objective 2.3: Determine whether CR signatures associated with clay-EtOH interactions are reversible when the EtOH is removed, thereby providing information on the persistence of clay-organic reactions.

Research topic 3: Complex Resistivity Signatures of Ethanol Biodegradation in Porous Media.

Objective 3.1: Determine the electrical properties of real-time EtOH biodegradation in porous media;

Objective 3.2: Determine whether temporal changes in aqueous chemistry are consistent with changes in the CR response

This thesis includes 6 chapters and it is structured as follows,

- Chapter 1 : Introduction (current part).
- Chapter 2: Complex resistivity method and modeling.
- Chapter 3: Electrical signatures of ethanol-liquid mixtures: implications for monitoring biofuels migration in the subsurface.
- Chapter 4 : Spectral Induced Polarization (SIP) Signatures of Ethanol in Sand-Clay Medium
- Chapter 5 : Spectral induced polarization characterization of ethanol biodegradation processes in porous media
- Chapter 6 : Conclusions and future work

CHAPTER 2: METHODS

2.1. Basic principles of geophysical data acquisition and electric conduction

Unlike direct sampling of the subsurface which is generally destructive and expensive, geophysical methods offer the potential for spatially continuous data acquisition of earth materials non-invasively and cost-effectively. Data acquisition with active geophysical methods (e.g. electrical resistivity (ER), induced polarization (IP), spectral IP (SIP) or complex resistivity (CR), ground-penetrating radar (GPR), electromagnetic (EM)), are based upon the same principle. Basically, a source of signals (e.g. electrical current or an electromagnetic wave) is applied to a volume of the subsurface material and the resulting signal response is measured either at the surface or in boreholes.

When applying an electric field to a porous medium, electric conduction can occur as a result of electrolytic conduction through interconnected pores, electronic conduction in the presence of metals, and surface conduction in the electrical double layer (EDL) at the grain fluid interface (Figure 1.3). The electrolytic conductivity is controlled by the conductivity of the pore-filling electrolyte (σ_w), along with the size and interconnectedness of the pores. The electronic conductivity occurs mainly as a result of electron mobility in a metallic conductor. The surface conductivity ($\sigma^*_{surface}$) primarily depends upon the grain-fluid interfacial area and grain-surface morphology, and is also controlled by the pore fluid chemistry.

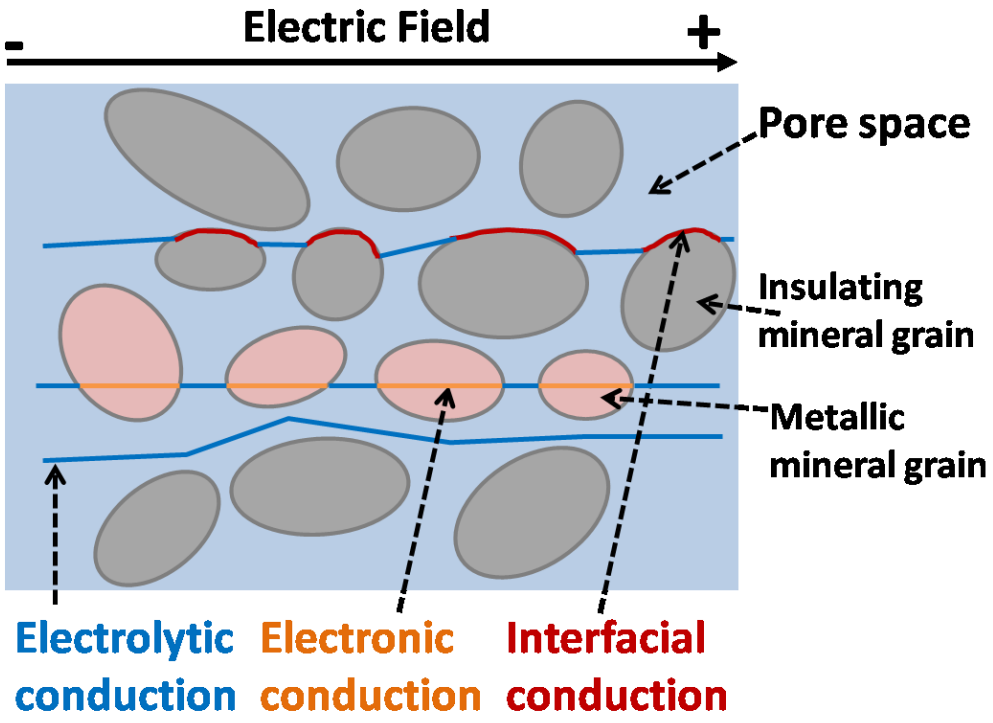

Figure 2.1: Electric conduction in porous medium

Figure showing electric conduction (electrolytic, electronic and surface conduction) in a porous medium

2.2. Complex resistivity method: data acquisition, modeling and interpretations

In my research, I applied complex resistivity (CR) method, also known as spectral induced polarization (SIP), for the investigation of EtOH-water and EtOH-clay interactions as well as EtOH biodegradation processes in the subsurfaceThe complex resistivity (CR) method measures the frequency dependent polarization associated with electrochemical charge migration and accumulation in the electrical double layer (EDL) at the mineral-fluid interface of soils and rocks [*Weller et al.*, 2010; Kemna et al., 2012]. Although traditionally developed for detecting disseminated metallic ores [*Marshall and Madden*, 1959; *Sumner*, 1976] and to a lesser extent for groundwater exploration

[*Vacquier et al.*, 1957], the CR method has increasingly been applied in a wide variety of environmental investigations [*Vanhala*, 1997; *Slater and Lesmes*, 2002; *Kemna et al.*, 2004; *Sogade et al.*, 2006; *Williams et al.*, 2009; *Flores Orozco et al.*, 2011; *Flores Orozco et al.*, 2012]. The CR method is sensitive to changes in pore fluid chemistry, pore space geometry and solid-fluid interface chemistry. These changes could occur as a result of EtOH-water and EtOH-mineral interactions, and EtOH biodegradation processes in porous media.

Induced polarization (IP) measurements are conventionally performed with a four-electrode configuration system consisting of two current injection electrodes and two potential recording electrodes. The measurements can be performed in the time domain or in the frequency domain. Note that the time domain IP measurement is only briefly mentioned here as the frequency domain IP measurement is utilized in this thesis. In the time domain, a transient decay of the voltage between two time intervals is recorded after the current injection to a volume of earth materials is stopped [*Binley and Kemna*, 2005] (Figure 2.2).

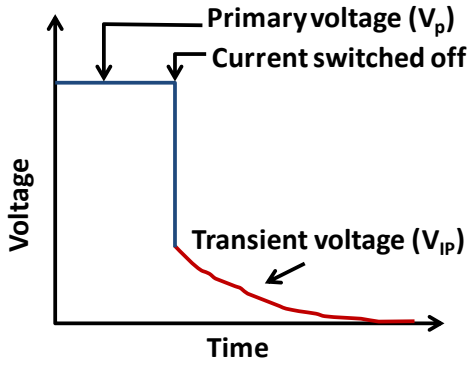

Figure 2.2: Illustration of measurement of time domain induced polarization

Figure showing measurement of time domain induced polarization with the primary voltage (Vp) remaining constant when the current is switched on followed by a gradual decrease of the transient (or secondary) voltage with time when the current is switched off.

This decay of the voltage can be defined by an apparent measure of chargeability, m_{app}, as follows,

$$m_{app} = \frac{1}{t_2 - t_1} \frac{1}{V_p} \int_{t_1}^{t_2} V_{IP}(t)dt \quad (1)$$

where t_1 and t_2 are the time window of the recording transient (or secondary) voltage (V_{IP}), and V_p is the primary voltage during the current injection.

In the frequency domain mode, a CR instrument (e.g. dynamic signal analyzer) records, at different frequencies of the applied current, the magnitude and the phase shift (ϕ) of the potential voltage waveform across the sample relative to the current waveform across a reference resistor. Typical theoretical variations in amplitude and phase driven by applied source of current are shown in Figure 2.3.

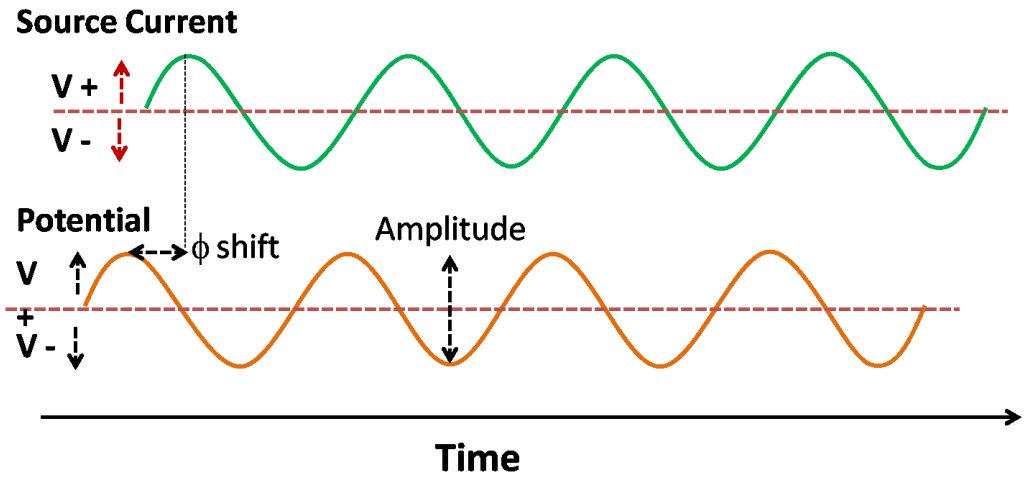

Figure 2.3: Theoretical variations in amplitude and phase driven by applied source of current.

Figure showing the phase (ϕ) shift of the potential voltage relative to the source current voltage as well as the amplitude of the potential voltage.

Knowing the sample measurement geometry factor, this complex impedance can be described as the vector sum of both in-phase energy loss (real conductivity, σ') and out of-phase energy storage /polarization (quadrature or imaginary conductivity, σ''). In terms of measured conductivity magnitude $|\sigma|$ and ϕ, the complex impedance is given by:

$$|\sigma| = \sqrt{(\sigma')^2+(\sigma'')^2} \quad (2),$$

$$\phi = tan^{-1}\left(\sigma''/_{\sigma'}\right) \quad (3).$$

The real and imaginary conductivity are then given by:

$$\sigma' = |\sigma| cos\ \phi \quad (4),$$

$$\sigma'' = |\sigma| sin\ \phi \quad (5).$$

In non-metallic porous media, the electrolytic and surface conductivity are often assumed to add in parallel (Figure 2.4). Thus, the complex conductivity (σ*) is given by:

$$\sigma^* = \sigma_{el} + \sigma^*_{surf} \quad (6).$$

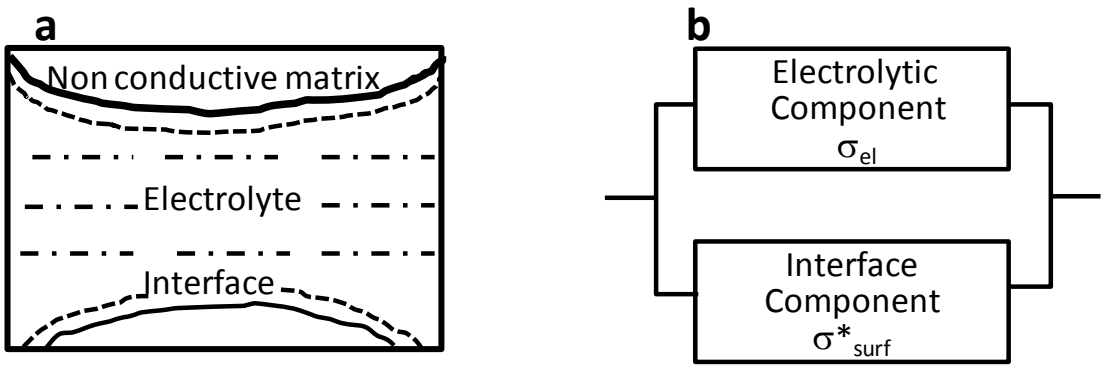

Figure 2.4: Illustration of electrolytic and surface conductivity adding in parallel in porous medium

Figures showing a) Electrolytic (σ_{el}) and surface conductivity (σ^*_{surf}) adding in parallel in a porous medium, and b) equivalent circuit showing σ_{el} and σ^*_{surf} component of the complex conductivity (σ^*).

The σ' and σ'' are commonly expressed as a function of electrolytic (σ_{el}) and surface conductivity ($\sigma*_{surf}$) as :

$$\sigma' = \sigma_{el} + \sigma'_{surf} \quad (7),$$

$$\sigma'' = \sigma''_{surface} \quad (8),$$

where σ'_{surf} and σ''_{surf} are the real part and imaginary parts of the complex surface conductivity (σ^*_{surf}), respectively.

As per Archie's Law [*Archie*, 1942], σ_{el} is given by:

$$\sigma_{el} = \frac{1}{F}\,\sigma_w \quad (9),$$

thus,

$$\sigma' = \frac{1}{F}\sigma_w + \sigma'_{surface} \quad (10),$$

where *F* is the true formation factor, defined as:

$$F = \frac{\sigma_w}{\sigma_{el}} = \Phi^{-m} \quad (11),$$

(Φ is the porosity and m is the cementation index i.e. a function of the effective grain shape).

An apparent formation factor, F_{app}, can be defined from the measurements of σ_w and σ' as follows:

$$F_{app} = \frac{\sigma_w}{\sigma'} = \frac{\sigma_w}{\sigma_{el} + \sigma'_{surf}} \quad (12).$$

Therefore, $F_{app} \approx F$ if σ'_{surf} is very small ($\sigma'_{surf} \approx 0$).

The mechanisms responsible for generating the CR responses in soils and rocks are not yet fully understood. In non-metallic porous media, the CR response could be associated with (a) grain polarization, (b) electrolytic or membrane polarization and (c) Maxwell Wagner polarization. In metallic porous media, electrode polarization could dominate the electrical response.

Grain polarization is mainly attributed to polarization of the Stern layer (the layer between the mineral surface and the inner surface of the diffuse layer) in the EDL at low frequencies (≤ 100 Hz) of the applied electrical current. Stern layer polarization results from accumulation of electrical charge due to attraction of counterions to the mineral surface (approximately the edge of the inner layer of the EDL) and tangential movement of charge along the grain surface. [*Leroy et al.*, 2008; *Revil and Florsch*, 2010; *Schmutz*

et al., 2010; *Revil and Skold*, 2011; *Vaudelet et al.*, 2011a; *Vaudelet et al.*, 2011b; *Revil et al.*, 2012a].

Membrane polarization *[Vinegar and Waxman*, 1984; *Reynolds*, 1997] is traditionally attributed to a blockage and selective flow of ions within the pore channels due primarily to pore constrictions and local ion congestion by clays lining pores. As most minerals are negatively charged, positive ions in the fluid phase are attracted and bound to the mineral surface. Under an applied electric field, zones with different number of cation and anion transport and local concentration gradients are formed within the pore channels.

Maxwell Wagner (MW) polarization is associated with the discontinuity of displacement of electrical charges in the pore space among the different phases of a composite medium at higher frequencies of the applied electrical current (≥ 100 Hz) [*Leroy et al.*, 2008, *Leroy and Revil*, 2009]. The MW polarization is controlled by the characteristics of the different phases of a composite medium including tortuosity, pore-volume fractions, conductivity and permittivity.

Electrode polarization results from the presence of conductive minerals such as metallic sulfide acting as electrodes distributed through the rocks and soils. Electrode polarization is controlled by electrochemical reactions and charge transport in the EDL at the interface between the metallic mineral and the ionic pore fluid [*Zonge et al.*, 2005].

Two main conceptual models have been proposed for interpreting the polarization in the EDL at the mineral-fluid interface that causes CR response, (a) polarization of the EDL itself surrounding a mineral grain, also termed as grain polarization [e.g. Lesmes and Morgan, 2001; Ulrich and Slater, 2004; *Leroy et al.*, 2008; *Revil and Florsch*, 2010; *Schmutz et al.*, 2010; *Revil and Skold*, 2011; *Vaudelet et al.*, 2011a; *Vaudelet et al.*, 2011b; *Revil et al.*, 2012a], and (b) polarization of pore throats [*Titov et al.*, 2002; *Scott and Baker*, 2003; *Titov et al.*, 2004, *Ulrich and Slater*, 2004, *Slater et al.*, 2007, *Blascheck and Hordt*, 2009, *Kruschwitz et al.*, 2010]. Grain polarization, as discussed above, results from polarization of the Stern layer in the EDL and is dependent upon the physical and chemical characteristics at the interface (grain size, surface area, surface charge density, surface ionic mobility, and pore fluid chemistry). A simplistic representation of grain polarization mechanism is shown in Figure 2.5. Polarization of pore throats, pertaining to membrane polarization, is controlled by the pore throat size. Under an applied electric field, charge transport occurs through a sequence of large and narrow pores and results in a surplus of cations and a deficiency of anions within the short narrow pores. The difference in ion transport between wide and narrow pores can be linked with higher concentrations of cations than anions in the diffuse layer of the EDL. A simplistic representation of pore-throat controlled polarization mechanism is shown in Figure 2.6.

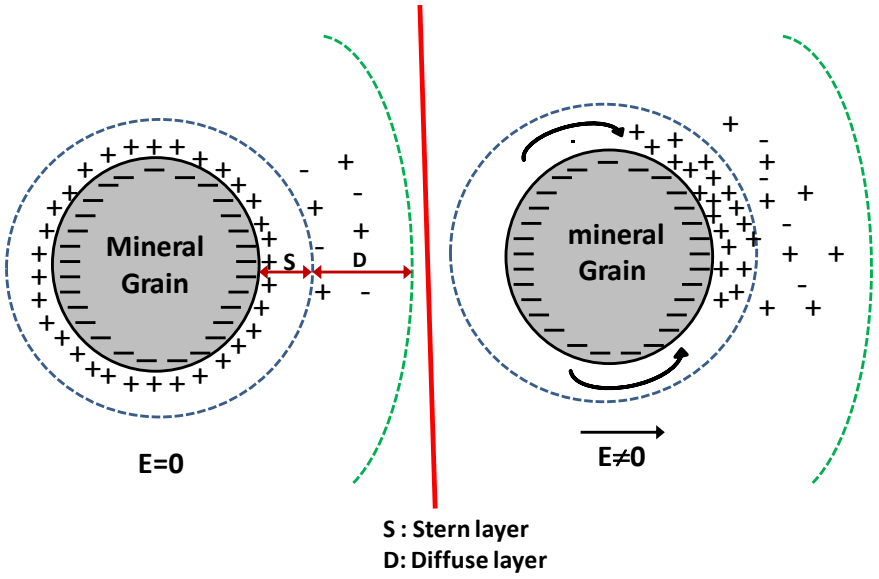

Figure 2.5: Possible polarization of the Stern layer of the EDL surrounding a mineral grain.

Figures showing the polarization associated with accumulation of charges in the Stern layer of the EDL due tangential movement of charges along the grain surface whereby cations move in the direction of the applied electric field (E≠0) and anions move in the opposite direction. When the electric field is terminated (E=0), the accumulated ions returned to neutral equilibrium distribution. Note that the stern layer is a very thin layer that is exaggerated in the figure. The mineral surface, a pH dependent surface charge, is negatively charged in the pH range above the point of zero charge.

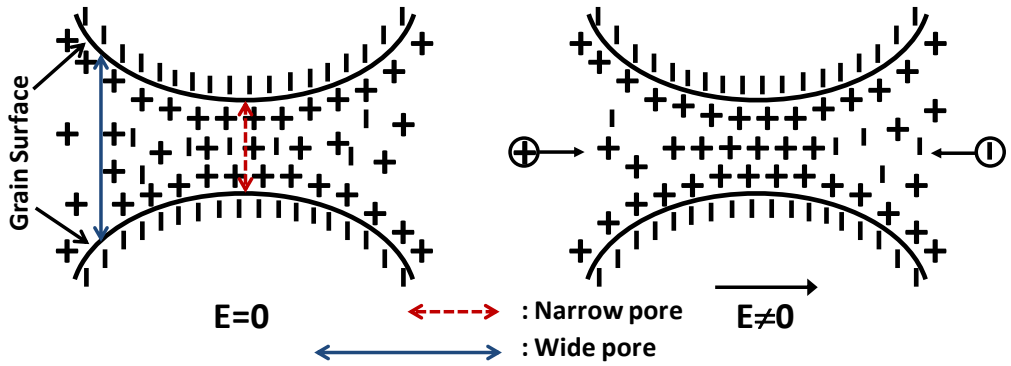

Figure 2.6: Possible pore-throat polarization during charge transport between wide and narrow pores.

This figure shows polarization effects associated with a surplus of cations and a deficiency of anions within the narrow pores as cations move in the direction of the applied electric field (E≠0) and anions move in the opposite direction. When the electric field is terminated (E=0), the charges are redistributed to neutral equilibrium.

During the last decade, important efforts have been made for developing mechanistic models to describe the micro-scale physical, chemical and biological properties of interest that govern polarization at the EDL and the CR responses [*Kemna et al.*, 2012]. For instance, some studies showed that the relaxation time closely correlated with the pore-throat size and geometry for sandstone samples [*Scott and Barker*, 2003; *Binley et al.*, 2005]. They suggested the potential application of CR technique for field determination of permeability as the diameter of pore-throat is closely related to the permeability. Some recent studies have reported contrasting results regarding the relationship between the magnitude of the electrical polarization (quantified as imaginary conductivity, σ'') and surface area to pore volume ratio (S_{por}). The σ''-S_{por} relation was described either by strong power-law functions for unconsolidated sediments [*Slater and Glaser*, 2003; *Slater et al.*, 2006; *Slater*, 2007], or by a single linear function for non-metallic sandstones and unconsolidated sediments, or a strong linear function for metallic samples [*Weller et al.*, 2010]. Other researchers reported only a weak σ''-S_{por} relation for sandstone samples [e.g. *Binley et al.*, 2005]. The effects of fluid chemistry on the polarization response were also examined. *Vaudelet et al.* [2011b] combined the Stern layer polarization model with a complexation model to explain changes in the complex conductivity as a function of pore fluid chemistry and competitive sorption of cations at the mineral-water interface. They showed a dependence of the phase response on cation (Na^+, $Cu^{2+)}$ exchange processes at the surface of the silica grain. *Weller and Slater* [2012] documented a simple positive power law dependence of σ'' on fluid conductivity (σ_w) at low salinities (<1 S/m) for sandstones and unconsolidated sediments. They showed that the Stern layer polarization and diffuse layer polarization models can be used to predict

the polarization response from an increase in surface charge density at increasing σ_w. These reported observations on the relationship between σ'' and S_{por}, and σ'' and σ_w provide insight into the potential application of CR measurements for lithologic discrimination and permeability estimation [*Weller and Slater*, 2012]. However, a definitive physicochemical model for interpretation of the complex conductivity response is still lacking.

Currently, empirical models like the Cole-Cole model and Debye Decomposition (DD) have been widely used for the interpretation of CR data. The Cole-Cole type models [*Cole and Cole*, 1941; *Davidson and Cole*, 1951] are useful to describe the dependence of σ^* on frequency, but one disadvantage is that the estimated model parameters may differ for each Cole-Cole variant even for the same CR data [*Nordsiek and Weller*, 2008]. Another disadvantage is that the Cole-Cole models may not adequately describe the data, especially when the shape of the spectra does not show a typical accentuated phase peak. An alternative is the Debye Decomposition (DD) approach that considers the spectra of conductivity amplitude and phase as a superposition of a finite number of different Debye relaxations. Unlike the Cole-Cole type models, the DD model can fit CR data of various spectral shapes [*Nordsiek and Weller*, 2008]. Recently, *Zisser et al.* [2010] proposed a variant of the DD approach as follows,

$$\sigma^*(\omega) = \frac{1}{\sigma_0}\left[1 - \sum_{k=1}^{n} m_k \left(1 - \frac{1}{1 + i\omega\tau_k}\right)\right] \quad (13),$$

where $\sigma_0 = 1/\rho_0$ is the DC conductivity, n is the number of individual Debye responses, m_k and t_k are, respectively a specific chargeability and relaxation time [*Zisser et al.*, 2010].

CHAPTER 3: ELECTRICAL SIGNATURES OF ETHANOL-LIQUID MIXTURES: IMPLICATIONS FOR MONITORING BIOFUELS MIGRATION IN THE SUBSURFACE[1]

Abstract

Ethanol (EtOH), an emerging contaminant with potential direct and indirect environmental effects, poses threats to water supplies when spilled in large volumes. A series of experiments was directed at understanding the electrical geophysical signatures arising from groundwater contamination by ethanol. Conductivity measurements were performed at the laboratory scale on EtOH-water mixtures (0 to 0.97 v/v EtOH) and EtOH-salt solution mixtures (0 to 0.99 v/v EtOH) with and without a sand matrix using a conductivity probe and a four- electrode electrical measurement over the low frequency range (1-1000 Hz). A Lichtenecker-Rother (L-R) type mixing model was used to simulate electrical conductivity as a function of EtOH concentration in the mixture. For all three experimental treatments increasing EtOH concentration resulted in a decrease in measured conductivity magnitude ($|\sigma|$). The applied L-R model fit the experimental data at concentration $\leq$ 0.4v/v EtOH, presumably due to predominant and symmetric intermolecular (EtOH-water) interaction in the mixture. The deviation of the

---

[1] This chapter is published as : Personna, Y. R., L. Slater, D. Ntarlagiannis, D. Werkema, and Z. Szabo (2013), Electrical signatures of ethanol-liquid mixtures: implications for monitoring biofuels migration in the subsurface, *Journal of contaminant hydrology*, *144*, 99-107.

experimental $|\sigma|$ data from the model prediction at higher EtOH concentrations may be associated with hydrophobic effects of EtOH-EtOH interactions in the mixture. The $|\sigma|$ data presumably reflected changes in relative strength of the three types of interactions (water-water, EtOH-water, and EtOH-EtOH) occurring simultaneously in EtOH-water mixtures as the ratio of EtOH to water changed. No evidence of measurable polarization effects at the EtOH-water and EtOH-water-mineral interfaces over the investigated frequency range was found. Our results indicate the potential for using electrical measurements to characterize and monitor EtOH spills in the subsurface.

3.1. Introduction

In the last two decades, the production of EtOH, one of the most common biofuels in the USA, has substantially increased due to regulations aimed at reducing air pollution and providing a supplement to petroleum. Accidental releases of large volumes of EtOH, particularly during transportation [*Spalding et al.*, 2011] and at storage facilities [*McDowell et al.*, 2003], have raised concerns about its environmental fate and potential risks to groundwater [*Powers et al.*, 2001a]. Ethanol is currently treated as an emerging contaminant [*Gomez and Alvarez*, 2010] that may induce substantial adverse effects in the subsurface environment [*EPA*, 2011]. As a powerful disinfectant that has been long used as an antiseptic, EtOH at concentrations as low as 6% v/v is toxic to soil and aquifer microorganisms [*Nelson et al.*, 2010]. Ethanol toxicity can lead to major alterations in microbial growth, metabolism, viability [*Ingram*, 1989; *Nelson et al.*, 2010] and community structure [*Cápiro et al.*, 2008; *Ma et al.*, 2011]. The persistence of EtOH toxicity in the subsurface may ultimately lead to a substantial decrease in microbial

population and activity, thus affecting the overall subsurface microbial processes including biodegradation of contaminants.

Ethanol contamination may also result in secondary adverse impacts on water quality. It has been shown that high EtOH concentration in water can exert cosolvency effects on existing BTEX (benzene, toluene, ethyl-benzene and xylene) contaminants [*Powers et al.*, 2001b; *Da Silva et al.*, 2002; *Corseuil et a*l., 2004; *Stafford et al.*, 2009]. Ethanol is an amphiphilic molecule that is fully miscible in water. Ethanol is characterized by (1) a hydrophilic part (hydroxyl) allowing it to partition into water, and (2) a hydrophobic part (2-carbon alkyl chain) facilitating the remobilization and redistribution of organic compounds in the aqueous phase. Therefore, a high aqueous EtOH concentration can potentially lead to an enhancement of organic contaminant concentration in water [*Powers et al.*, 2001b]. Ethanol can also affect the natural degradation of BTEX compounds [*Corseuil et al.*, 1998; *Powers et al.*, 2001b; *Ruiz-Aguilar et al.*, 2003; *MacKay et al.*, 2006; *Gomez and Alvarez*, 2009 & 2010; *Freitas et al.*, 2011] due mainly to its preferential biodegradation and subsequent depletion of dissolved oxygen and other electron acceptors during this process, thereby limiting the degradation of the other compounds. As anaerobic conditions develop, EtOH degradation may generate methane in potentially hazardous concentrations by exceeding the explosive limit [*Nelson et al.*, 2010; *Freitas et al.*, 2010, *Spalding et al.*, 2011].

Ethanol and water chemically form a complex mixture, which can be mainly attributed to the amphiphilic or bi-functional nature of ethanol molecules. These molecules are characterized by the hydrophilic hydroxyl group favorable to hydrogen-bonding formation with water molecules and the alkyl chain conferring hydrophobic effects [*Franks and Ives*, 1966]. The complexity of EtOH-water media, partially attributable to the hydrogen-bond formation among the water and ethanol molecules, leads to complex molecular interactions [*Atamas and Atamas*, 2009; *Mizuno et al.*, 1995] and distinct physical properties of the solution (e.g. density and sound velocity) [*Petek et al.*, 2001; *Parke and Birch*, 1999] as the EtOH/water ratio changes.

Few studies have examined the potential of non-invasive geophysical measurements for monitoring the effects of EtOH releases in the subsurface environment. *McNaughton et al*. [2009] demonstrated the potential of using high frequency ground penetrating radar (GPR) to image sequential gasoline-EtOH releases in the near sub-surface. *Petong et al.* [2000] studied the dielectric relaxation of EtOH-water mixtures at different compositions and temperatures between 1 MHz and 24 GHz. At the low frequencies (< 1 KHz) used for electrical conductivity and induced polarization methods, only *Henderson et al.* [2009] reported initial results that suggested the potential application of electrical measurements for EtOH detection in the subsurface.

Owing to the increasing likelihood of undesired EtOH releases, potential risks to humans and the environment exist, particularly in a scenario of a large EtOH spill and

contamination of drinking water supplies. Such risks call for the preparation of adequate remediation responses. Yet, the design and application of relevant remediation actions depend both upon a comprehensive understanding of EtOH-water chemistry and the availability of cost-effective tools to characterize and monitor the spatial and temporal evolution of EtOH in the near surface. Therefore, basic research on the electrical properties of EtOH in water and porous media is needed in order to improve the understanding of the potential for electrical monitoring of ethanol contamination in the subsurface. In this paper, we investigate the low frequency (<1 KHz) geophysical behavior of EtOH-liquid (water and salt solution) mixtures at the laboratory scale. The main objective of this study was to determine the low-frequency electrical properties of EtOH in water and a porous medium. Our results indicate the dependence of electrical conductivity measurements on EtOH concentration, highlighting the potential of electrical measurements for detection and monitoring of EtOH in the subsurface.

3.2. Electrical properties

When applying an electrical current to a porous medium, electric conduction can occur as a result of electrolytic conduction through interconnected pores, electronic conduction in the presence of metals, and surface conduction in the electrical double layer (EDL) at the grain fluid interface. The electrolytic conductivity is controlled by the conductivity of the pore-filling electrolyte (σ_w), along with the size and interconnectedness of the pores. The electronic conductivity occurs mainly as a result of electron mobility in a metallic conductor. The surface conductivity ($\sigma^*_{surface}$) primarily depends upon the grain-surface morphology, and is also controlled by the pore fluid chemistry.

Electrical measurements are commonly used to determine the complex conductivity (σ^*) of a material by measuring the conductivity magnitude ($|\sigma|$) and phase shift (ϕ) of a sample relative to a reference resistor. These measurements are related to an in-phase energy loss term (conduction) represented by the real conductivity (σ') and an out-of-phase energy storage term (polarization) represented by the imaginary conductivity (σ'') as follows,

$$|\sigma| = \sqrt{(\sigma')^2 + (\sigma'')^2} \quad (1),$$

$$\phi = tan^{-1}\left(\sigma''/_{\sigma'}\right) \quad (2).$$

Therefore, the real and imaginary components are related to the phase as follows,

$$\sigma' = |\sigma| \cos\phi \quad (3),$$

$$\sigma'' = |\sigma| \sin\phi \quad (4).$$

The electrolytic and surface conductivity are often simply assumed to add in parallel for a porous medium [*Waxman and Smits*, 1968]. In this case, the real and imaginary parts of the complex electrical conductivity (σ^*) can be expressed as a function of the fluid conductivity (σ_w) and the surface conductivity ($\sigma^*_{surface}$) by:

$$\sigma' = \frac{1}{F}\sigma_w + \sigma'_{surface} \quad (5),$$

$$\sigma'' = \sigma''_{surface} \quad (6),$$

where F is the electrical formation factor (discussed further below), and single and double scripts represent real and imaginary part of the conductivity, respectively. Note that when surface conductivity is small,

$$|\sigma| \cong \sigma' \cong \frac{1}{F}\sigma_w \quad (7).$$

3.3. Materials and methods

3.3.1. Preparation of ethanol-water and ethanol-salt solution mixtures

Pure ethanol (ethyl alcohol 200 proof, absolute ACS/USP grade, 99.98 % assay v/v) was used in this experiment. We prepared EtOH-water mixtures (0 to 0.97 v/v EtOH) by adding the desired volumes of pure EtOH and tap water in a volumetric flask and stirring at room temperature (26.0 ± 0.5 ^{o}C). Ethanol-salt solution mixtures (0 to 0.99 v/v EtOH) were prepared the same way. The salt solution, a Bushnell Haas Broth, was initially prepared in deionized water and comprised 0.81 mM of $MgSO_4.7H_2O$, 0.14 mM of $CaCl_2.2H_2O$, 7.35 mM of KH_2PO_4, 5.74 mM of K_2HPO_4, 12.44 mM of NH_4NO_3 and 0.18mM of $FeCl_3.6H_20$. This salt solution is commonly used to examine microorganisms capable of degrading fuels and it can also be expected to serve as a surrogate for potentially mineralized groundwater where large spills of EtOH may occur.

Prepared salt solutions were sterilized by autoclaving at 121 ^{o}C for 30 minutes to prevent microbial growth of airborne bacteria that may be able to degrade EtOH and afterwards kept enclosed at ambient air and allowed to reach room temperature before being mixed with ethanol in a volumetric flask. The solution was cooled down to room temperature to prevent EtOH volatilization during the mixture.

3.3.2. Conductivity measurements

We performed conductivity measurements for water, salt solution, EtOH-water and EtOH-salt solution mixtures using both a conductivity probe (Orion 013010A Thermo

Electron Corporation) to measure σ_w and a four electrode electrical technique to measure complex conductivity (σ^*). As pure EtOH is highly resistive, neither method could be used to measure conductivity of EtOH directly. The $|\sigma|$ of EtOH-water mixtures varied dramatically but followed a second order polynomial function ($R^2 \approx 1$) at EtOH > 90% v/v. The conductivity of pure EtOH was estimated by extrapolation based on the second order polynomial function of $|\sigma|$ of the mixture as a function of EtOH concentration, from 90% to 97% EtOH v/v.

We directly measured fluid conductivity of the mixtures by inserting a probe in a sufficient volume of the fluid that was transferred into a clean beaker. Prior to each set of measurements, the probe was calibrated in a standard conductivity solution. The probe was rinsed with deionized water and wiped with task tissues after every single measurement.

The electrical measurement used a four-electrode configuration, utilizing two electrodes as current injection and two additional electrodes to record the resulting potential difference. These measurements were performed between 1-1000 Hz using a two-channel dynamic signal analyzer (DSA) (NI-4461) on a flow through column (inner diameter=4.0c m, length= 17.3 cm) [*Slater and Lesmes*, 2002]. Figure 3.1 shows a schematic of the column, including the location of two coiled Ag-AgCl current electrodes at each end and two Ag-AgCl potential electrodes (4.3 cm apart) along the side. Unlike the probe, the electrical method determines the complex conductivity of a porous

material, and also allows measurements on a much larger volume than the probe. In the case of solution mixtures only, the probe and electrical measurements should be equal (assuming homogeneous mixing of ethanol and water).

For measurements in the presence of a sand matrix, the column was dry-packed with Ottawa Sand (SiO2 > 99%, specific gravity= 2.65, d_{50}= 0.5mm), with gentle tapping applied to minimize variations in the amount of compaction along the column.

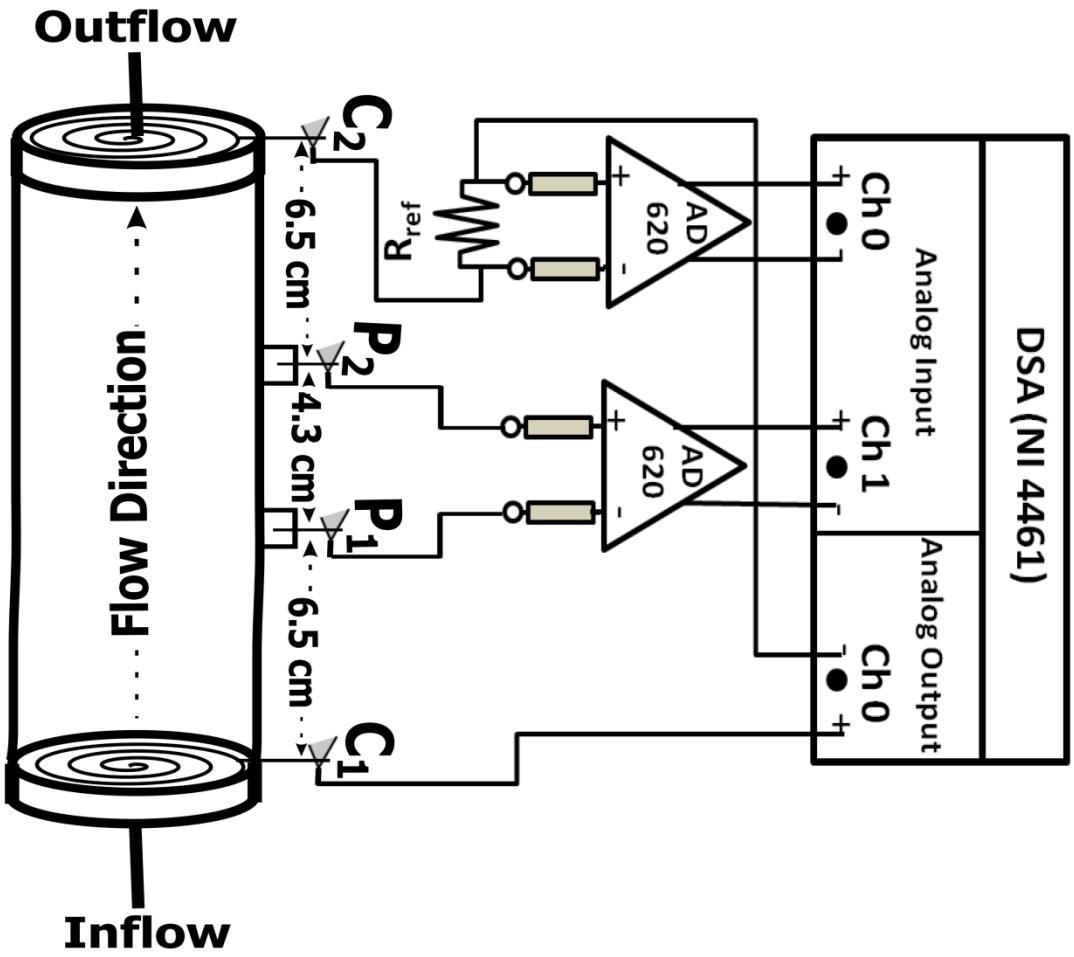

Figure 3.1: Schematic of experimental setup.

Schematic of experimental setup showing dynamic signal analyzer (NI 4461) with analog input and output, reference resistance ($R_{ref.}$), location of preamplifier (AD 620),

column configuration with two coiled Ag-AgCl current electrodes (C_1 & C_2) and two Ag-AgCl potential electrodes (P_1 & P_2), inflow and outflow valves and flow direction.

3.3.3. Determination of the electrical formation factor

The electrical formation factor (F) is defined as the ratio of the conductivity of the water to the conductivity of a water-saturated porous medium [*Archie*, 1942]. We determined F of the sand samples from the slope of the real conductivity (σ') at 1 Hz versus the fluid conductivity (σ_w) (Figure 3.2) as per equation (5) [See *Lesmes and Friedman*, 2005 for review].

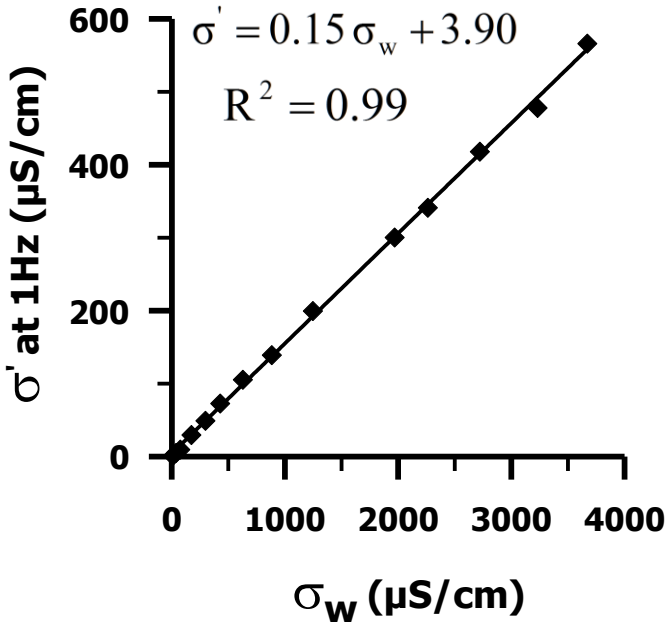

Figure 3.2: Plot of real conductivity (σ') at 1Hz versus fluid conductivity (σ_w).
In this plot, the dark squares are experimental data while the dark line is the linear regression fit of the data. The equation of this regression is shown as well as the R^2 value. The formation factor (F) and $\sigma'_{surface}$ are 6.62 and 3.90 µS/cm, respectively.

3.3.4. Application of a mixing model

The Lichtenecker-Rother (L-R) model, an effective medium theory, follows the symmetric Bruggeman rule that symmetric electromagnetic interactions occur among the components of a geomaterial [*Cosenza et al.*, 2009]. Such models offer a semi-analytical approach to examine a conceptual elementary volume of a geomaterial in terms of its constituent components. Effective medium theories are generally conceptualized on a simple cell containing a sub-spherical solid grain such as quartz sand embedded into a surrounding volume of fluid such as water. Commonly used in soil physics, they are valuable for characterizing the relationships between electromagnetic properties and hydrological variables [see *Cosenza et al.*, 2009 for review]. When ethanol is introduced into water, an arrangement of water molecules occurs as a result of attractive forces between the two components so that multi-hydration layers form around EtOH molecules [*Frank and Wen*, 1957; *Parke and Birch*, 1999]. Therefore, like a solid grain of sand in water, an EtOH molecule can be seen as being embedded in many water molecules.

We applied a simple L-R model [*Zakri et al.*, 1998; *Cosenza et al.*, 2009] to our experimental data. We used the conductivity magnitude $|\sigma|$ measured with the DSA as input data, although the same results would be obtained using real conductivity (σ') (e.g. Eq. 7). Assuming a negligible surface conduction in a two-phase mixture, this model is given by,

$$|\sigma|^{\alpha} = (1-n)\sigma_2^{\alpha} + n\sigma_1^{\alpha} \quad (8),$$

where σ_1 is the conductivity of water (236.34 µS/cm) or the salt solution (3633.60 µS/cm), σ_2 is the conductivity of EtOH (0.252 µS/cm), n is the relative volume concentration of the water phase or salt-solution phase ($0 \leq n \leq 1$) and α is a fitting parameter ($0 \leq \alpha \leq 1$). All parameters were known except α, which was estimated from a least squares regression of the above models against the experimental data.

To account for the presence of the sand matrix in the case of an EtOH-salt solution in a sand matrix, the data were fit to the following adjusted model:

$$|\sigma|^{\alpha} = \frac{1}{F}\left[(1-n)\sigma_2^{\alpha} + n\sigma_1^{\alpha}\right] \quad (9),$$

where F (6.62) is the electrical formation factor.

3.4. Results

The results of this experiment are summarized in Figures 3.3 to 3.5. Figure 3.3 shows a clear decrease in measured conductivity magnitude ($|\sigma|$) for the three experimental treatments (EtOH-water mixture, EtOH-salt solution mixture, and EtOH-salt solution mixture in sand matrix) with increasing EtOH concentration. The decrease in $|\sigma|$ shows a similar trend for all three experimental treatments. At very high EtOH concentration (≥ 0.70 v/v), the drop in $|\sigma|$ of the mixtures becomes much steeper.

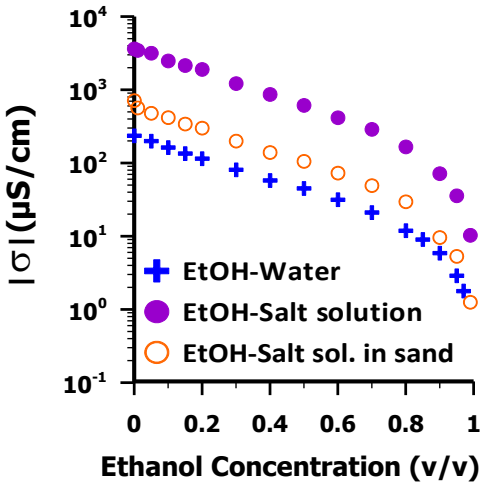

Figure 3.3: Variation in measured conductivity magnitude |σ|.

Variation in measured conductivity magnitude |σ| for all three experimental treatments: ethanol-water mixture (plus sign), ethanol-salt solution mixture (dark circles) and ethanol-salt solution mixture in sand matrix (open circles) at increased ethanol concentration.

The comparison between the experimental and modeled |σ| data for EtOH-water mixtures (0-0.97 v/v EtOH) and EtOH-salt solution mixtures (0-0.99 v/v EtOH) with and without sand matrix is shown in Figure 4. The fitting parameter (α), determined from the least-squares regression approach, is respectively, 0.28 ± 0.01, 0.33± 0.01 and 0.37± 0.01for EtOH -water mixtures, EtOH-salt solution mixtures and EtOH-salt solution mixtures in the sand matrix. The model fits the experimental data at concentration ≤ 0.4 v/v EtOH, but it cannot fit the data recorded at ≥ 0.4 v/v EtOH. In all three cases, measured |σ| is greater than that predicted by the model at concentration ≥ 0.4 v/v EtOH.

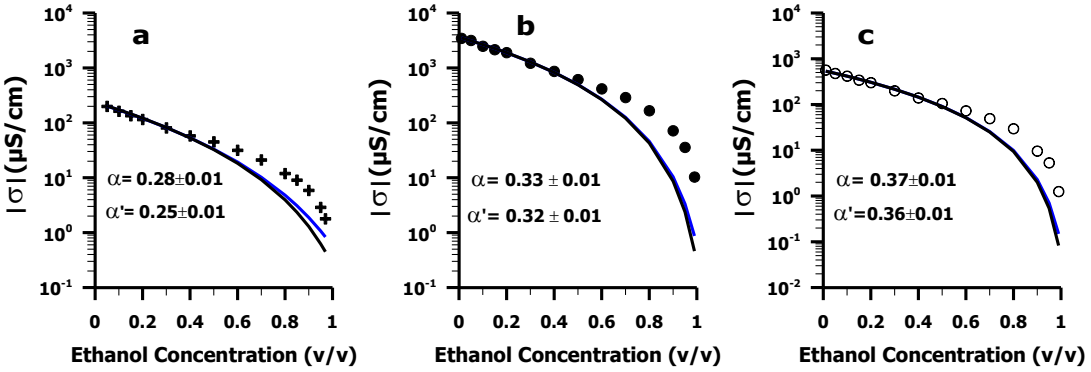

Figure 3.4: Comparison of measured and modeled conductivity magnitude (|σ|).

Comparison of measured conductivity magnitude (|σ|) between the Lichtenecker-Rother modeled data (black line for our estimated pure ethanol electrical conductivity of 0.252 μS/cm and blue line for the value of 0.554 μS/cm reported by Prego et al., 2000) and a) ethanol-water mixture experimental data (plus sign), b) ethanol-salt solution mixture experimental data (dark circles), and c) ethanol-salt solution mixture in sand matrix experimental data (open circles). The fitting parameters (α and α' for ethanol conductivity of 0.252 and 0.554 μS/cm, respectively), determined from the least-squares regression approach, are shown.

Figure 3.5 shows the variation in the measured phase response for selected concentrations of EtOH mixed with either water or salt solution (with or without a sand matrix). In all cases, the phase responses are negligible (~ 0.1 mrad) for all the mixtures at the low frequency range (≤ 100 Hz). The increase in phase response at ≥ 100 Hz likely in part results from instrumentation effects such as capacitive coupling associated with the wiring to potential electrodes. However, it may also reflect the existence of other polarization mechanisms becoming important at higher frequencies.

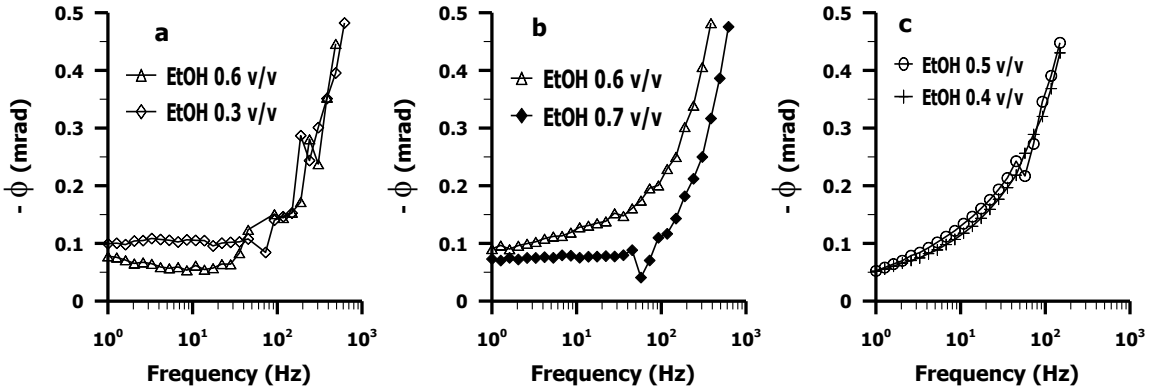

Figure 3.5: Variation in phase (ϕ) for selected ethanol concentration

Figure showing variation in phase (ϕ) for selected ethanol concentration, a) ethanol-water mixture, b) ethanol-salt solution mixture and c) ethanol-salt solution mixture in sand matrix

3.5. Discussion

3.5.1. Electrical properties of ethanol-liquid mixtures

The decrease in $|\sigma|$ shows a similar trend for all three media (EtOH-water mixture, EtOH-salt solution mixture with and without sand matrix) as EtOH concentration increases (Figure 3.3). The initial conductivity values of the mixture components were 236.34 µS/cm for water, 3633.60 µS/cm for the salt solution and 0.252 µS/cm (estimated) for pure EtOH. Our estimated conductivity of EtOH is comparable with that of 0.554 µS/cm obtained in a previous study using a conductivity meter designed for very low conductivity measurement [*Prego et al.*, 2000]. Since pure EtOH is highly resistive, its addition to the mixtures reduces the mixture $|\sigma|$. However, an equal increment of EtOH does not result in a linear or an exponential decrease in $|\sigma|$, thus suggesting varied and complex intermolecular interactions between the components of the mixtures as the ratio of EtOH to water or salt solution changed. Previous studies have shown that EtOH and

water chemically interact (hydrogen bonding) to form a complex mixture [*Franks and Ives*, 1966; *Parke and Birch*, 1999, *Atamas and Atamas*, 2009].

That ethanol molecules have both a hydrophilic hydroxyl group favorable to hydrogen-bonding with water molecules and an alkyl chain conferring hydrophobic effects may shed light on the complexity and types of interactions involved in EtOH-water mixtures and their influence on the electrical conductivity observed here. Unlike dissolution, a kinetic process that is quantified by its rate, solvation (interaction of a solute with a solvent leading to a solution whereby the solute species is stabilized, [*IUPAC*, 2006]) could better explain the types of interaction and association occurring in EtOH-water mixtures. During this solvation process, different types of attractive forces are involved among water and EtOH molecules. The mobility of water molecules may have been affected as they are attracted and form multi-hydration layers around EtOH molecules. The formation of immobilized water layers was documented previously for ion-solvent interaction in aqueous solutions [*Frank and Wen*, 1957] and inferred elsewhere for EtOH-water interaction [*Parke and Birch*, 1999]. As a result, the ionic mobility of the solution could be affected. *Bhat and Shetty* [2011], observing a rapid decrease in limiting molar conductance of water containing sulfacetamide sodium following the addition of EtOH, suggested a reduction in solvated ionic mobility as a result of the formation of intermolecular hydrogen bonding. Therefore, a relation is inferred between the measured $|\sigma|$ values and the solvation driven changes in the ionic mobility of EtOH-water and EtOH-salt solution. The steeper decrease in $|\sigma|$ at very high EtOH concentration $\geq$ 0.7v/v probably reflects limited availability of ions in the small volume proportion of water or

salt solution in the mixtures. Measurements performed directly on the EtOH-water and EtOH-salt solution mixtures using the conductivity meter (data not shown) were comparable to those with the electrical method, confirming the accuracy and precision of the electrical measurements.

3.5.2. Modeling of ethanol-liquid mixtures

The applied Lichtenecker-Rother (L-R) model yields similar results for both our estimated $|\sigma|$ value for ethanol (0.252 µS/cm) and the value of 0.554 µS/cm of pure EtOH reported elsewhere (Prego et al, 2000). The model fits the $|\sigma|$ data for EtOH concentration $\leq$ 0.4 v/v while deviations from the model are observed at higher EtOH concentration in the mixture (Figure 3.4). These findings likely result from the complexity and different types of interactions of EtOH and water molecules. *Atamas and Atamas* [2009] described three types of interactions occurring in water-ethanol mixtures: water-water interaction, EtOH-water interaction and EtOH-EtOH interaction (Figure 3.6).

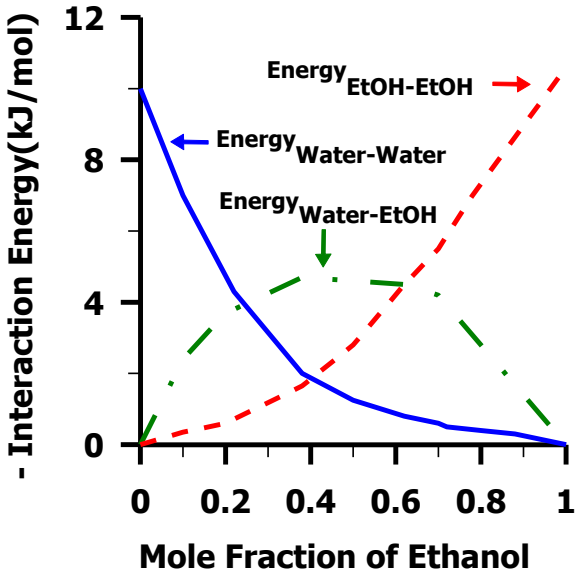

Figure 3.6: Types and complexity of water–ethanol mixtures interactions.
Adapted from Atamas and Atamas (2009).

As EtOH concentration increases, it can be seen (Figure 3.6) that the water-water energy interaction decreases while the EtOH-EtOH interaction increases. However, the water-EtOH energy interaction shows a multiphase profile curve with: a) a rapid increase up to ~ 0.4 v/v EtOH, b) a relative plateau from ~ 0.4 to 0.7 v/v EtOH and, c) a rapid decrease after ~ 0.7 v/vEtOH. The fit of the L-R model with the experimental data at EtOH concentration ≤ 0.4 v/v is consistent with a strong water-EtOH interaction mainly through intercomponent hydrogen bonding formation. Although several forces can act simultaneously during the solvation process occurring in water-EtOH media, hydrogen bonding remains predominant in defining their association [*Atamas and Atamas*, 2009]. As EtOH is introduced into water, a structural rearrangement of water molecules occurs such that EtOH and water are strongly attracted. As depicted in the modeled and the experimental curves (Figure 3.4), the log of $|\sigma|$ is linearly related to EtOH concentration at ≤ 0.4 v/v. This trend can be explained by the fact that the water-EtOH interaction is optimized and more influential than the water-water and EtOH-EtOH interactions. In that range, the modeled and experimental data fit because the applied L-R model assumes a symmetric interaction between the two components of the mixture. Note that EtOH is toxic to soil and aquifer microorganisms at concentration ≥ 0.06 v/v [*Nelson et al.*, 2010], but its biodegradation can occur at lower concentration if sufficient nutrients, along with O_2 or other terminal electron acceptors are available. The biodegradation of EtOH may result in various byproducts including dissolved acetic and carbon acid that can lead to changes in fluid conductivity and, subsequently, in bulk conductivity. However, we did not observe visible contamination indicative of microbial activity and/or EtOH biodegradation.

Our results are therefore consistent with the rapid increase of water-EtOH energy interaction illustrated in Figure 3.6. Furthermore, they are in agreement with previous studies showing a minimum in the apparent specific volumes of EtOH in water at low EtOH concentrations (~ 25 % w/w) [*Franks and Ives*, 1966; *Parke and Birch*, 1999], thus indicating a better packing efficiency between EtOH and water molecules due to strong intermolecular interactions. Our findings are also supported by previous observations on solution properties of EtOH in water such as the maximum in the sound velocity, the formation of a more compact hydration layer (minimum value of the isentropic compressibility coefficient) as a result of strong intercomponent hydrogen bonding formation, and the increased number of water molecules displaced by EtOH molecules (compressibility hydration numbers) at low EtOH concentrations [*Parke and Birch*, 1999]. All of these parameters indicate the extent of high and predominant water-EtOH or EtOH-salt solution interactions in the mixtures.

The existence of hydrophobic effects, which start to occur at ~ 0.4 - 0.5 v/v EtOH as suggested in Figure 3.6, could explain the observed deviation between the modeled and experimental $|\sigma|$ data at high EtOH concentrations. These effects may take place in water-EtOH mixtures as a result of the formation of linear chains or rings of self-associated EtOH molecules [*Mizuno et al.*, 1995; *Franks and Ives*, 1966], which removes their hydrophobic parts from contact with water [*Wiggins*, 1997]. *Atamas and Atamas* [2009] pointed out that the water-EtOH mixture forms an ideal solution at ~ 0.4 v/v EtOH and follows Raoult's law, thus indicating an equilibrium state in the solution. At ethanol concentration $\geq$ 0.4 v/v, the solution structure has changed. The aforementioned

predominant intercomponent hydrogen bonding at concentration ≤ 0.4 v/v EtOH is presumably weakened as EtOH-EtOH interaction increases over the point of equilibrium (Figure 3.6). *Weaver et al.* [2009] showed a gradual increase in hydrophobicity in EtOH-water-hydrocarbon system at ~ 0.4 ≤ EtOH ≤ 0.7 v/v, followed by a complete phase separation into a predominantly aqueous-alcohol phase and a predominantly oil phase at ~ EtOH > 0.7 v/v. As pure ethanol (ethyl alcohol 200 proof, absolute ACS/USP grade, 99.98 % assay v/v) (i.e. hydrocarbon content < 0.02 % v/v) was used in our experiment, a phase separation with an oil phase is not plausible. Instead, in our binary EtOH-water system, it is most likely that the influence of hydrophobic effects becomes particularly important at very high EtOH concentration (> 0.70 v/v) such that water or salt solution clusters (partial phase separation into EtOH and water or salts) could potentially occur. Similar observations of water cluster formation and enhancement of water-water interaction energy in the bulk of water-pyridine system were reported previously [*Sinoti et al.*, 1996]. Both the weakening of water-EtOH interaction and the formation of water and salt solution clusters could facilitate ionic mobility in the solution. Therefore, they could be responsible for observed higher experimental $|\sigma|$ values in comparison with the modeled data. As the applied L-R model is based on the assumptions of symmetric interactions between the components of the mixtures, it cannot reflect such asymmetric changes occurring in the media at high EtOH concentrations. Our observations herein are consistent with previous studies that reported an increase of water-water aggregation [*Atamas and Atamas*, 2009] and a decrease of water-EtOH molecules interacting by hydrogen bonding [*Parke and Birch*, 1999; *Atamas and Atamas*, 2009] at very high EtOH concentration in water-EtOH media.

Subsurface EtOH contamination can potentially vary from very low to high concentration. Previous studies have shown that EtOH transport in porous media resulted in high EtOH concentration, with ethanol trapped in the unsaturated zone and slowly diffusing into the shallow groundwater [*Cápiro et al.*, 2007; *Stafford and Rizey*, 2011; *Freitas and Barker*, 2011a; *Freitas and Barker*, 2011b]. In such situations, EtOH concentration may potentially exceed 0.4 v/v in the unsaturated zone, the concentration beyond which the applied L-R model becomes invalid based on our results. However, owing to high EtOH-water miscibility, it is likely that EtOH dilution occurs as it partitions into a sufficient volume of pore water in the unsaturated zone and the capillary fringe. Furthermore, fluctuations in the water table may potentially increase the mixing of EtOH with the saturated and unsaturated zone pore water, such that EtOH may be significantly diluted near the source zone.

3.5.3. Interfacial polarization of ethanol-liquid mixtures

The electrical $|\sigma|$ measurements show no evidence of interfacial polarization effects at the EtOH-liquid interfaces (Figure 3.5). As an electric current is applied to the EtOH-liquid mixture, the presence of an interface between EtOH and water could conceivably result in an electrical double layer (EDL). The migration and redistribution of ions in the EDL could result in an electrochemical polarization effect as charges tend to built up at the interface. However, if such an EDL does form, the signal associated with its polarization is clearly too weak to be detected with conventional electrical methods as our measurements of phase responses are negligible ($\leq$ 0.1 mrad) in all EtOH-liquid mixtures at the low frequency measurements ($\leq$ 100 Hz) (Figure 3.5). At frequencies $\geq$ 100Hz, the Maxwell-Wagner polarization (MW) could potentially occur at the interface [e.g. *Leroy*

et al., 2008]. However, we mainly attribute the small phase response observed (0.2 - 0.5 mrad) in the frequency range $\geq$ 100Hz as being instrumentation effects associated with the wiring to potential electrodes.

3.5.4. Influence of sand matrix on the polarization effects

We also observed no evidence of substantial interfacial polarization effects at the EtOH/liquid/mineral interface. Similar to the discussion above, the double layer polarization and the MW polarization could potentially exist at the ethanol/liquid/mineral interface. However, the phase responses remain very small (0.2-0.5 mrad) over the measured frequency range. Therefore, our results show no clear evidence of changes in the polarization effects due to the presence of the sand matrix. Furthermore, the measurements in the sand matrix confirmed that the $|\sigma|$ results could simply be scaled by the formation factor (F) as indicated by the comparable fitting parameter ($\alpha = 0.33 \pm 0.01$ and $\alpha = 0.37 \pm 0.01$, respectively) obtained from the conductivity model for measurements performed with and without sand matrix (Figure 3.4). We recognize that this experiment was conducted in a simple sand matrix while more complex environmental conditions may prevail in the field. As different environmental settings may influence substantially the polarization effects, further investigations need to be conducted to establish the potential effects of EtOH in more complex matrices (e.g. in the presence of clays).

3.6. Conclusions

Our experiment has demonstrated the sensitivity of electrical conductivity measurements to the interactions occurring in EtOH-liquid mixtures as EtOH concentration is varied. The measured $|\sigma|$ values were related to the changes in solution properties, which may reflect solvation driven changes in ionic mobility. We also demonstrated that a simple mixing model can be combined with electrical data to reasonably estimate EtOH concentration at ≤ 0.4 v/v EtOH in the mixture. The model could not fit the experimental data at ≥ 0.4 v/v EtOH presumably due to subtle asymmetric changes in water-EtOH mixtures associated with important hydrophobic effects of EtOH molecules. Our results highlight the potential for using non-invasive and cost-efficient geophysical techniques to detect and monitor EtOH concentrations in the subsurface. Such tools may ultimately serve to assess EtOH-contaminated sites and aid in the decision-making process regarding appropriate remediation strategies.

CHAPTER 4: COMPLEX RESISTIVITY SIGNATURES OF ETHANOL IN SAND-CLAY MIXTURES[2]

Abstract

We performed complex resistivity (CR) measurements on laboratory columns to investigate changes in electrical properties as a result of varying ethanol (EtOH) concentration (0% to 30% v/v) in a sand-clay (bentonite) matrix. We applied a Debye Decomposition, a phenomenological model commonly used to fit CR data, to determine model parameters (time constant: τ, chargeability: m, normalized chargeability: m_n). The CR data showed a significant ($P \leq 0.001$) time-dependent variation in the clay driven polarization response (~ 12 mrad) for 0% EtOH concentration. This temporal variation probably results from the clay-water reaction kinetics trending towards equilibrium in the sand-clay-water system. The clay polarization is significantly suppressed ($P \leq 0.001$) for both measured phase (ϕ) and imaginary conductivity (σ'') with increasing EtOH concentration. Normalized chargeability consistently decreases (by up to a factor of ~2) as EtOH concentration increases from 0% to 10% and 10 to 20%, respectively. We propose that such suppression effects are associated with alterations in the electrical double layer (EDL) at the clay-fluid interface due to (a) strong EtOH adsorption on clay, and (b) complex intermolecular EtOH-water interactions and subsequent changes in ionic

---

[2] This chapter is published as: Personna, Y. R., L. Slater, D. Ntarlagiannis, D. Werkema, and Z. Szabo (2013), Complex resistivity of ethanol in sand-clay mixtures, *Journal of contaminant hydrology*, 149, 76-87.

mobility on the surface in the EDL. Changes in the CR data following a change of the saturating fluid from EtOH 20% to plain water indicate strong hysteresis effects in the electrical response, which we attribute to persistent EtOH adsorption on clay. Our results demonstrate high sensitivity of CR measurements to clay-EtOH interactions in porous media, indicating the potential application of this technique for characterization and monitoring of ethanol contamination in sediments containing clays.

4.1. Introduction

The development of non-invasive geophysical techniques for characterizing organic contaminants in the subsurface is desirable as most organic contaminants cause environmental and health problems. Low-frequency complex resistivity (CR) measurements could potentially be applied for monitoring the spatiotemporal distribution of subsurface contaminant plumes, thus for assessing the effectiveness of remediation design efforts aimed at reducing organic contaminant concentrations in clayey soils. Organic contaminants may affect the petrophysical properties as result of induced changes in pore fluid chemistry and mineral surface properties via mineral-fluid interactions, leading to a distinctive geophysical response. The potential application of low-frequency (<1000Hz) electrical geophysics for mapping clay-organic interactions was first investigated in the mid 1980s [*Olhoeft*, 1985; *Olhoeft*, 1986; *Sadowski*, 1988]. *Olhoeft* [1985] performed a series of CR measurements that showed a significant difference in phase (ϕ) response between uncontaminated and organic-contaminated clayey (either montmorillonite or smectite) soils. This work stimulated further research on clay-organic interactions and associated changes in the CR response. Significant ϕ

responses as high as ~ 100 mrad were recorded from CR measurements on clay-toluene mixtures [*Sadowski*, 1988; *Olhoeft and King*, 1991]. These authors concluded that toluene oxidizing polymerization reactions in the presence of clays led to distinctive electrochemical signatures detectable by CR measurements.

Such work stimulated experimentation regarding the sensitivity of CR for detecting chlorinated solvents, particularly dense non aqueous phase liquid (DNAPL) pollution [*Olhoeft*, 1985; *Sadowski*, 1988; *Olhoeft and King*, 1991]. However, efforts by others to confirm that clay-organic interactions impact CR measurements and to test the capabilities of complex resistivity technique for mapping DNAPL have been inconsistent [*Börner et al.*, 1993; *Vanhala*, 1997; *Roberts and Wildenschild*, 2004; *Brown et al.*, 2004; *Ustra et al.*, 2012]. For example, *Brown et al.* [2004] attempted unsuccessfully to reproduce the reported high ϕ response associated with clay-toluene interactions despite conducting a series of laboratory experiments that closely mimicked those of *Olhoeft* [1985]; instead finding a barely distinguishable ϕ response for clay containing samples contaminated with toluene. These inconsistent previous findings encourage further research to determine whether or not the interactions of organic contaminants with clay minerals result in useful geoelectrical responses. In this paper, we focus on the potential application of CR as a tool for monitoring clay-ethanol interactions.

Ethanol is an emerging contaminant [*Gomez and Alvarez*, 2010] that poses potential risks to groundwater resources [*Powers et al.*, 2001a] when accidental releases of large

volumes occur during transportation [*Spalding et al.*, 2011] or from storage facilities [*McDowell et al.*, 2003]. Ethanol contamination in the subsurface has recently become more likely as its production and use as a biofuel blend (EtOH blended with conventional gasoline) has increased exponentially [*ITRC*, 2011] as a result of regulatory stimuli in the USA to reduce air pollution and provide an alternative to petroleum. Potential adverse impacts of EtOH on groundwater include, (1) increases in aqueous phase BTEX (benzene, toluene, ethyl-benzene and xylene) compounds contained in gasoline [*Powers et al.*, 2001b] due to cosolvency effects [*Powers et al.*, 2001b; *Da Silva et al.*, 2002; *Corseuil et al.*, 2004; *Stafford et al.*, 2009], (2) slower natural degradation of BTEX compounds [*Corseuil et al.*, 1998; *Powers et al.*, 2001b; *Ruiz-Aguilar et al.*, 2003; *Mackay et al.*, 2006; *Gomez and Alvarez*, 2009 & 2010; *Freitas et al.*, 2011] attributed to the preferential biodegradation of EtOH and associated rapid depletion of dissolved oxygen and other electron acceptors, and (3) methane production associated with anaerobic degradation of EtOH reaching the explosive limit level [*Nelson et al.*, 2010; *Freitas et al.*, 2010, *Spalding et al.*, 2011]. EtOH may also quickly become toxic to soil and aquifer microorganisms (Nelson et al., 2010), affecting their growth [*Ingram*, 1989; *Nelson et al.*, 2010] and community structure [*Cápiro et al.*, 2008; *Ma et al.*, 2011].

In this paper, we report on CR signatures associated with clay-ethanol interactions. Our main objectives were to determine (a) the electrical properties of EtOH in a sand-clay medium, (b) if clay-organic reactions associated with EtOH enhance or suppress the CR response, and (c) whether CR signatures associated with clay-EtOH interactions are

reversible when the EtOH is removed, thereby providing information on the persistence of clay-organic reactions.

4.2. Potential interactions in a clay-ethanol-water system

Clay mineral surfaces generally carry a net negative charge due to isomorphous substitutions of some electropositive elements of similar size but lower valence [*Van Olphen*, 1977]. This negative charge is generally compensated for by sorption of exchangeable cations in the interlayer and onto the external clay surfaces such that clay minerals, in their natural form, are hydrophilic [*Yariv and Cross*, 2002]. In the type 2:1 clay minerals (i.e. those having 2 tetrahedral sheets on each side of an octahedral sheet (T-O-T)), water molecules can be readily adsorbed onto the existing exchangeable cations as part of the associated electrical double layer (EDL).The EDL is the most common model used to describe charge distribution at the mineral/water interface associated with chemical reactions between the surface sites and ions in water. The EDL includes (a) a Stern layer i.e. the layer between the mineral surface and the inner surface of the diffuse layer resulting from sorbed ions (counterions) directly to mineral surface, and (b) a diffuse layer i.e. a layer that extends beyond the Stern layer and includes an excess of counterions and a depletion of co-ions moving mostly freely. Two types of water may be distinguished from the water-cation interactions: type 1 whereby an inner or primary hydration shell is directly coordinated to the cation, and type 2 whereby an outer or secondary hydration shell is indirectly coordinated to the cation [*Theng*, 1974; *Sposito et al.*, 1999]. The outer hydration shell is less stable than the inner shell and, hence, more likely to be displaced by other competing compounds for the cation sites.

Various interactions are possible between organic molecules and the type 2:1 clay minerals including hydrogen bonding, cation-dipole interaction, coordination bonds, acid-base reactions, charge transfer and van der Waals forces [see *Kowalska et al.*, 1994; *Yariv and Cross*, 2002; *Lagaly et al.*, 2006 for review]. Like water molecules, the adsorption of EtOH molecules can occur on the existing cation sites in clay. As water and EtOH are both polar compounds, they will essentially compete for the same cation sites in the clay structure [*Dowdy and Mortland*, 1967; *Theng*, 1974). *German and Harding* [1969] demonstrated adsorption of large amounts of EtOH, n-propanol and n-butanol on Ca^{2+} and Na^{+} of montmorillonite. Among these primary n-alcohols, EtOH has been shown to be capable of displacing water even in the inner hydration shell around cations such as Ca^{2+} , Cu^{2+} and Al^{3+} in clay [*Dowdy and Mortland*, 1967] though the ratio of EtOH to water does play a role in these reactions [*Brindley and Hoffman*, 1962]. The adsorption of EtOH by displacement of water is a favorable reaction that results in a gain of entropy by the system [*Theng*, 1974].

Competition for adsorption on available cation sites in the clay structure aside, water and EtOH molecules in solution show complex intermolecular interactions [*Franks and Ives*, 1966; *Parke and Birch*, 1999; *Atamas and Atamas*, 2009]. These molecules are subject to different attractive forces such that multi-hydration layers may be formed around the EtOH molecules. This type of solvent-solute interaction also known as solvation [*IUPAC*, 2006] may impede the ionic mobility of the solution, thus affecting its conductivity. The reduction in solvated ionic mobility in water-sulfacetamine sodium mixtures has been

associated with a rapid decrease in molar conductance [*Bhat and Shetty*, 2011]. *Personna et al.* [2013a] interpreted a significant non-linear decrease in conductivity magnitude measured for mixtures with varying amounts of EtOH (very resistive) and mineralized water (very conductive) to result from complex intermolecular interactions in the mixtures.

4.3. Complex resistivity

The CR method measures the frequency dependent polarization (≤ 1000 Hz) associated with the reversible capacitive characteristics of soils to electrical charges as a current is applied and terminated [*Summer*, 1976]. Originally primarily developed for detecting disseminated metallic ores [*Marshall and Madden*, 1959; *Sumner*, 1976], the CR method has since been applied in a wide variety of environmental investigations [*Slater and Lesmes*, 2002] including characterization of metal containing soils [*Williams et al.*, 2005; *Slater et al.*, 2005; *Wu et al.*, 2005; *Slater and Binley*, 2006; *Wu et al.*, 2006; *Mansoor and Slater*, 2007, *Personna et al.*, 2008] and organic contamination [*Olhoeft*, 1985; *Olhoeft*, 1986; *Sadowski*, 1988, *Olhoeft and King*, 1991; *Börner et al.*, 1993; *Jones*, 1997; *Vanhala*, 1997; *Roberts and Wildenschild*, 2004; *Brown et al.*, 2004; *Ustra et al.*, 2012].

Complex resistivity measurements are commonly performed with a four-electrode configuration consisting of two current injection electrodes and two potential recording electrodes. In the frequency domain mode, a CR instrument (e.g. a dynamic signal analyzer) records both the magnitude impedance and ϕ shift of the potential voltage waveform across the sample relative to the current waveform across a reference resistor.

Knowing the sample geometric factor, this complex impedance can be described by the vector sum of both in-phase energy loss (real) and out of phase energy storage /polarization (quadrature or imaginary) components and expressed in terms of conductivity magnitude ($|\sigma|$) and ϕ as follows,

$$|\sigma| = \sqrt{(\sigma')^2+(\sigma'')^2} \quad (1),$$

$$\phi = tan^{-1}\left(\sigma''/_{\sigma'}\right) \quad (2),$$

where single prime superscript represents the real part and double superscript represents the imaginary part of the complex conductivity ($\sigma*$) [*Lesmes and Frye*, 2001]. The real and imaginary parts are therefore given as a function of measured $|\sigma|$ and ϕ by:

$$\sigma' = |\sigma| cos\ \phi \quad (3),$$

$$\sigma'' = |\sigma| sin\ \phi \quad (4).$$

In a non-metallic porous medium, electrical conduction can occur as a result of (a) electrolytic conduction controlled by the conductivity of the pore-filling electrolyte, and the size and interconnectedness of the pores, and (b) surface conduction occurring in the electrical double layer at the grain fluid interface and depending upon the grain-surface morphology and the pore fluid chemistry. The electrolytic and surface conductivity are often simply assumed to add in parallel [*Waxman and Smits*, 1968]. With this assumption, σ' and σ'' can be expressed as a function of the fluid conductivity (σ_w) and the surface conductivity ($\sigma*_{surf}$) by:

$$\sigma' = \frac{1}{F}\sigma_w + \sigma'_{surf} \quad (5),$$

$$\sigma'' = \sigma''_{surf} \qquad (6),$$

where F is the formation factor, defined as the ratio of the conductivity of the saturating water to the conductivity of the water-saturated porous medium [*Archie*, 1942].

However, the mechanisms responsible for generating a CR signature in soils are not yet fully understood. Surface conductivity is complex as it results from electrochemical processes that depend on the physical and chemical characteristics of soils. Two main electrochemical mechanisms associated with charge transport in the EDL at the fluid-mineral interface have been widely used to interpret polarization processes in non-metallic and bacteria-free porous media: grain polarization and electrolytic or membrane polarization. At low frequencies of the applied electrical current (≤ 100 Hz), grain polarization is mainly attributed to polarization of the Stern layer in the EDL. Stern layer polarization results from (a) accumulation of electrical charge due to attraction of counterions to the mineral surface (approximately the edge of the inner layer of the EDL) , and (b) tangential movement of charge along the grain surface as the dipole moment associated with the charge transfers points in the opposite direction of the applied electrical field [*Leroy et al.*, 2008; *Revil and Florsch*, 2010; *Schmutz et al.*, 2010; *Revil and Skold*, 2011; *Vaudelet et al.*, 2011a; *Vaudelet et al.*, 2011b; *Revil et al.*, 2012a). Membrane polarization [*Vinegar and Waxman*, 1984; *Reynolds*, 1997] is traditionally attributed to a blockage and selective flow of ions within the pore channels due primarily to pore constrictions and local ion congestion to clays lining pores due to an applied current. At higher frequencies of the applied electrical current (≥ 100 Hz), Maxwell

Wagner (MW) polarization, associated with the accumulation of electrical charges in the pore space among the different phases of a composite medium, becomes important [*Leroy et al.*, 2008, *Leroy and Revil*, 2009].

A physicochemical model for interpretation of the CR response of complex systems such as soils containing clay-EtOH-water mixtures does not yet exist. Empirical models, such as Cole-Cole relaxation models or their variants [*Cole and Cole* 1941; *Davidson and Cole*, 1951], can instead be used to describe the CR dependence on applied electrical frequency. While the Cole-Cole type models are useful, each variant may result in different estimated values of the model parameters even for the same CR data [*Nordsiek and Weller*, 2008]. *Nordsiek and Weller* [2008] proposed a Debye Decomposition (DD) approach as an alternative to fit CR spectra data. Unlike the Cole-Cole type models, DD can fit a wide range of spectral shapes to data over a limited frequency range. The DD approach considers the spectra of conductivity amplitude and phase to result from a superposition of a finite number of different Debye relaxations. A variation of the *Nordsiek and Weller* [2008] DD approach was recently proposed as follows,

$$\sigma^*(\omega) = \frac{1}{\sigma_0}\left[1 - \sum_{k=1}^{n} m_k \left(1 - \frac{1}{1 + i\omega\tau_k}\right)\right] \qquad (7),$$

where n is the number of individual Debye responses, m_k and t_k are, respectively, a specific chargeability and relaxation time [*Zisser et al.*, 2010]. This approach utilizes a decomposition of the CR spectra into a number of individual discrete Debye responses with specific chargeability (m_k) and relaxation time (τ_k). As described in *Zisser et al.*

[2010] and *Nordsiek and Weller* [2008], this continuous function can be discretized into a system of linear equations by normalizing the complex conductivity with respect to the DC conductivity (σ_0), separating the normalized complex conductivity into its real and imaginary parts, weighting the obtained real and imaginary parts, and weighting by the frequency. The application of DD is thus useful to fit measured CR data to obtain quantifiable CR parameters.

4.4. Methodology

4.4.1. Sample preparation and experimental treatments

Samples consisted of small cylindrical transparent PVC columns (length =0.029 m, and inner diameter 0.025 m) that were dry-packed with either Ottawa Sand (SiO_2 > 99%, specific gravity= 2.65, and d_{50}= $0.5x10^{-3}$ m) from Fisher Scientific or a mixture of sand and clay (bentonite, lot AO16747601) from Acros Organics, New Jersey, USA. The sand (98% w/w) and clay (2% w/w) were mechanically mixed in an effort to render the mixture as homogenous as possible. A 0.45 μm cellulose membrane (Whatman) from Fisher Scientific was placed on the bottom and the top of each column to prevent clay from moving out of the column under fluid flow. The saturating fluid was either water or water-ethanol mixtures, which were made from pure ethanol (ethyl alcohol 200 proof, absolute ACS/USP grade, and 99.98 % assay v/v) from Pharmco AAPER and a well characterized water sample to represent a natural groundwater ($23.63x10^{-3}$ S/m at 26.0 ^{o}C) (major anions: Cl^-, and $S0_4^{-2}$ and minor anions: F^-, and NO_3^- ; major cations: Na^+, K^+, $Ca^{2+,}$ and Mg^{2+} and minor cations: Cu^{2+}, Mn^{2+} , Zn^{2+} , Fe^{2+} / Fe^{3+}, and Al^{3+}). These

mixtures were prepared at room temperature (26.0 ± 0.5 ^{o}C) in a volumetric flask over a magnetic stirring plate.

We defined two experimental phases, hereafter referred as Period I and Period II (Figure 4.1) based on the experimental treatments applied for CR measurements. Experimental treatments for each sample are summarized in Figure 4.1. All clay containing samples had a clay concentration of 2% (w/w). During Period I (Day 1 to Day 35/36), we applied four different experimental treatments in replicate: (a) sand (clay 0%) saturated with water-EtOH mixture (EtOH 10%, v/v) (clay blank or control sample) , (b) sand- clay mixture saturated with water (EtOH blank or control sample) (c) sand-clay mixture saturated with water-EtOH mixture (EtOH 10% , v/v), and (d) sand-clay mixture saturated with water-EtOH mixture (EtOH 20%, v/v). The first treatment determined the CR response of EtOH in sand in the absence of clay. The second treatment determined the CR response of clay in the absence of EtOH. The third and fourth treatments examined the effect of increasing EtOH concentration (and clay-organic interactions) on the clay polarization. Each experimental treatment was performed by first setting the packed columns and their corresponding saturating fluid in a clean and sterilized beaker. We then saturated the sample using a saturation chamber, which consists of a vacuum container operated by a pump. Each sample was submerged in the saturating fluid in a beaker and then placed in the vacuum container for 30 minutes to allow pore-filling by the saturating fluid.

During Period II (Day 36/37 to Day 51), we performed three additional experimental treatments by changing only the saturating fluid of some samples ran in Period I as follows (Figure 4.1) : (a) water-EtOH mixture (EtOH 20%, v/v) replaced water-EtOH (EtOH 10%, v/v) as saturating fluid in a sand-clay column, (b) water-EtOH mixture (EtOH 30%, v/v) replaced water-EtOH (EtOH 10%, v/v) as saturating fluid in a sand-clay column, and (c) plain water replaced water-EtOH mixture (EtOH 20%, v/v) as saturating fluid in a sand-clay column. The first two experimental treatments in Period II were performed to investigate the effects of further increasing EtOH concentration on the electrical responses of samples previously exposed to a lower EtOH concentration. The third experimental treatment was applied to test if the EtOH effect on the clay polarization is reversible when the saturating fluid is switched back to background water.

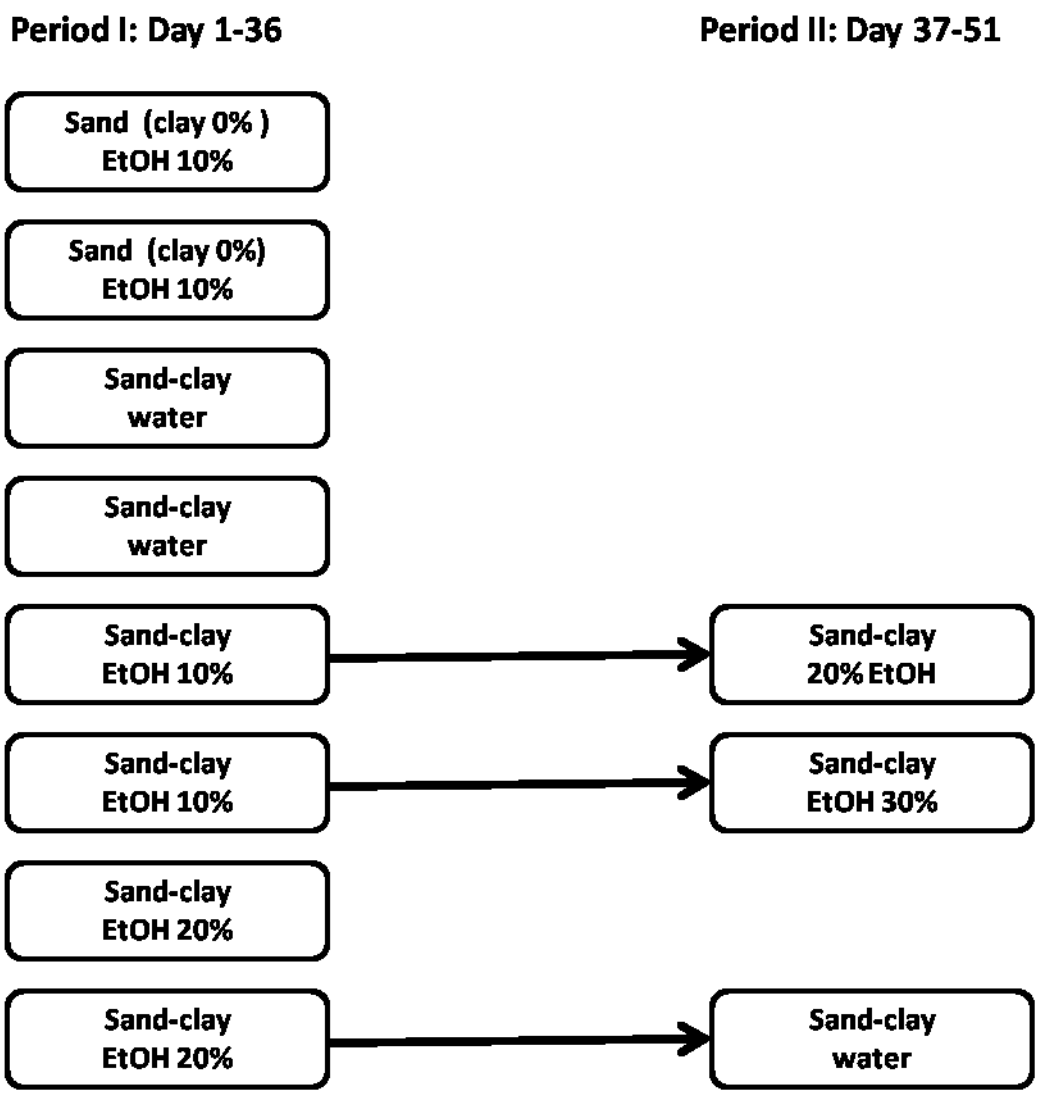

Figure 4.1: Summary of the experimental treatments

Summary of the experimental treatments applied during Period I (Day 1 to 36): four treatments in replicate in sand-clay or sand (clay 0%) saturated with water or a mixture of EtOH-water (EtOH 10% and 20% v/v, respectively), and Period II (Day 37 to 51): three additional treatments by changing only the saturating fluid (transition at Day 37) of selected samples run in Period I.

4. 4.2. Complex resistivity measurements and modeling

We performed CR measurements (0.1 to 1000 Hz) using a two-channel dynamic signal analyzer (DSA) (NI-4461) (Slater and Lesmes, 2002). The CR measurements were recorded using a four-electrode configuration: two coiled Ag-AgCl electrodes placed at the ends of the column were used to inject current into the sample and two Ag-AgCl point electrodes (0.049 m apart) were used to record the resulting potential difference (Figure 4.2). We recorded both the impedance magnitude and phase shift of the potential voltage waveform across the sample relative to the current waveform on a reference resistor. Each sample was transferred from the beaker containing the saturated fluid solution into the sample holder for CR measurements under flow through conditions after passage of at least 2-pore volumes as estimated from the sample porosity. After each measurement (~ twice a week), the samples were returned to a beaker filled with the saturating fluid until the next measurement. Figure 4.2 schematically illustrates the experimental setup including the DSA, the reference resistor, geometry and dimensions of the sample in the sample holder, the location of the inflow/outflow as well as the current and potential electrodes.

To determine the CR model parameters, we applied a Debye Decomposition (DD) approach to fit the measured CR data to a specific integral chargeability (m_k) and mean relaxation time (τ_k) (cf. Eq. 7). Analysis of variance (ANOVA), performed with Minitab 16 statistical software, was used to test the statistical significance (α=0.05) of the changes

in the CR data and DD derived model parameters as a function of time and EtOH concentration.

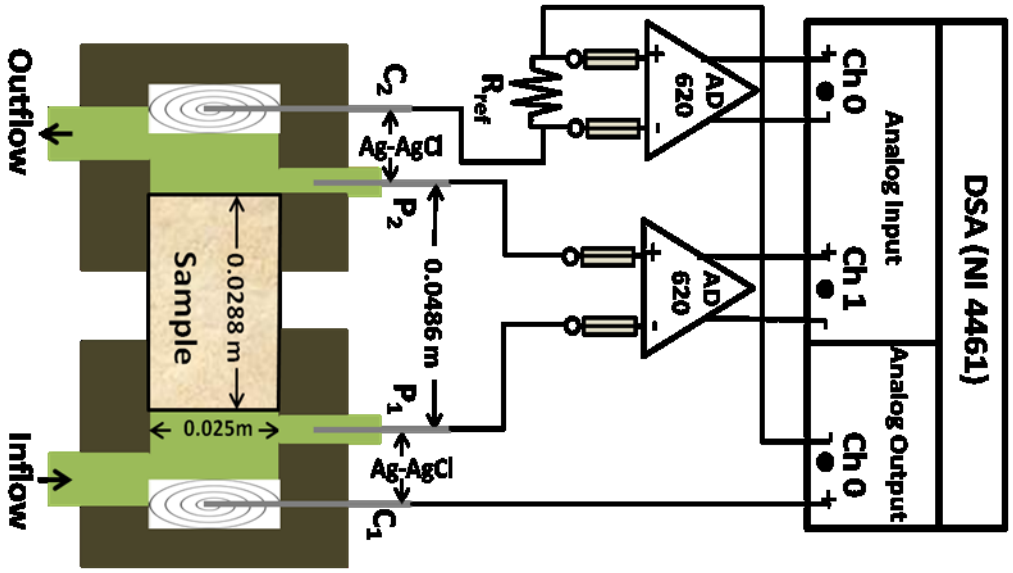

Figure 4. 2: Schematic of experimental setup

Schematic of experimental setup showing dynamic signal analyzer (NI 4461) with analog input and output, reference resistance ($R_{ref.}$), location of preamplifier (AD 620), sample location in sample holder, location of two coiled Ag-AgCl current electrodes (C_1 and C_2) and two Ag-AgCl potential electrodes (P_1 and P_2), inflow and outflow location and flow direction.

4.5. Results

Results of this experiment are presented in Figures 4.3 through 4.6 and Table 4.1. Figure 4.3 shows an unexpected time-dependent variation in the electrical response (ϕ and σ'') during Period I over the entire frequency range at selected days that is most pronounced for sand-clay samples saturated with water (EtOH 0%). Single frequency (7 Hz) measurements of ϕ (3g) and σ'' (3h) for all temporal datasets are shown for the sand-clay samples saturated with water (EtOH 0%), EtOH 10% v/v and EtOH 20% v/v. The

ϕ and σ'' show a clear time-dependent variation of the clay-driven polarization for the sand-clay sample saturated with water (Figures 4.3 a, b, g and h). The time-dependent response is less pronounced (particularly at frequency ≤ 100 Hz) for the two other experimental treatments containing EtOH. Figures 4.3g and 4.3h show that the ϕ and σ'' for the sample saturated with water increases up to Day 5 and shows minimal variation thereafter until Day 36. Minimal variation is observed from Day 1 to Day 36 for the two other experimental treatments containing EtOH. The CR spectra for most of the measurements show evidence for two mechanisms (1) EDL polarization dominant at the lower frequency (≤ 100 Hz), and (2) MW polarization dominant at the higher frequency (≥ 100 Hz) (e.g. sand-clay samples saturated with water: Figures 4.3a, 4.3b, 4.4a and 4.4b). The high frequency response might also partly result from errors caused by the circuitry used to interface the sample with the instrument. We focus our analysis on the EDL polarization of primary interest here as field CR measurements can only be performed at the lower frequency range.

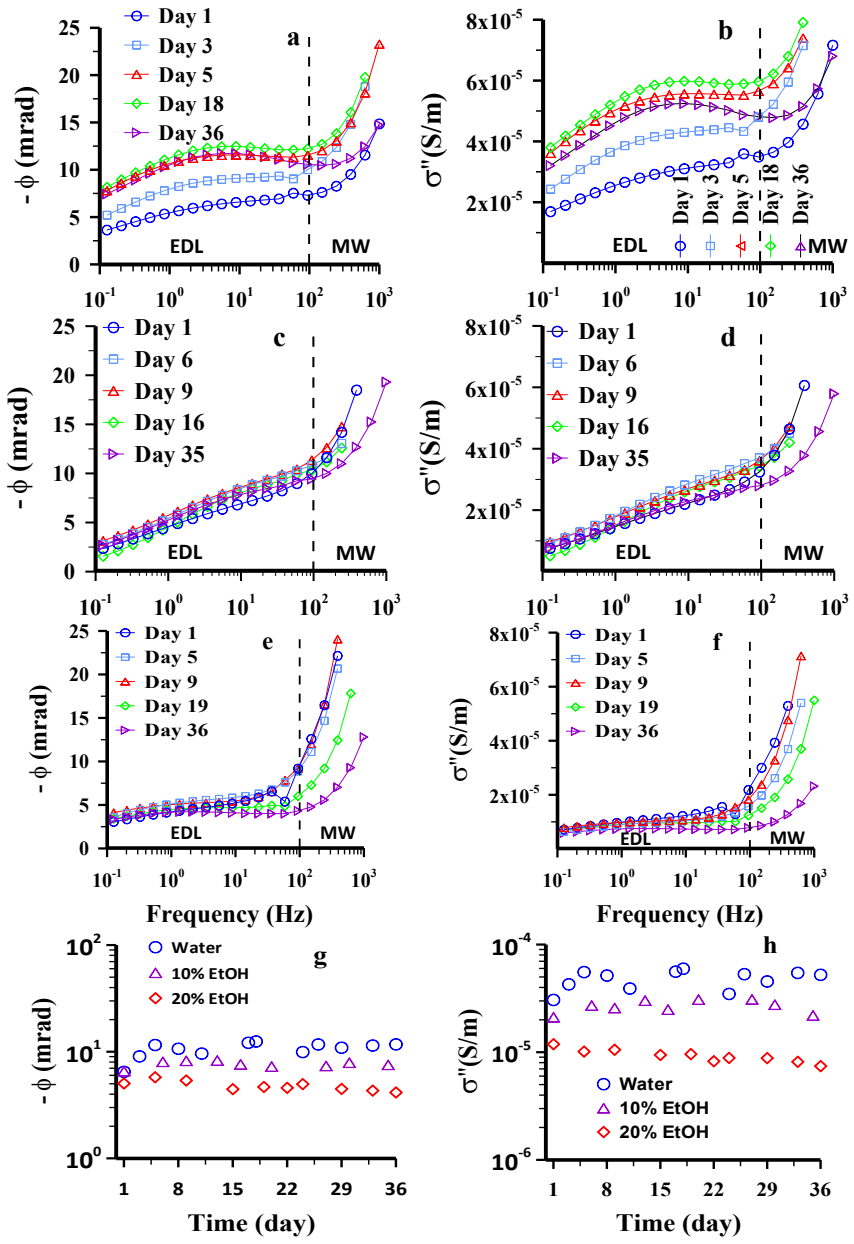

Figure 4.3: Time-dependent variation in the electrical response (ϕ and σ'')

Time-dependent variation in the electrical response (ϕ and σ'') during Period I over the entire frequency range at selected days for sand-clay samples saturated with: a) and b) water (EtOH 0%); c) and d) EtOH-water mixtures (EtOH 10% v/v); and e) and f) EtOH-water mixtures (EtOH 20% v/v). Phase (g) and σ''(h) measurements as a function of time for a single frequency (7 Hz) are shown for sand-clay samples saturated with water (EtOH 0%), EtOH 10% v/v, and EtOH 20% v/v in EtOH-water mixtures. The dash line indicates the assumed demarcation between where electrical double layer polarization dominates the spectra (EDL <100 Hz) and where Maxwell Wagner polarization (and instrumentation errors) become more important (MW> 100 Hz).

A striking observation regarding our results is that the polarization (ϕ and σ'') is largely suppressed as EtOH concentration increases from 0% to 10% and 20% v/v in the water-EtOH mixtures (Figures 4.4a and 4.4b). The observed trend in the suppression of measured ϕ and σ'' is very consistent between treatments (Figures 4.4a and 4.4b). Previous exposure of the samples to lower EtOH concentration (10% v/v) still results in consistent suppression of the polarization as EtOH concentration increases (20% and 30% v/v), particularly for the σ'' (Figures 4.4c and 4.4d). After the samples were exposed to EtOH 10% v/v, the polarization is further suppressed at EtOH 20% v/v and further still when increased to 30% v/v (Figures 4.4c and 4.4d). Note that the CR measurements for sand saturated with water (data not shown) exhibit no significant response.

Another key observation is the minimal changes in ϕ and σ'' after a transition of the saturating fluid from EtOH 20% v/v back to water (Figure 4.5). Figure 4.5 suggests that the suppression effects of EtOH on the clay-driven polarization responses are not readily reversible. The σ'' remains small and relatively unchanged (frequency ≤ 100 Hz) 14 days (12 pore-volumes) after the saturating fluid transitions back to plain water.

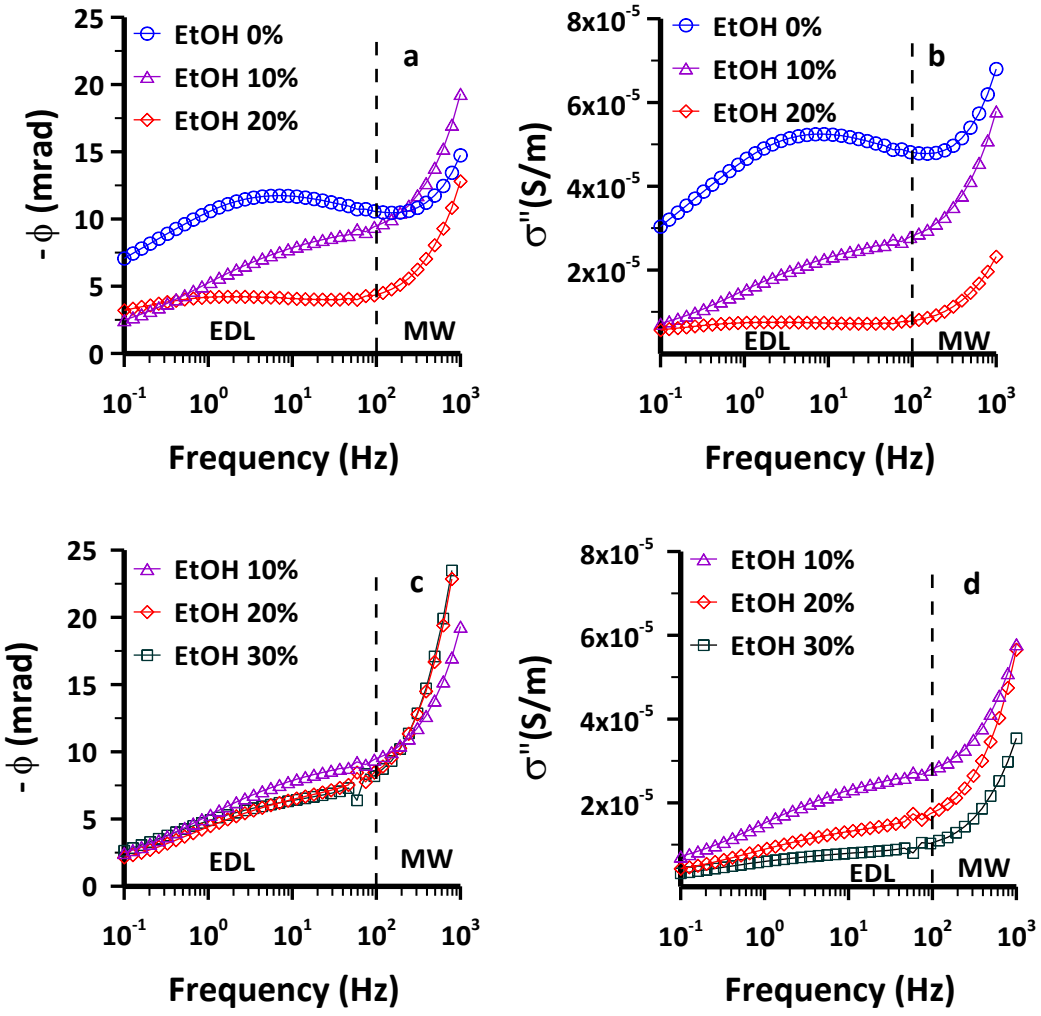

Figure 4.4: Phase (ϕ) and imaginary conductivity (σ'') responses as a function of ethanol concentration

Phase (ϕ) and imaginary conductivity (σ'') responses as a function of ethanol concentration (v/v) (water i.e. EtOH 0%, EtOH 10%, 20%, and 30%, v/v): a) and b) at Day 35/36 from Period I (Day 1-35/36), and c) and d) at Day 51 from Period II (columns initially saturated with EtOH 10% during Period I were switched at Day 36/37 to saturation fluids of EtOH 20% and 30% v/v, respectively). The dashed line indicates the assumed demarcation between where electrical double layer polarization dominates the spectra (EDL <100 Hz) and where Maxwell Wagner polarization (and instrumentation errors) become more important (MW> 100 Hz).

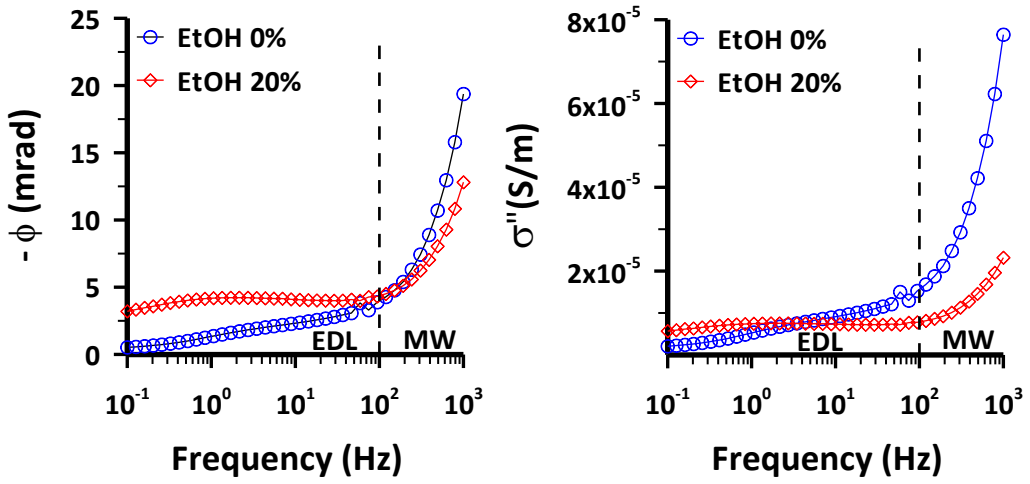

Figure 4.5: Phase (ϕ) and imaginary conductivity (σ'') responses

Phase (ϕ) and imaginary conductivity (σ'') responses of water (EtOH 0%) at Day 51 from Period II i.e. after 14 days of saturating fluid transition from EtOH 20% v/v (Period I) to water (Period II). ϕ and σ'' at Day 36 during Period I for EtOH 20% v/v are also shown for comparison with those obtained at Day 51 following the saturating fluid changes. The dashed line indicates the assumed demarcation between where electrical double layer polarization dominates the spectra (EDL <100 Hz) and where Maxwell Wagner polarization (and instrumentation errors) become more important (MW> 100 Hz).

The changes in the values of CR model parameters derived from the DD follow what is observed in the measurements. The normalized chargeability (m_n) decreases as EtOH concentration increases in the water-EtOH mixtures (Table 4.1). The fitting of the models with the observed CR data is strong (R^2= 0.99) as illustrated for three typical example datasets in Figure 4.6. The observed decrease in m_n with increasing EtOH concentration is highly consistent with what is observed in the σ'' data.

The ANOVA for a level of significance α = 0.05 shows that the changes in ϕ and σ'' occurring with time (Day 1, 18 and 36) are statistically significant (P ≤ 0.001) for the sand-clay sample saturated with water. The suppression of the clay-driven polarization

response with increasing EtOH concentration is also statistically significant ($P \leq 0.001$) for both ϕ and σ'' when comparing the three experimental treatments for the sand-clay sample (2% clay w/w) during Period I (saturating fluid of EtOH 0%, 10% and 20% v/v of water-EtOH mixtures, respectively). During Period II, the observed decrease in σ'' at EtOH 20% and 30% v/v after following previous sample exposure to EtOH 10% v/v is also statistically significant ($P \leq 0.001$).

Table 4.1: Selected Complex Resistivity Parameters

Selected CR parameters (τ: relaxation time, m: chargeability and $m_n = m/\rho_0$: normalized chargeability) at Day 35/36 from Period I (Day 1 to 35/36) and at Day 51 from Period II (Day 36/37 to 51) based on the Debye Decomposition Model. The saturating solution of the columns in Period I was changed during Period II. The CR parameters during Period I are presented with square brackets under Period II for comparison with those obtained at Day 51 following the saturating fluid changes.

Period I : Day 1 to 35/36			
	Day 35/36		
EtOH (v/v)	**τ**	**m**	**m_n**
0	0.052	0.098	4.18E-04
0.1	0.031	0.099	2.75E-04
0.2	0.296	0.069	1.19E-04
Period II : Day 36/37 to 51			
	Day 51		
EtOH (v/v)	**τ**	**m**	**m_N**
[0.1]	[0.031]	[0.099]	[2.75E-04]
0.2	0.177	0.118	2.27E-04
0.3	0.162	0.120	1.41E-04
[0.2]	[0.296]	[0.069]	[1.19E-04]
0	0.085	0.077	2.92E-04

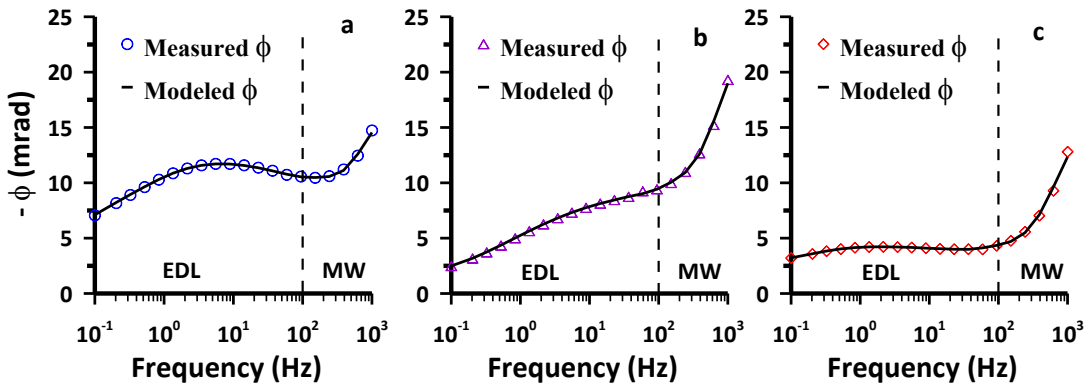

Figure 4.6: Fits of selected measured ϕ data and modeled data from Debye Decomposition

Fits of selected measured ϕ data and modeled data from Debye Decomposition for sand-clay medium saturated with: a) water at Day 36, b) EtOH 10% v/v at Day 35 and c) EtOH 20% v/v at Day 36. The dashed line indicates the assumed demarcation between where electrical double layer polarization dominates the spectra (EDL <100 Hz) and where Maxwell Wagner polarization (and instrumentation errors) become more important (MW> 100 Hz).

4.6. Discussion

4.6.1. Origin of the time dependent electrical response

We observed a clear temporal variation in the electrical response of the sand-clay sample saturated with water (Figure 4.3a). This temporal CR variation likely results from the fact that clay-water interactions are not instantaneous; instead these interactions evolve to a near equilibrium state in about 5 days (Figures 4.3g and 4.3h). After this time, ϕ and σ'' show only minor variations with time (pseudo-steady-state). Considering the clay-EtOH experimental treatment, faster reaction kinetics between clay and EtOH towards a near equilibrium state might explain why both ϕ and σ'' show no obvious time-varying response (Figures 4.3g, 4.3h). *Brindley and Hoffman* [1962] and *Brindley et al.* [1969]

indicate reactions take place rapidly (within hours) between the clay surface and EtOH because of the preference of the surface for EtOH. The water-rock mineral interaction processes, described mainly by transport (diffusion or advection) of ions or compounds to and from the mineral surface coupled with chemical reactions on the mineral surface [*Schott et al.*, 2009, *Steefel and Maher*, 2009], can be envisioned as dynamically evolving processes that tend towards equilibrium. As this equilibrium is reached, ionic movement and reaction rates remain relatively constant with time. The observed temporal variation in ϕ and σ'' may therefore reflect the dynamic evolution toward equilibrium of transport and chemical processes occurring at the clay-water and clay-EtOH interfaces.

4.6.2. Suppression of clay-driven polarization by ethanol

The CR spectra show a clear suppression in the clay-driven electrical polarization response (ϕ and σ'') with increasing EtOH concentration (Figure 4.4). This suppression is consistent as EtOH concentration increases from 0% to 10% and 20% v/v (Figures 4.4a and 4.4b). The differences in the CR spectra with increasing EtOH concentration are statistically significant ($P \leq 0.001$, $\alpha = 0.05$), as confirmed by ANOVA. We suggest that the suppression effect of EtOH on the clay-driven polarization results from complex interactions in the clay-EtOH-water system. Among the plausible explanations, we focus on a) preferential adsorption of EtOH over water on clay and subsequent possible modification of the clay structure, and b) complex intermolecular EtOH-water interactions that may induce significant changes in mobility of ions in the electrical double layer (EDL) at the mineral surface. The combination of EtOH adsorption on clay and EtOH-water interactions presumably altered the EDL at the clay-fluid interface,

resulting in an overall suppression of the polarization response, being more pronounced with increasing EtOH concentration. Among the possible interactions between organic molecules and the type 2:1 clay minerals [for a review see *Kowalska et al.*, 1994; *Yariv and Cross*, 2002; *Lagaly et al.*, 2006], cation-dipole interactions could potentially explain EtOH adsorption on clay [*Dowdy and Mortland*, 1967; *Bissada et al.*, 1967; *Mortland*, 1970; *Theng*, 1974]. These interactions presumably, (1) result in preferential and stronger adsorption of EtOH relative to water on clay [*Russel and Farmer*, 1964, *Hiltabrand, 1971*; *Theng*, 1974; *Clausen et al.*, 2009], and (2) cause significant alterations of clay surfaces [*Brindley et al.*, 1969], particularly their ability to attract counterions and repel co-ions in solution. For example, the adsorption of amphipolar molecules (e.g. EtOH) can potentially change the interfacial tension and the EDL structure at the solid-liquid interface [*Brindley and Hoffman*, 1962; *Van Olphen*, 1977]. Such influence of adsorbed EtOH on the clay surface chemistry would likely be more important with increasing EtOH concentration in the water-EtOH mixtures. *Theng* [1974] reported that organic adsorption on clay minerals correlates with organic concentration. In addition, complex intermolecular water-EtOH interactions [*Franks and Ives*, 1966; *Parke and Birch*, 1999, *Atamas and Atamas*, 2009] may further affect ionic mobility [*Bhat and Shetty*, 2011] on the surface in the EDL. Such an effect could also partly contribute to the observed polarization suppression response.

The presumed reduction in the capacity of the clay surface to hold charges as a result of increasing EtOH adsorption associated with higher EtOH concentration is supported by the observed decrease in σ'' (Figures 4.4b and 4.4d). This decrease in σ'', which is

statistically significant (P≤0.001) for all experimental treatments, indicates the important influence of surface processes, namely clay surface alteration by EtOH adsorption, on the overall polarization response. In addition, the decrease in m_n approximately by a factor of 2 as EtOH concentration increases respectively from 0 to 10% v/v, and 10 to 20% v/v, in the water-EtOH mixtures is consistent with the observed trend in σ''. Such consistency is expected given that m_n is generally proportional to σ'' [*Slater and Lesmes*, 2002].

Our findings are inconsistent with early studies by Olhoeft and colleagues on complex resistivity measurements of clay-organic interactions [*Olhoeft*, 1985; *Olhoeft*, 1986; *Sadowski*, 1988; *Olhoeft and King*, 1991]. These authors documented a distinctive large increase in ϕ response (~ 100 mrad) with the addition of toluene and interpreted this increase from clay-toluene polymerization. Instead, our results are consistent with more recent studies on clay-organic interactions [*Börner et al.*, 1993; *Brown et al.*, 2004; *Ustra et al.*, 2012]. *Ustra et al.* [2012], performing laboratory-scale experiments on clay-toluene interactions designed to replicate the experiments of Olhoeft and colleagues, found a statistically significant decrease in polarization associated with increasing concentrations of toluene. *Brown et al.* [2004] also observed a very low ϕ response associated with clay-toluene interactions in contrast to the reported large ϕ response by Olhoeft and colleagues. *Börner et al.* [1993] found a decrease in σ'' in a clay-benzene system while other organic contaminants (oil, hexane) exhibited similar σ'' responses to that of a clean (water matrix only) sample. Finally, interactions of clay with trichloroethylene (TCE) resulted in a reduced ϕ response with increasing TCE

concentration, probably due to alterations of clay exchangeability and other chemical reactions [*Roberts and Wildenschild*, 2004]. Our findings clearly support the concept that clay-organic interactions suppress rather than increase the clay-associated polarization as EtOH concentration increased.

4.6.3. Polarization response hysteresis due to ethanol adsorption on clay

Our results also indicate hysteresis in the CR response to EtOH concentration as the clay polarization was not recovered upon returning a sand-clay sample back to a water only solution (Figure 4.5). Measured ϕ and calculated σ'' exhibit minimal changes after 14 days of a transition of the saturating fluid from EtOH 20% v/v back to water (Figure 4.5). We interpret this hysteresis of the CR polarization response to be associated with persistent and strong EtOH adsorption on the exchangeable cations and sites of clay. We assume that the observed CR response reflects the high affinity of EtOH for the available exchangeable cations and sites resulting in a very stable interaction with clay. Our interpretation is supported by the fact that adsorption of EtOH is a more favorable reaction than that of water in the presence of clay as the system gains a large amount of entropy [*Theng*, 1974]. In addition, strong adsorption of EtOH may have induced significant or perhaps nearly irreversible changes in the clay structure so that only limited clay-water interactions subsequently become possible even in fully water saturating conditions at least within the time frame of the investigation we conducted. For example, *Lu and Pignatello* [2002] reported irreversible changes in the structure (pore deformation) of natural organic matter materials associated with sorption hysteresis of

organic contaminants. Structural changes are reported by *Brindley et al.* [1969] in montmorillinite when exposed to EtOH. Therefore, we infer herein that EtOH adsorption on clay exerts a memory effect that has a persistent influence on the electrochemical processes occurring in the system and, subsequently, on the observed CR response.

4.6.4. Implications for monitoring of EtOH contamination, chemical ion exchange and kinetics

Our findings support the potential for using CR measurements as an effective tool to monitor and characterize EtOH contamination in clayey soils. The percentage clay content (2%) used in our experiment is comparable to the unconfined sand aquifer at the Canadian Forces Base, in Borden Ontario [*Mackay et al.*, 1986]. Numerous field studies on ethanol transport behavior have been recently performed at this site [e.g. *Molson et al.*, 2002; *Freitas et al.*, 2011; *Freitas and Barker*, 2013]. However, we recognize that higher clay content sediments may act as low permeability media for the storage and persistent release of organic contaminants. CR measurements should be effective in studying higher clay content systems as the imaginary conductivity scales with surface area normalized by pore volume [e.g. *Weller et al.*, 2010] and more sites for EtOH sorption would be available**.** The clay-EtOH interactions result in a distinctive suppression of the electrical response as EtOH concentration increases, indicating the sensitivity of the CR measurements to EtOH contamination. The EtOH adsorption clearly shows strong hysteresis effects. We have demonstrated that, even when pore fluids were returned back to water, the initial effects on the CR response observed with EtOH 20% v/v as saturating fluid persisted. Our findings emphasize the importance of considering hysteresis effects

in the interpretations of geophysical data with regards to the fate of EtOH and other organic contaminants in the subsurface. On one hand, such hysteresis effects associated with persistent and strong EtOH adsorption on clay may result in geochemical sampling of pore fluids showing inconsistencies with the geophysical data, thus complicating geophysical interpretations of clay-organic interactions. On the other hand, the hysteresis effects might provide useful information on the contamination history in the subsurface even after the concentration of the contaminants in the pore-fluid falls below an undetectable level, particularly if there are other geophysical indicators or geochemical characteristics that could provide complementary information. The strong sorption and subsequent hysteresis effects of clay-EtOH interactions could in part explain the long term persistence of EtOH in the unsaturated and capillary fringe reported in previous field studies [e.g. *Spalding et al.*, 2011; *Freitas and Barker*, 2013]. Therefore, CR measurements could be useful for long-term monitoring of EtOH contamination, particularly when associated with low permeability media, such as sand admixed with clay or clay-silt matrix.

Our findings also indicate the potential for CR measurements to capture chemical ion exchange and kinetics reactions. The observed changes in ϕ and σ'' presumably reflect the overall chemical processes occurring in the clay-EtOH-water system towards a near equilibrium state. In the clay-water system, both ϕ and σ'' exhibit a gradual increase during the first 5 days of measurement, then plateau until the end of the measurements. The gradual increase in ϕ and σ'' may be attributed to varied ion exchange processes and kinetics during the initial stage of clay-water interactions in the system. The observed

plateau in both ϕ and σ'' can be associated with a relatively constant ion exchange and kinetics rate of reactions, thereby indicating a near equilibrium state in the system. Clay-EtOH interactions result in a near immediate suppression response and minimal variation in both ϕ and σ'' with time, thus indicating a relatively constant ion exchange and kinetic reaction rates in the system, suggesting that a near equilibrium state is reached rapidly in the clay-EtOH system, similar to observations of *Brindley et al.* [1969]. Our findings indicate the sensitivity of CR measurements to chemical ion exchange and kinetics reactions and that CR can be a useful tool for predicting both non-equilibrium and equilibrium state of chemical reactions.

The CR method, applied for our experiment at the laboratory scale, is potentially deployable in the field. As in the laboratory, a four electrode arrangement is used for CR measurements on the ground surface or in boreholes. Borehole measurements could be acquired with a down-hole probe, in order to determine fine-scale variations in ethanol concentrations with depth along a borehole. Although lower resolution in comparison with laboratory and borehole measurements, CR imaging from the surface is possible and could be implemented to non-invasively characterize and monitor sites of ethanol contamination. Some recent examples of field-scale CR measurements for environmental applications include characterization of hydraulic properties [*Hördt et al.*, 2007], monitoring of bioremediation of heavy metals [*Williams et al.*, 2009; *Flores Orozco et al.*, 2011] and mapping of organic contaminants [*Vanhala*, 1997; *Kemna et al.*, 2004; *Flores Orozco et al.*, 2012].

4.7. Conclusions

Unlike some previous studies reporting a large increase in ϕ response associated with clay-toluene interactions, our research demonstrates that clay-EtOH interactions generate distinctive CR responses that indicate a strong reduction in clay polarization with increasing EtOH concentration in agreement with other recent studies. The CR responses are presumably sensitive to EtOH adsorption on clay, and overall chemical ion exchange and kinetics reactions in clay-water-EtOH media. The CR polarization response hysteresis during saturating fluid transitions, due presumably to strong and persistent EtOH adsorption on clay, may provide insight into the contamination history of organic compounds in the subsurface, especially if considered in the context of other geophysical and geochemical data and site history. Our findings highlight the sensitivity of the CR technique to clay-organic interactions and its potential application for minimally invasive, non-invasive and cost-effective monitoring and characterization of subsurface organic contamination. Further laboratory and field investigations are necessary to test the effectiveness of this CR technique with a variety of organic contaminants in clayey soils.

CHAPTER 5: COMPLEX RESISTIVITY SIGNATURES OF ETHANOL BIODEGRADATION IN POROUS MEDIA[3]

Abstract

Numerous adverse effects are associated with the accidental release of ethanol (EtOH) and its persistence in the subsurface. Geophysical techniques may permit non-invasive, real time monitoring of microbial degradation of hydrocarbon. We performed complex resistivity (CR) measurements in conjunction with geochemical data analysis on three microbial-stimulated and two control columns to investigate changes in electrical properties during EtOH biodegradation processes in porous media. A Debye Decomposition approach was applied to determine the chargeability (*m),* normalized chargeability (m_n) and time constant (τ) of the polarization magnitude and relaxation length scale as a function of time. The CR responses showed a clear distinction between the bio-stimulated and control columns in terms of real (σ') and imaginary (σ'') conductivity, phase (ϕ) and apparent formation factor (F_{app}). Unlike the control columns, a substantial decrease in σ' and increase in F_{app} occurred at an early time (within 4 days) of the experiment for all three bio-stimulated columns, which is opposite to previous studies on hydrocarbon biodegradation. These columns also exhibited increases in ϕ (up

---

[3] This chapter is submitted (May 1st, 2013) as: Personna, Y. R., L. Slater, D. Ntarlagiannis, D. Werkema, and Z. Szabo, Complex resistivity signatures of ethanol biodegradation in porous media, *Journal of contaminant hydrology*.

to ~9 mrad) and σ'' (up to two order of magnitude higher) 5 weeks after microbial inoculation. Variations in m and m_n were consistent with temporal changes in ϕ and σ'' responses, respectively. Temporal geochemical changes and high resolution scanning electron microscopy imaging corroborated the CR findings, thus indicating the sensitivity of CR measurements to EtOH biodegradation processes. Our results offer insight into the potential application of CR measurements for long-term monitoring of biogeochemical and mineralogical changes during intrinsic and induced EtOH biodegradation in the subsurface.

5.1. Introduction

Microorganisms have long played an important role in geochemical cycles and transformations of earth systems [*Konhauser*, 2007]. Recently, biogeophysics has emerged as a sub-discipline of the geosciences concerned with the geophysical signatures arising from the presence of microbial cells in the near surface, the interaction between these cells and the geologic media, and the alterations of the physical properties of geologic media as result of microbial activity [*Atekwana and Slater*, 2009; *Atekwana and Atekwana*, 2010; *Slater and Atekwana*, 2013]. Microorganisms are capable of extracting energy from electron donors (e.g. organic contaminants or other carbon sources) to build biomass, and catalyzing chemical reactions into numerous intermediate and end products during the respiration of oxygen under aerobic conditions, and other terminal electron acceptors (e.g. sulfate, iron) under anaerobic conditions. The metabolic activity of microorganisms can alter the petrophysical properties of porous media and potentially induce substantial changes in electrical conductivity of pore fluids through changes in

fluid chemistry (ionic strength and composition) and electrical surface conductivity through changes in surface area and roughness, pore geometry and porosity [see *Atekwana and Slater*, 2009; *Atekwana and Atekwana*, 2010 for review]. Using either electrical resistivity (ER) or complex resistivity (CR) methods, recent biogeophysical research has reported distinctive geophysical properties associated with active hydrocarbon (e.g. light non-aqueous phase liquid/LNAPL) biodegradation [*Werkema Jr et al.*, 2003; *Abdel Aal et al.*, 2004; *Atekwana et al.*, 2004a, b, c, d; *Abdel Aal et al.*, 2006; *Allen et al.*, 2007], microbial stimulated metal sulfide mineralization [*Ntarlagiannis et al.*, 2005b; *Williams et al.*, 2005; *Slater et al.*, 2007; *Personna et al.*, 2008] and microbial growth or biofilm formation [*Ntarlagiannis et al.*, 2005a; *Davis et al.*, 2006; *Ntarlagiannis and Ferguson*, 2009; *Abdel Aal et al.*, 2010].

Ethanol, the most common biofuel used in the USA and in Brazil, is an emerging contaminant [*Gomez and Alvarez*, 2010] that can be released, potentially at high concentrations, into the environment, e.g. during transportation accidents [*Spalding et al.*, 2011] or from leaking storage facilities [*McDowell et al.*, 2003]. Numerous adverse effects are associated with subsurface EtOH contamination. For instance, ethanol at concentration ≥ 6% v/v is toxic to soil and water borne microorganisms [*Nelson et al.*, 2010]. Ethanol may therefore affect microbial growth [*Ingram*, 1989; *Nelson et al.*, 2010] and community structure [*Cápiro et al.*, 2008; *Ma et al.*, 2011], and may impede intrinsic biodegradation of organic contaminants, as well as biomineralization of toxic metals in the subsurface. A high concentration of EtOH in groundwater can result in colsovency effects [*Powers et al.*, 2001b; *Da Silva and Alvarez*, 2002; *Corseuil et al.*, 2004; *Stafford*

et al., 2009] that enhance the aqueous concentration of BTEX (benzene, toluene, ethyl-benzene and xylene) compounds contained in gasoline. When present in the subsurface at low concentration, EtOH is readily and preferentially degraded by microorganisms in comparison with the BTEX compounds [*Corseuil et al.*, 1998; *Powers et al.*, 2001b; *Ruiz-Aguilar et al.*, 2003; *Mackay et al.*, 2006; *Gomez and Alvarez*, 2009; 2010; *Freitas et al.*, 2011] and thereby increases the likelihood that these compounds will persist long enough to migrate away from the spill site. Anaerobic degradation of EtOH can potentially lead to methane production at concentrations reaching the explosive limit level [*Freitas et al.*, 2010; *Nelson et al.*, 2010; *Spalding et al.*, 2011].

Despite the growing literature providing insights into the electrical signatures arising from biodegradation of organic contaminants, studies of the geophysical signatures arising from microbial degradation of EtOH are lacking. Detection of EtOH in soils using ER and CR has recently been investigated [*Henderson et al.*, 2009; *Personna et al.*, 2013a, *Personna et al.*, 2013b]. *Personna et al.* [2013a] demonstrated that ER measurements were dependent on EtOH concentration, whereas *Personna et al.*, [2013b] showed that CR measurements were sensitive to clay-EtOH interactions as a result of the suppression of interfacial polarization associated with clays.

We report here on CR signatures during microbial-stimulated EtOH degradation in porous media columns. Our main objectives were to determine (a) changes in the electrical properties due to EtOH biodegradation in porous media, and (b) whether

temporal changes in aqueous chemistry are consistent with changes in the CR response. Our results show the sensitivity of CR measurements to EtOH biodegradation, characterized by a substantial decrease in real conductivity (σ') within days and an increase in imaginary conductivity (σ'') and phase (ϕ) within weeks after microbial inoculation. While our findings on the increase in (σ'') and ϕ agree with previous studies on biomineralization of metal sulfide, the observed early-time decrease in σ' contrasts with previous studies on hydrocarbon biodegradation.

5.2. Potential EtOH biodegradation pathways

Understanding potential EtOH biodegradation pathways is important for predicting changes in the physical, chemical and geophysical properties of geologic media. Figure 5.1 illustrates possible EtOH biodegradation pathways and processes driving changes in the electrical properties of porous media.

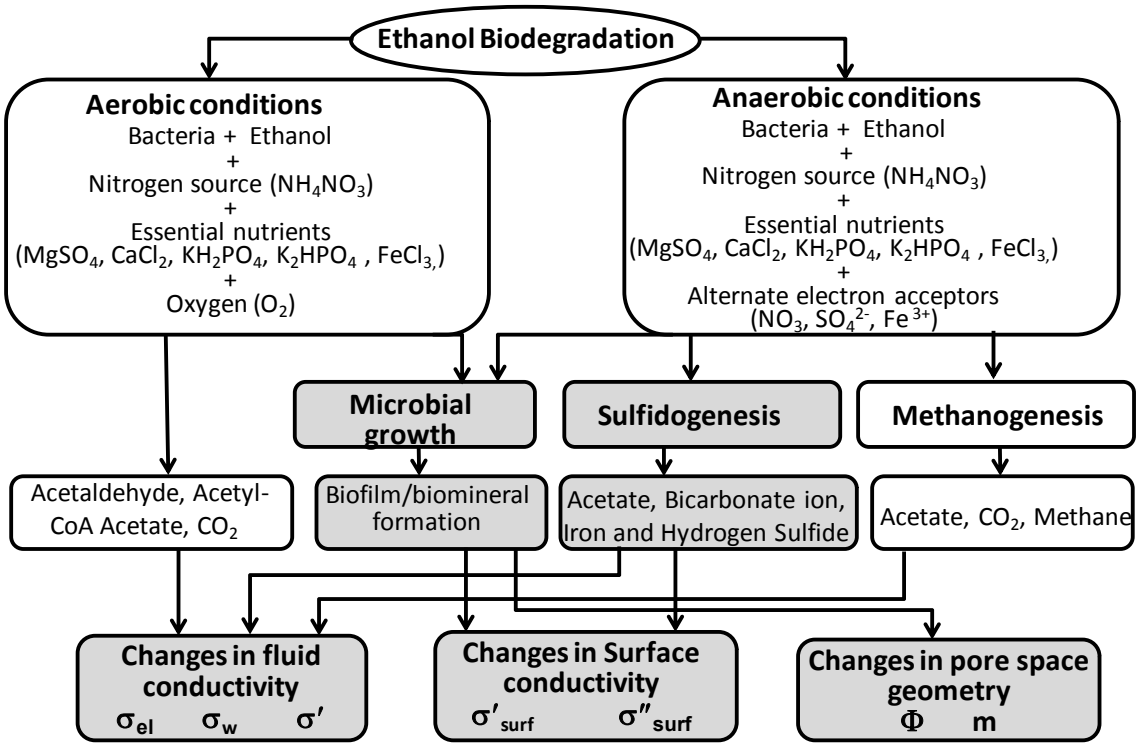

Figure 5.1: Possible ethanol biodegradation pathways and potential resulting induced changes in electrical properties of porous geologic media.

Possible ethanol biodegradation pathways and potential resulting induced changes in electrical properties of porous geologic media (σ_w: fluid conductivity, σ_{el}: electrolytic conductivity, σ': real conductivity, σ'_{surf} : real part of surface conductivity, σ''_{surf} : imaginary part of surface conductivity, Φ : porosity, m= cementation index i.e. a function of the effective grain shape). Shaded areas highlight predominant pathways and processes driving changes in the electrical properties observed in this experiment.

Ethanol is a carbon and energy source that can be readily degraded by most common bacteria in nature for building biomass [*Powers et al.*, 2001b]. Microbial-mediated EtOH degradation in porous media can occur under both aerobic and anaerobic conditions, depending on temperature, pH, availability of nutrient, oxygen and other terminal electron acceptors (TEAs) [see *Powers et al.*, 2001b for review]. In the presence of oxygen, EtOH is readily oxidized to carbon dioxide (CO_2) and H_2O by most common aerobic bacteria through the Krebs cycle [*Powers et al.*, 2001b]. The common

intermediate metabolites include acetaldehyde, acetyl-CoA and acetate. In aquifers contaminated by gasoline-EtOH mixtures, the available oxygen will be rapidly consumed due to the high biochemical oxygen demand associated with preferential EtOH biodegradation, leading to anaerobic conditions. Under these conditions, many groups of bacteria (e.g. acetogens and methanogens) can act separately or synergistically in the degradation of EtOH to acetate (CH_3COOH) and hydrogen (H_2), and ultimately to carbon dioxide (CO_2) and methane (CH_4) [*Powers et al.*, 2001b] as per the following equations:

$$CH_3CH_2OH + H_2O \rightarrow CH_3COOH + 2H_2 \quad (1)$$

$$CH_3COOH \rightarrow CO_2 + CH_4 \quad (2)$$

$$2H_2 + \tfrac{1}{2} CO_2 \rightarrow \tfrac{1}{2} CH_4 + H_2O \quad (3)$$

However, if sulfate (SO_4^{2-}) is the primary TEA, sulfate reducing bacteria (SRB) may dominate anaerobic EtOH biodegradation processes. *Bryant et al.* [1977] demonstrated that, in a mixed culture of desulfovibrio and methanogens growing on EtOH, the production of methane decreased in stoichiometric amount with increasing sulfate concentration; an excess of sulfate completely halted methane production. This observation suggests that anaerobic oxidation of EtOH by SRB was a preferential pathway as long as a sufficient sulfate was available in the system. The utilization of EtOH as an energy source by SRB, reducing sulfate to hydrogen sulfide (HS^-) and producing acetate, is a common and thermodynamically favorable process [*Widdel*, 1988; *Nagpal et al.*, 2000]. Acetate can be further converted to bicarbonate (HCO_3^-) while aqueous hydrogen sulfide reactions with many metals in solution, especially

ferrous iron, can lead to metal sulfide precipitates. These multi-step chemical reactions can be expressed by the following equations:

$$CH_3CH_2OH + 0.5SO_4^{2-} \rightarrow CH_3COO^- + 0.5HS^- + 0.5H^+ + H_2O \quad (4)$$

$$CH_3COO^- + SO_4^{2-} \rightarrow 2HCO_3^- + HS^- \quad (5)$$

$$Fe^{2+} + HS^- \rightarrow FeS + ½\ H_2 \quad (6)$$

5.3. Complex resistivity method

The complex resistivity (CR) method measures the frequency dependent polarization associated with electrochemical charge migration and accumulation in the electrical double layer (EDL) at the mineral-fluid interface of soils and rocks [*Weller et al.*, 2010; *Kemna et al.*, 2012]. Although traditionally developed for detecting disseminated metallic ores [*Marshall and Madden*, 1959; *Sumner*, 1976], the CR method has increasingly been applied in a wide variety of environmental investigations [*Vanhala*, 1997; *Slater and Lesmes*, 2002; *Kemna et al.*, 2004; *Sogade et al.*, 2006; *Williams et al.*, 2009; *Flores Orozco et al.*, 2011; *Flores Orozco et al.*, 2012]. The CR method is sensitive to changes in pore fluid chemistry, pore space geometry and solid-fluid interface chemistry, all of which may be driven by microbial activity as summarized in Figure 5.1 for the case of ethanol biodegradation. Polarization of the EDL forming at mineral-fluid interfaces is commonly assumed to be the major CR signature of interest, although the CR method also provides information on electromigration within the interconnected pore space and along interconnected interfaces. Abiotic and biotic redox processes at metal-fluid interfaces can dramatically enhance polarization due to the electron transport

characteristics of semi-conductors. Furthermore, bacterial cells are negatively charged and form in contact with water an additional EDL [*Poortinga et al.*, 2002] that can generate a polarization response [*Prodan et al.*, 2004; *Prodan et al.*, 2008; *Revil et al*., 2012b; *Zhang et al.*, 2013]. Many studies have reported CR applications for the characterization of microbial mediated changes in -and interactions with- geologic media, particularly during microbial growth and development of biofilms, biotransformation of heavy metals and radionuclides and biomineralization of organic contaminants [see *Atekwana and Slater*, 2009; *Atekwana and Atekwana*, 2010 for review]. For instance, *Davis et al.* [2006] and *Abdel Aal et al.* [2010] reported an increase in the imaginary component (σ'') of the complex conductivity ($\sigma*$) during microbial growth and associated attachment to mineral surfaces. They inferred an enhancement of the EDL polarization due to the colonisation of the pore space by microbial cells (large surface area to pore volume ratio (S_{por})).

Complex resistivity measurements are conventionally performed using a four-electrode configuration: one pair of electrodes is used for current injection and another pair of electrodes is used to record the resulting voltage drop independent of electrode polarization effects. In the frequency domain mode, a dynamic signal analyzer (DSA) is used to record the magnitude and phase (ϕ) shift of the potential voltage waveform across the sample relative to the current waveform across a reference resistor. This complex impedance is a vector sum of the in-phase conductivity associated with electromigration of charges, represented by the real conductivity (σ'), and the out-of-phase reversible

energy storage (polarization), represented by the imaginary conductivity (σ'') . In terms of measured conductivity magnitude $|\sigma|$ and ϕ, the complex impedance is given by,

$$|\sigma| = \sqrt{(\sigma')^2+(\sigma'')^2} \quad (7),$$

$$\phi = tan^{-1}\left(\sigma''/_{\sigma'}\right) \quad (8),$$

The σ' and σ'' are then derived as follows,

$$\sigma' = |\sigma| cos\, \phi \quad (9),$$

$$\sigma'' = |\sigma| sin\, \phi \quad (10).$$

The σ' and σ'' are commonly expressed as a function of electrolytic (σ_{el}) and surface conductivity (σ^*_{surf}), which are most often assumed to add in parallel in porous media, i.e.

$$\sigma^* = \sigma_{el} + \sigma^*_{surf} \quad (11).$$

The real and imaginary components are most commonly presented as,

$$\sigma' = \sigma_{el} + \sigma'_{surf} = \frac{1}{F}\sigma_w + \sigma'_{surf} \quad (12),$$

$$\sigma'' = \sigma''_{surf} \quad (13),$$

where F is the true formation factor from Archie's Law [*Archie*, 1942] given by,

$$F = \frac{\sigma_w}{\sigma_{el}} = \Phi^{-m} \quad (14),$$

(Φ is the porosity and m is the cementation index i.e. a function of the effective grain shape). We define an apparent formation factor, F_{app}, directly calculated from the CR measurements as,

$$F_{app} = \frac{\sigma_w}{\sigma'} = \frac{\sigma_w}{\sigma_{el} + \sigma'_{surf}} \quad (15).$$

If σ'_{surf} is very small ($\sigma'_{surf} \approx 0$), then $F_{app} \approx F$.

Empirical models like the Cole-Cole model and Debye Decomposition (DD) have been widely used for the interpretation of CR data as no definitive physicochemical models currently exist. The Cole-Cole type models [*Cole and Cole*, 1941; *Davidson and Cole*, 1951] are useful to describe the dependence of σ^* on frequency, but one disadvantage is that the estimated model parameters may differ for each Cole-Cole variant even for the same CR data [*Nordsiek and Weller*, 2008]. Another disadvantage is that the Cole-Cole models may not adequately describe the data, especially when the shape of the spectra does not show a typical accentuated phase peak. An alternative is the Debye Decomposition (DD) approach that considers the spectra of conductivity amplitude and phase as a superposition of a finite number of different Debye relaxations. Unlike the Cole-Cole type models, the DD model can fit CR data of various spectral shapes [*Nordsiek and Weller*, 2008]. Recently, *Zisser et al.* [2010] proposed a variant of the DD approach as follows,

$$\sigma^*(\omega) = \frac{1}{\sigma_0}\left[1 - \sum_{k=1}^{n} m_k \left(1 - \frac{1}{1 + i\omega\tau_k}\right)\right] \quad (16),$$

$$m = \sum_{k=1}^{n} m_k \quad (17),$$

$$m_n = m/\rho_0 \quad (18),$$

$$\tau = \exp\left(m^{-1} \sum_{k=1}^{n} \ln(\tau_k) m_k\right) \quad (19),$$

where $\rho_{0=1/}\sigma_0$ is the DC resistivity, n is the number of individual Debye responses, m_k and t_k are, respectively, a specific chargeability and relaxation time for a single Debye relaxation, m is the total chargeability, m_n is the normalized chargeability and τ is the mean relaxation time.

5.4. Materials and methods

We performed CR measurements coupled with aqueous geochemical sampling and scanning electron microscopy (SEM) analyses to investigate microbial mediated ethanol degradation in porous media.

5.4.1. Microbial growth test and determination of column geometric factor

Prior to the experiment, we performed, at room temperature (23.5 ± 1 ^{o}C), a microbial growth test in several tubes containing mixtures of a diluted (by factor of 2) Bushnell Haas Broth (BHB) medium and ethanol (1-5% EtOH v/v). The BHB, a favorable medium for hydrocarbon degraders, includes [in g/L] magnesium sulfate (0.2), calcium chloride (0.02), monopotassium phosphate (1.0), dipotassium phosphate (1.0), ammonium nitrate (1.0) and ferric chloride (0.05) [*Bushnell and Haas*, 1941]. We added to the mixtures 1 ml of groundwater samples collected from an EtOH contaminated site (Cambria, Minnesota) [*Spalding et al.*, 2011] as microbial source. Visual observations of the tubes turning turbid within a week suggest a maximum microbial growth at 2% EtOH v/v.

We also performed, prior to the experiment, conductivity measurements on two different sets of known conductivity solutions (sodium chloride /NaCl: ~ 500 µS/cm and ~ 1000 µS/cm) to determine the exact geometric factor (the area/length ratio) defining the

measurement geometry of the five columns to be used in the experiment. For this purpose, a DSA and a four-electrode configuration were used.

5.4.2. Complex resistivity and geochemical measurements

The sampling intervals of the CR and geochemical measurements for the duration of the experiment (day1-71) are summarized in Table 5.1. The measurements were performed on five columns: two control columns (C1 and C2) and three active columns (C3, C4, and C5). Each column (inner diameter: 0.038 m and length: 0.22 m) had six Ag-AgCl potential electrodes spaced equidistant (0.043 m) along one side. The columns, placed in vertical position, were wet-packed with sterilized sand and deionized water (DIW), following identical procedures in an effort to minimize packing differences among columns. Columns were then circulated with the diluted BHB and 2% EtOH v/v (added as solely organic source) at a steady flow rate of ~ 20 cm/day (i.e. ~ 1 pore volume day) from bottom to top using a multichannel peristaltic pump. Note that a small amount of a bactericide, mercury chloride ($HgCl_2$ 5 mg/L), having minimal effect (< 1%) on fluid conductivity, was added in the influent of the control columns to reduce the possibility of contamination. Note that the starting fluid conductivity (0.18 S/m) was higher than that of typical natural shallow ground water. The schematic of the experimental set-up is shown in Figure 5.2.

Table 5.1: Summary of geophysical and geochemical sampling intervals or frequency of measurements

Measurements	Instrumentation/ Analytical methods	Sample collection period	Sample collection frequency
CR	DSA	Day 1-71	at least twice/week
Redox potential	ORP probe	Day 1-71	at least twice/week
pH	pH probe	Day 1-71	at least twice/week
Acetate	HPLC	Day 1-61	at least twice/week
Methane	GC	Day 1-47	at least twice/week
Hydrogen Sulfide	hydrogen sulfide kit	Day 63-70	twice

We performed CR measurements between 0.1-1000 Hz under continuous flow of the sand column saturated with the BHB containing 2 % EtOH during pre-microbial inoculation (day 1 to 8) and post-microbial inoculation (day 9 to 71). The measurements were performed on the three adjacent potential electrode pairs (P1-P2, P2-P3 and P3-P4) (Figure 5.2). Note that some of the CR measurements on the microbial inoculated columns were performed at 0.01-1000 Hz, whereas other measurements were limited to 0.1-1000 Hz due to time constraints (measurement of CR data takes much longer at 0.01 Hz compared with at 0.1 Hz). We applied a Debye Decomposition model to fit the CR data to the specific integral chargeability (m_k) and mean relaxation time (τ_k) (Cf. Eq. 16). At day 8, a dense microbial solution (1 mL), prepared on the diluted BHB version containing 2% EtOH and concentrated by centrifugation, was inoculated in three columns (so-called active columns C3, C4, C5) from the septum/sampling valve located at the middle of each column (Figure 5.2). The two control columns (C1, C2) continued to run without microbial injection. The flow in the active columns was halted for 48 h after the microbial inoculation to prevent undesired flushing of microbes. Fresh diluted BHB, not

sparged to remove dissolved oxygen, and 2% EtOH v/v solution was used to refill the inflow bottles nearly once a week to ensure optimal microbial growth conditions.

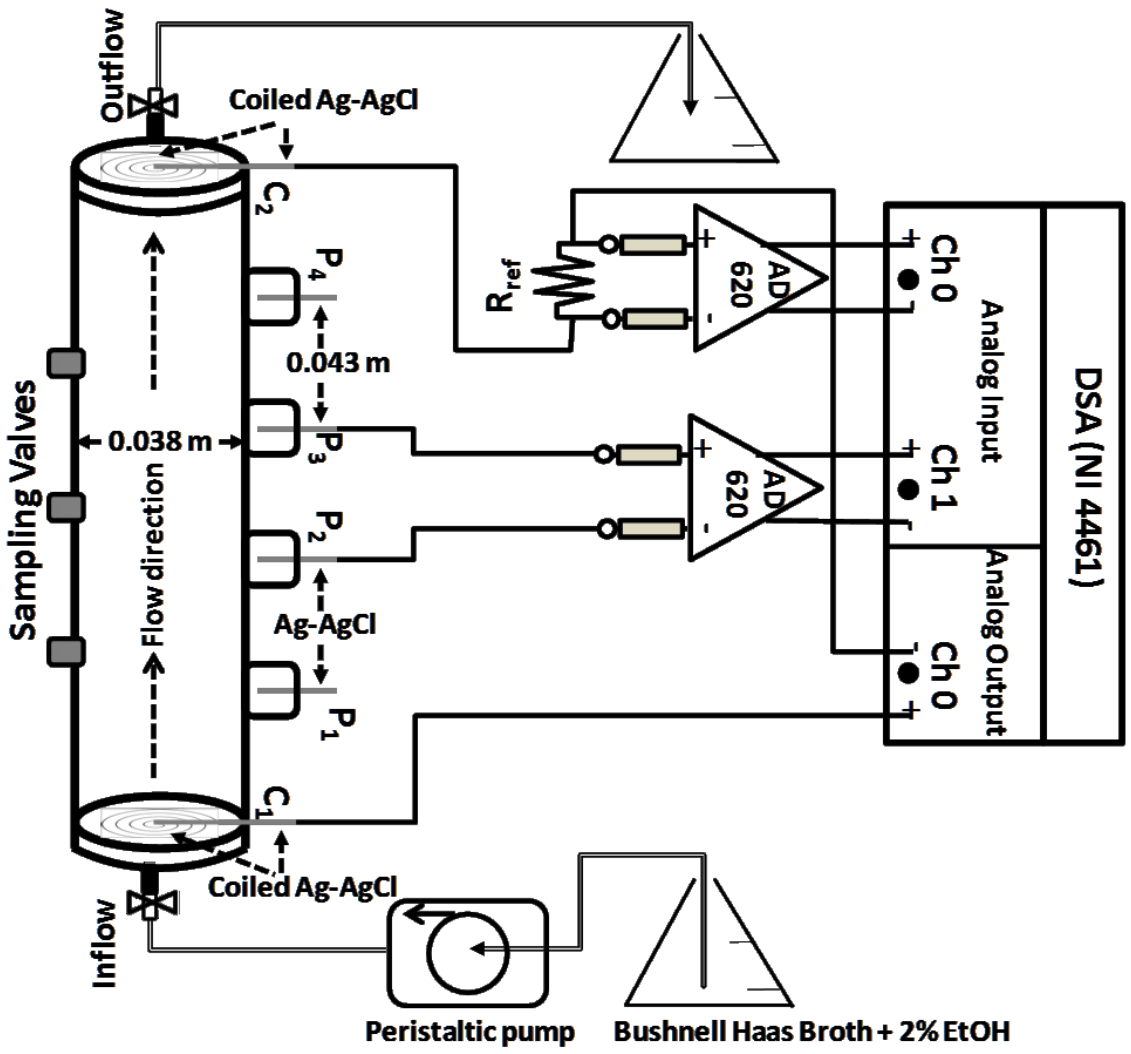

Figure 5.2: Schematic of experimental setup

Schematic of experimental setup showing vertically oriented column with coiled Ag-AgCl electrodes for current injection (C1 and C2) at each end, Ag-AgCl potential electrodes (P1, P2, P3 and P4) housed in pore fluid chambers along a column side, sampling/injection valves on the opposite side, flow direction from bottom to top and two-channel dynamic signal analyzer (DSA) for complex resistivity measurements at frequency of 0.01-1000Hz.

Geochemical measurements of acetate, sulfate, methane, pH, redox potential and fluid conductivity were also performed during pre- and post-microbial inoculation. The outflow tubing of each column was plugged directly into a perforated hole on the cap of a 25 mL-tube for collecting geochemical samples at least twice a week for analysis. We used a sterile syringe to collect 1mL of fluid sample from each tube, that was further filtered at 0.2 μm (Fisherbrand), transferred into a microcentrifuge tube and kept frozen at - 20 ^{o}C until acetate analysis using high performance liquid chromatography (Beckman HPLC, Pump 125, Detector 168). Similarly, we collected and transferred 1.5 mL fluid-samples into 3.5ml O_2-free vials (atmosphere of N_2: 95% and H_2: 5%) for methane analysis; these samples were stored at 4 ^{o}C until analysis by gas chromatography (GC Fischer 1200). We measured pH and redox potential and fluid conductivity using a pH-meter (Accumet), redox potential (MI-800-XXX, Microelectrodes Inc.) and conductivity (Orion 013010A Thermo Electron Corporation) probes, respectively. We used a hydrogen sulfide kit (HACH model, HS-WR) to measure aqueous sulfide during the last week of the experiment to confirm whether sulfide production from sulfate reduction had occurred in the columns. We also purposely halted the flow in the control column (C2) and the active column (C5) at day 44 for five days and again at day 51 for five days to limit the circulation of fresh oxygenated solution (from the inflow bottles) and further explore the corresponding electrical responses that could be associated with metal sulfide formation during EtOH biodegradation processes.

5.4.3. Scanning electron microscopy (SEM) analysis

At the end of the experiment, sand samples were collected by destructive column analysis for high resolution imaging of potential biofilms and biominerals using SEM. We

followed the method described by *Vandevivere and Baveye* [1992] for sample collection and preservation for SEM analysis. We built small cylindrical copper cores (inner diameter: 2.8 mm, length: 13 mm) to collect several undisturbed samples from each column. Then, we capped the core end with a fine nylon mesh and immersed the samples overnight in 2.5% solution of glutaraldehyde in phosphate buffer (pH=7.2). The samples were rinsed in phosphate buffer (0.05M) for 4 h and dehydrated in EtOH-water mixtures of10%, 25%, 50%, 75%, 90% EtOH v/v and 3 times 100% EtOH for 1 hour each. Finally, the samples were dried at ambient air**.** Thin layers of treated sand samples were mounted on the discs and studied by SEM (Zeiss Gemini, Energy spread: 0.5 to 30 eV, Schottky FEG electron gun, Gun vacuum = 10^{-9} Torr).

5.5. Results

5.5.1. Geochemical data

The geochemical data are shown in Figures 5.3 and 5.4. Fluid conductivity (σ_w) varied from about 0.15 to 0.20 S/m (Figures 5.3a, 5.3b). In the control columns (Figure 5.3a), σ_w mainly showed values above 0.17 S/m during the whole experiment although a trend to lower values in C2 and C1 was observed at about day 28 and 44, respectively. However, σ_w of all active columns decreased substantially to reach values mostly below 0.17 S/m from day 12 to day 71 (Figure 5.3b).

The redox potential (ORP) showed large positive values (> 200 mV) during the first 24 days of the experiment indicating oxidizing conditions in both control and active columns

(Figures 5.3c, 5.3d). However, ORP values dropped sharply to less than -200 mV in all active columns at day 25 (Figure 5.3d), indicating a transition to reducing conditions. From day 25 to the experiment end, the active columns showed overall reducing conditions (ORP < 0) although some fluctuations in columns C4 and C5 (ORP near 0) could indicate temporarily alternating strongly reducing and weakly oxidizing conditions. ORP values remained positive until day 61 in the control columns (Figure 5.3c), indicating that oxidizing conditions prevailed. Negative ORP values indicated reducing conditions in column C2 only during the last 10 days of the experiment (presumed microbial contamination).

Both control and active columns showed circum-neutral pH (6.7 < pH< 7.3) conditions during the whole experiment (Figures 5.3e, 5.3d). Methane remained below detection limits for samples collected at least twice a week during the first 47 days of the experiment (data not shown for brevity). Stringent odor of rotten eggs suggested production of hydrogen sulfide, which was confirmed by two measurements revealing concentrations as high as 11.9 mg/L at day 70 in the active columns compared to 0 mg/L and 2.65 mg/L in the control columns C1 and C2 (C2 presumed to have microbial contamination by about day 61), respectively.

Microbial EtOH degradation led to high aqueous acetate concentration (≥ 150 ppm) in all active columns (Figure 5.4). Acetate concentration in columns C3 and C5 showed an abrupt increase post-microbial inoculation, almost concurrently with visual observations

of black precipitates (day 27), and remained afterwards elevated between 71 to 190 ppm. The other active column (C4) showed an early production of acetate (21ppm) at day 15, followed by a dramatic decline to reach negligible values. However, acetate production rebounded in column C4 to a peak of 150 ppm at day 49 i.e. 2 days after visual black precipitates (day 47) occurred. In the control column, acetate concentration was negligible in column C1 for all samples collected during the first 37 days of the experiment (Figure 5.4). However, control column C2 showed acetate concentrations as high as 77 ppm at day 37 (Figure 5.4).

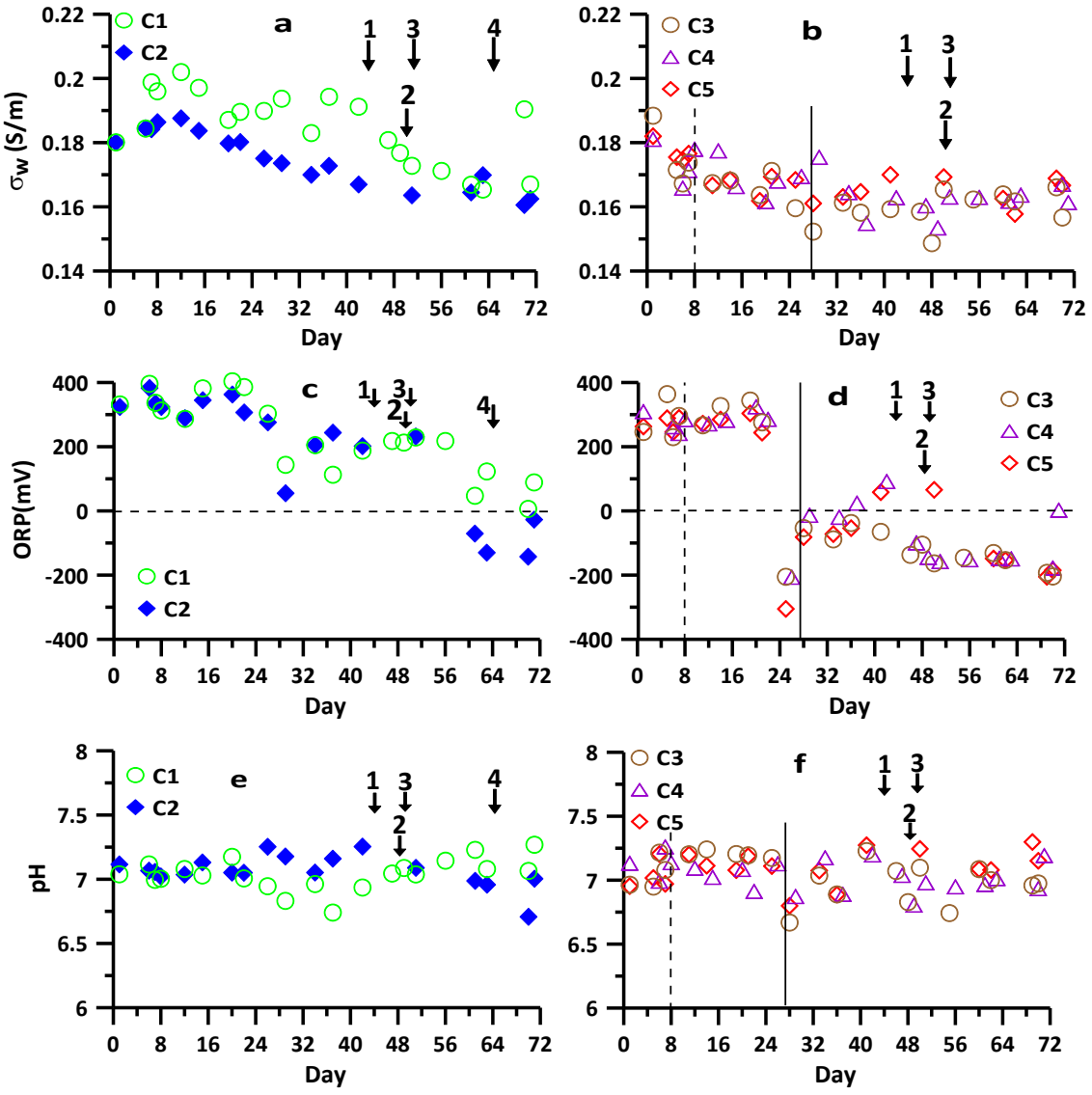

Figure 5.3: Temporal variation in geochemical data for control (C1, C2) and active (C3, C4, C5) columns

Temporal variation in geochemical data for control (C1, C2) and active (C3, C4, C5) columns: a) and b) fluid conductivity (σ_w), c) and d) redox potential (ORP), and e) and f) pH. The vertical dashed line indicates microbial inoculation in all active columns; the solid line indicates first visible black precipitates in C3 and C5. The horizontal dashed line in ORP indicates the theoretical demarcation between oxidizing conditions (ORP > 0) and reducing conditions (ORP < 0). The black arrows 1 and 3 indicate when columns C2 and C5 were intentionally halted ; the black arrow 2 indicates subsequent rerun of C2 and C5; the black arrow 4 indicates observation of black precipitates in control column C2.

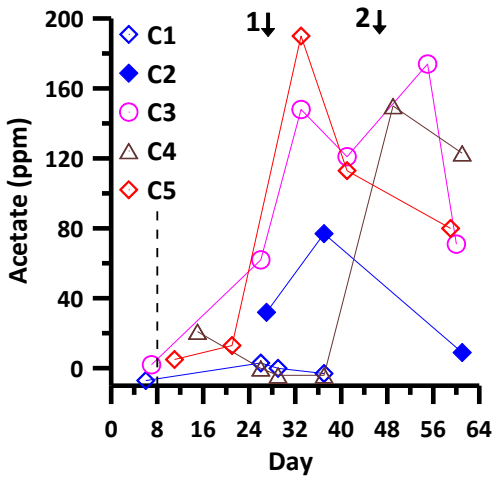

Figure 5.4: Temporal variation in acetate concentration for control (C1, C2) and active (C3, C4, C5) columns.

Figure showing the temporal variation in acetate concentration for control (C1, C2) and active (C3, C4, C5) columns. The dashed line indicates microbial inoculation in all active columns. Black arrows 1 and 2 indicate first visible black precipitates in C3/C5 and C4, respectively.

5.5.2. Geoelectrical responses

The geoelectrical responses are summarized in Figures 5.5, 5.6 and 5.7. The responses varied spatially and temporally among the columns, but changes were more pronounced around the electrode pair P3P4 close to the outflow. For the sake of brevity and clarity, we report only the electrical responses recorded on pair P3P4 of both control (C1, C2) and active (C3, C4, C5) columns. As the peak of relaxation frequency was mainly between 0.1-1Hz, we focus on the 0.8 Hz frequency for presentation of some data.

The phase (ϕ) response is presented only for the active column C5 as the other active columns showed a similar trend although lower response. The temporal variation and

frequency dependence of measured and modeled (from Debye Decomposition, DD) phase (ϕ) data are shown in Figures 5.5a-e while temporal variation at a single frequency (0.8 Hz) is summarized in Figure 5.5f. The DD model describes the measured CR data well (Figures 5.5a-f), as expected given the flexibility of this approach for fitting a wide range of CR curves [*Nordsiek and Weller*, 2008]. As can be seen in these figures, the ϕ response in C5 exhibited a clear temporal variation characterized by a) a slight increase (up to ~ 1.5 mrad) post-microbial inoculation until day 35 (Figure 5.5a) , b) a slight decrease from day 35 to 41 (Figure 5.5b), c) an abrupt jump from day 41 to 43 reaching a peak value of ~9 mrad at 0.2 Hz (Figure 5.5c), d) a decrease after day 43 (except between day 44-46 where a small increase was observed) until returning to pre-inoculation values at day 62 (Figure 5.5d), and e) an increase again from day 62 to 70 (Figure 5.5e). These time periods can also be seen in Figure 5.5f for the single frequency (0.8 Hz) datasets. In the control columns, the phase response remained negligible (<0.5 mrad) until day 65 (data not shown for brevity).

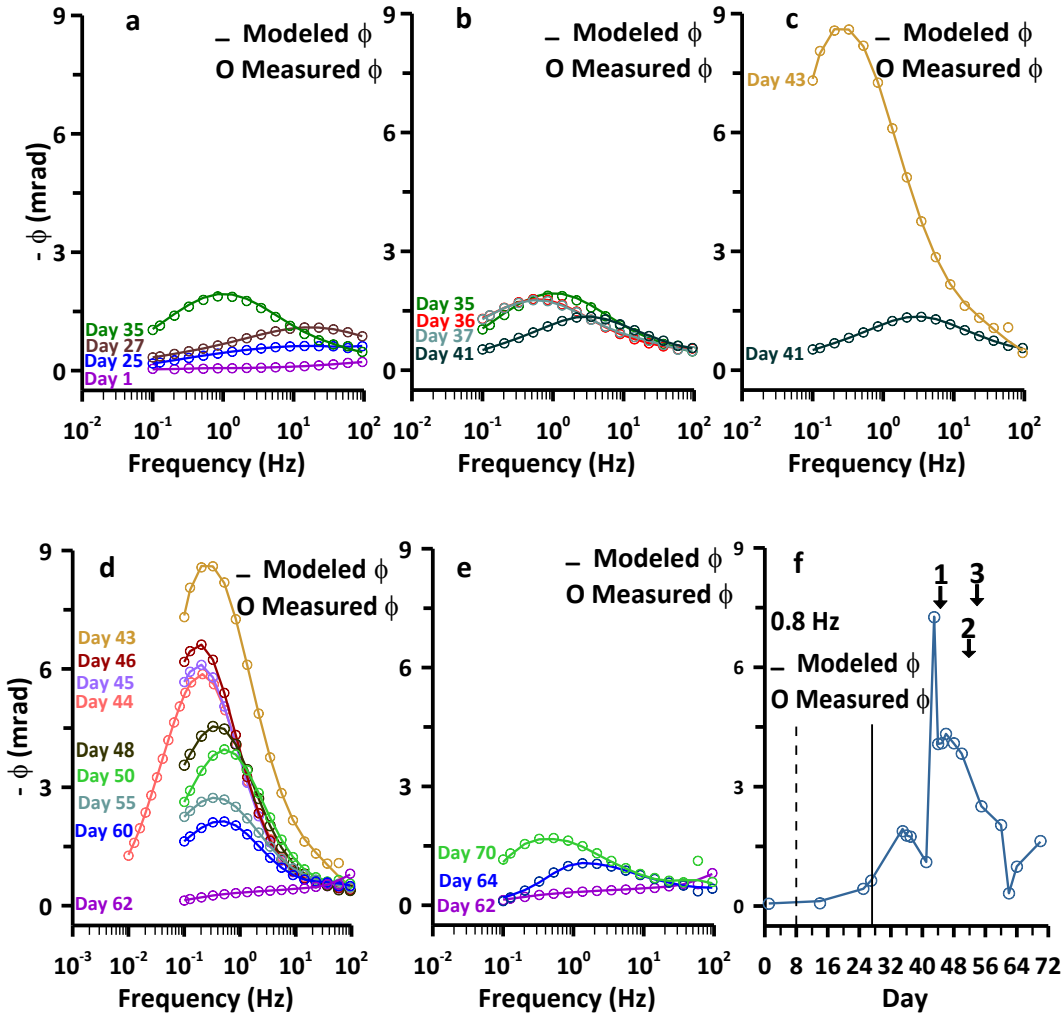

Figure 5.5: Temporal variation and frequency dependence (0.01-100Hz) of measured ϕ data and modeled data obtained from Debye Decomposition for the active column C5

Temporal variation and frequency dependent (0.01-100Hz) of measured ϕ data and modeled data obtained from Debye Decomposition for the active column C5: a) increase from day 1 to 35, b) decrease from day 35 to 41, c) abrupt increase from day 41 to 43, d)decrease from day 43 to 62, and e) increase from day 62 to 70. The temporal variation at a single frequency (0.8 Hz) for C5 is also shown in f). The vertical dashed line and solid line indicate microbial inoculation and first visible black precipitates, respectively. The black arrows 1 and 3 indicate when C5 was intentionally halted while the black arrow 2 indicates C5 rerun.

Real conductivity (σ') data for both control (C1, C2) and active (C3, C4, C5) columns at frequency of 0.8 Hz are shown in Figures 5.6a and 5.6b, respectively. The real conductivity exhibited a substantial decrease in all active columns within the first 4 days post-microbial inoculation and then remained relatively constant from day 12 to the experiment end (day 71). The σ' values remained substantially higher in the bacteria-free (non-inoculated) control columns for the first 40 days of the experiment than in the inoculated columns. The σ' then dropped progressively in the control columns until it reached values that were comparable with those of the active columns by day 56.

The apparent formation factor, F_{app}, for both control (C1, C2) and active (C3, C4, C5) columns at a frequency of 0.8 Hz is shown in Figures 5.6c and 6d, respectively. The F_{app} revealed an abrupt increase from ~ 6 to 10 in all active columns (Figure 5.6d) during the first 4 days post-microbial inoculation, but then remained relatively constant from day 12 to the experiment end. The F_{app} varied between ~ 5 to 7 in the control columns (Figure 5.6c) until day 48, but then increased substantially to about 10 and 8 in C1 and C2, respectively.

Imaginary conductivity (σ'') data for both control (C1, C2) and active (C3, C4, C5) columns at frequency of 0.8Hz are shown in Figures 5.6e and 5.6f, respectively. Both control and active columns showed relatively comparable σ'' values until day 24. However, almost concurrently with visual observation of black precipitates in columns C3 and C5 at day 27 and in C4 at day 44, the σ'' increased about an order of magnitude

in the active columns whilst remaining relatively unchanged (same order of magnitude) in the control columns. By day 44, σ'' values were two orders of magnitude higher in the active column C5 relative to the two control columns. However, the control columns showed a substantial increase in σ'' at about Day 60 (late time), reaching comparable values with the active columns by the end of the experiment. As discussed later, this likely reflects microbial contamination of the control columns at late time.

The DD model parameters, chargeability (m) and normalized chargeability (m_n), for the active column C5 are shown in Figure 5.7a. These parameters represent global estimates of the ratio of polarization to conduction, and an absolute measure of the polarization, respectively. Therefore, they should generally follow the trend of the phase and imaginary conductivity, respectively. These parameters exhibit a consistent temporal variation characterized by a) small values until about day 20 followed by an increase starting at day 25 (almost concomitantly with observed black precipitates at day 27) and reaching a peak at day 35, b) a decrease from day 35 to day 41, c) an abrupt increase from day 41 to day 43, and d) a decrease from day 43 to day 62, where the values become small again. For comparison, the variation in σ'' at 0.8 Hz is shown for C5 (Figure 5.7b). The changes in m and m_n followed changes in ϕ and σ'' as depicted by Figures 5.7a and 5.7b. The time constant (τ) varied between 0.04 to 0.78 seconds for all datasets, except for days 1, 35, and 36 where τ was 1.6, 6.1, and 5.4 seconds, respectively.

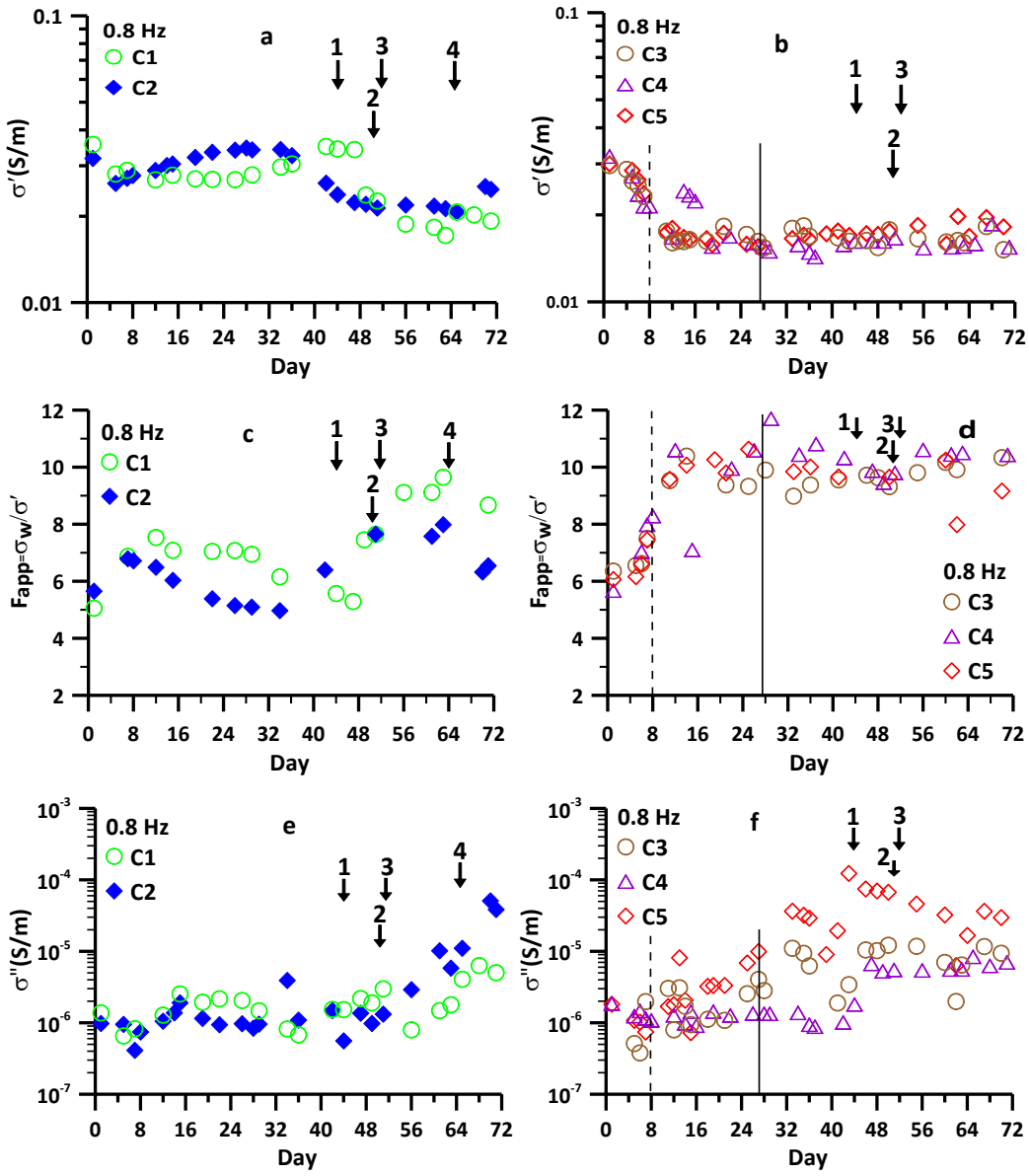

Figure 5.6 : Geoelectrical responses for control (C1, C2) and active columns (C3, C4, C5) as a function of time at 0.8 Hz

Geoelectrical responses for control (C1, C2) and active columns (C3, C4, C5) as a function of time at 0.8 Hz (a) and (b) real conductivity (σ'), (c) and (d) apparent formation factor (F_{app}), and (e) and (f) imaginary conductivity (σ''). The vertical dashed line indicates microbial inoculation in all active columns; the solid line indicates first visible black precipitates in C3 and C5. The black arrows 1 and 3 indicate when columns C2 and C5 were intentionally halted; the black arrow 2 indicates subsequent rerun of C2 and C5; the black arrow 4 indicates observation of black precipitates in control column C2.

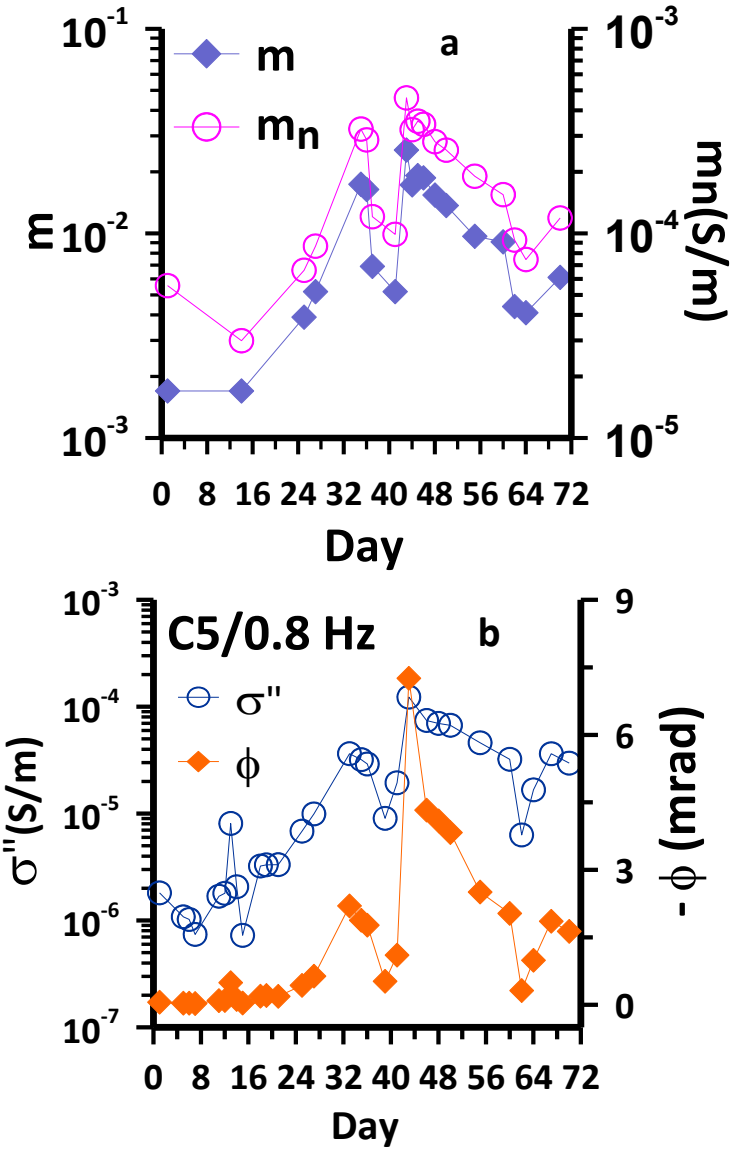

Figure 5.7: Temporal variation in chargeability and normalized chargeability

Figures showing a) Temporal variation in chargeability (m) and normalized chargeability ($m_n = m/\rho_0$) obtained from Debye Decomposition (DD) for the active column C5. b) the temporal variation in imaginary conductivity (σ'', as shown in Figure 5.6f) and phase (ϕ, as shown in Figure 5.5d) at single frequency (0.8 Hz) for the active column C5 are shown for comparison.

5.5.3. SEM results

The SEM analysis, performed on samples collected after the experiment ended showed evidence that the bacteria efficiently utilized EtOH (sole energy source or electron donor) and available electron acceptors in the system to build biomass. As revealed by high resolution SEM images, intense microbial activity and EtOH degradation in the active columns resulted in biofilm formation (Figure 5.8a), mineral precipitation as a dispersed phase (Figure 5.8b) and as presumed biomineral (mineral encrusted on bacterial cell surfaces) (Figure 5.8c). Like the active columns, the control columns showed biofilm formation for samples collected after the experiment ended, thus confirming suspected late time contamination.

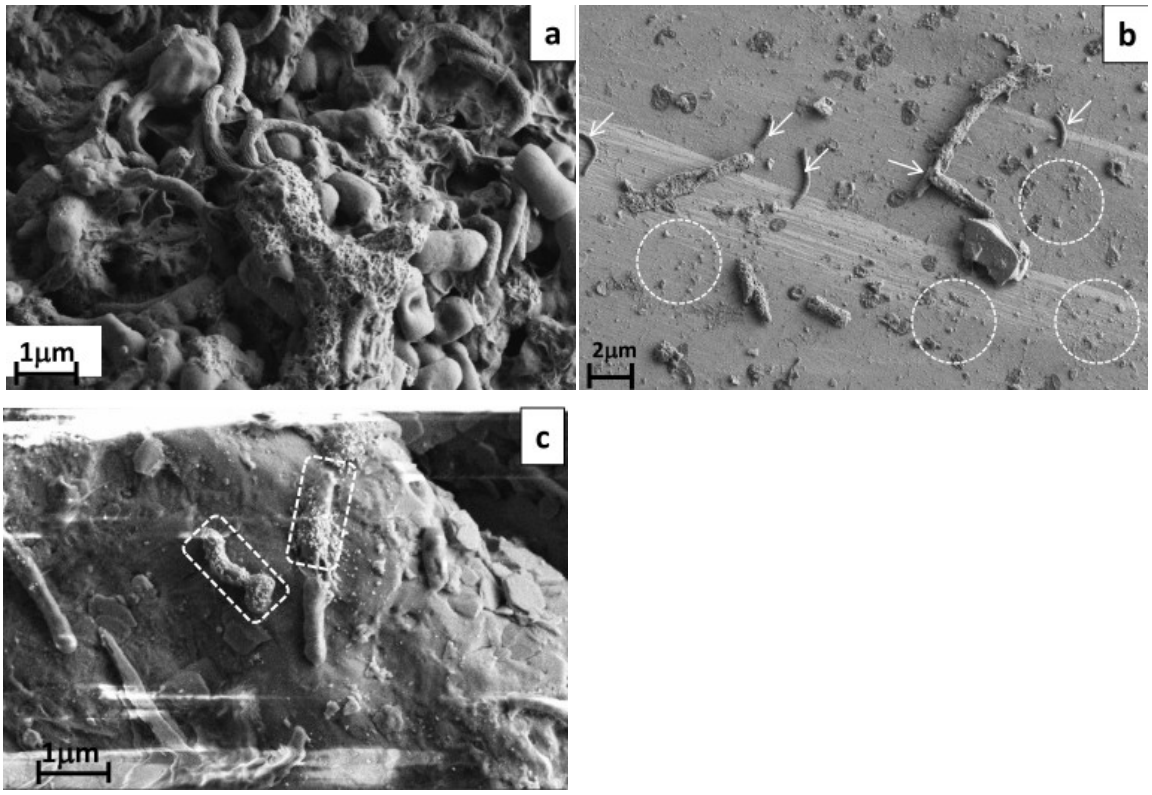

Figure 5.8: Selected SEM images from the active columns

Selected SEM images showing in the active column C3: a) biofilm formation and b) isolated bacteria (indicated by white arrows) and mineral precipitation as dispersed form (indicated inside the whilte circles) on grain surface; and in the active column C5 : c) mineral precipitation as presumed biomineral (mineral encrusted on bacterial cell surfaces as shown here inside the rectangles)

5.6. Discussion

5.6.1. Geochemical characteristics of EtOH degradation and sulfidogenesis

A rapid depletion of oxygen occurred within the active columns due to high biochemical oxygen demand associated with intense microbial activity during EtOH degradation. Such rapid oxygen depletion was previously reported for preferential EtOH biodegradation occurring in aquifer microcosms contaminated by gasoline-EtOH mixtures [*Corseuil et al.*, 1998]. Anaerobic conditions were likely to rapidly develop and prevail in the system, but periodic changes of inflow recipient with fresh oxygenated

solution may have led to transitory sub-aerobic conditions that revert to anaerobic conditions upon continuing biodegradation of the ethanol. The trend of occasionally alternating measured ORP (Figure 5.3d) indicates a possible strengthening and weakening of the anaerobic conditions during the experiment.

Anaerobic EtOH degradation by SRB appeared to be dominant in the system as indicated by visible black precipitates, most likely metal sulfide, developing in the active columns C3 and C5 within 2 weeks post-microbial inoculation. The degradation of EtOH by SRB in the presence of sulfate is a common and thermodynamically favorable process [*Widdel*, 1988; *Nagpal et al.*, 2000]. As H_2S is formed even at low concentration, metal sulfide could be produced almost stoichiometrically and removed rapidly owing to their low solubility [*Drzyzga et al.*, 2002]. In our system, CH_4 remained below detection limit, but a stringent odor of rotten egg suggested high H_2S production, which was confirmed for the two measurements taken during the last week of the experiment showing H_2S concentration as high as 11.9 mg/L in all active columns. This observation supported the predominance of sulfidogenesis over methanogenesis during anaerobic degradation of EtOH in our system as illustrated in Figure 5.1.

5.6.2. Distinctive electrical responses associated with microbial EtOH degradation

The geoelectrical response appears to reflect sequential and subtle changes occurring in the system as a result of EtOH biodegradation processes. In the active columns, the real conductivity (σ') captured changes at the early time of microbial growth on EtOH almost immediately post-microbial inoculation. In contrast, the imaginary conductivity (σ'') and

phase (ϕ) anomalies developed at a later time, almost concurrently with mineral precipitation in the system. Relative to the active columns, the bacteria-free (non inoculated) control columns showed small changes in σ', σ'' and ϕ responses.

A rapid decrease in σ' after microbial inoculation was observed in the active columns (Figure 5.6b) that was not seen in the control columns (Figure 5.6a). We attribute this decrease in σ' within the active columns to microbial activity associated with ethanol biodegradation and the resultant changes in the column matrixes. This finding is not consistent with previous experiments on electrical properties of hydrocarbon biodegradation that have found an increase in σ' attributed to an increase of total dissolved solids, solution ionic strength and conductivity resulting from either a direct release of metabolic organic acids or an indirect release of ions from enhanced mineral weathering by organic acids [*Werkema Jr et al.*, 2003; *Abdel Aal et al.*, 2004; *Atekwana et al.*, 2004a, b, c, d]. The decrease in σ' within four days after microbial inoculation could have been caused primarily by the removal of ions in solution during intense microbial respiration or by changes in porosity and pore space tortuosity associated with rapid microbial growth and biofilm formation. Rapid (≤ 5 days) microbial growth and biofilm development were expected within days in our system as, prior to the experiment onset, a) bacteria acclimation was performed in the growth medium, b) substantial microbial growth was visually observed within 5 days in the batch test, and c) bacterial solution was concentrated by centrifugation before inoculation. The sand-matrix could also provide a support for bacteria attachment and ease of use of EtOH and nutrients.

Agladze et al. [2003] reported substantial microbial growth, biofilm formation and attachment within 72 hours during the development of *Escherichia coli* under static and laminar flow conditions. During the oxidation of EtOH, it is plausible that bacteria utilized substantial amounts of aqueous terminal electron acceptors (e.g. SO_4^{-2} and Fe^{3+}), thus removing them from solution perhaps as precipitated solids, reducing pore fluid ionic strength, changing fluid composition and, consequently, decreasing fluid conductivity (σ_w). In fact, direct measurements of σ_w (Figures 5.3a and 5.3b) revealed much lower values with time in the active columns than in the control columns, although fluid of similar conductivity was used to fill the influent bottles of both the active and control columns. As per Eq. 12, a decrease in σ_w will result in a decrease in σ'. *Abdel Aal et al.* [2010] observed a decrease in σ' during microbial growth in porous media that they attributed to such microbial utilization of nutrients in solution. The removal of aqueous cations through sorption on bacterial surfaces could also contribute to the observed reduction in σ' in the active columns. Bacteria, whether gram positive or negative, are characterized by strong electronegative surface charges that are favorable to interactions and sorption of dissolved metal ions [*Schultze-Lam et al.*, 1996]. Adsorbed cations on cell surfaces may even serve as available sites for further interactions with other dissolved anions such as SO_4^{-2} and HCO_3^- [*Schultze-Lam et al.*, 1996]. In addition, bacterial growth and biofilm formation in the pore space, either attached on the grain surface or free in the pore water, could induce substantial changes in σ' through changes in porosity and tortuosity in our system.

Assuming insignificant surface conduction and no change in the pore space geometry, the relative changes in σ' and σ_w should be identical (Eq. 12). Under these conditions F_{app} will be constant. The increase in F_{app} in all active columns shortly after microbial inoculation (Figure 5.6d) could indicate either changes in the pore space geometry and/or changes in surface conduction. In the early time (within 4 days post-microbial inoculation) of the experiment where the abrupt increase in F_{app} occurred, no obvious changes in the imaginary conductivity were detected, suggesting that changes in F_{app} were unlikely to result from changes in surface conductivity (σ^*_{surf}). Therefore, the observed changes in F_{app} may indicate a reduction in the conductivity of the interconnected pore space, represented by Φ^m, due to biomass production. Numerous previous studies have correlated microbial presence and growth in porous media with a reduction in porosity, and subsequently in hydraulic conductivity [see *Baveye et al.*, 1998; *Thullner et al.*, 2002 for review].

In contrast to the real conductivity, the imaginary conductivity (σ'') exhibited a distinct increase at a later stage of the EtOH biodegradation processes. Following only moderate changes in both control and active columns until day 26 (Figures 5.6e and 5.6f), a substantial increase in σ'' occurred concurrently with visual observations of black precipitates in the active columns C3, C5 at day 27 and C4 at day 47. We suggest that this increase in σ'' results from the maturation of freshly formed biofilm (within days post-microbial inoculation) and the occurrence of metal sulfide precipitates (within weeks post-microbial inoculation). High resolution SEM imaging performed at the end of the

experiment (Figure 5.8) provided evidence of biofilm formation (Figure 5.8a) and mineral precipitation (presumably iron sulfide) in a dispersed state (Figure 5.8b), presumably as biominerals (Figure 5.8c). Biofilm and/or biomineral formation has commonly been noted where sulfate-reducing and other bacteria have achieved high biomass concentration resulting from the presence of a rich degradable organic source [*Baveye et al.*, 1998; *Thullner et al.*, 2002; *Personna et al.*, 2008]. Sorption and subsequent desorption of cations on the reactive groups of bacterial cells was recently incorporated into a model for the CR signatures of bacterial growth in porous media [*Revil et al.*, 2012b]. Under an applied electric field, polarization of the EDL could typically take place in the Stern layer (layer between the mineral/bacterial surface and the inner surface of the diffuse layer resulting from sorbed ions directly to mineral/bacterial surface) of counterions occurring in a brush of polymers coating the bacteria surface [*Revil et al.*, 2012b]. Consequently, biofilm formation and progressive maturation and attachment to the mineral surface would offer more surface area for enhanced interfacial polarization under an applied electrical field. *Abdel Aal et al.* [2010] interpreted an increase of ~ 120 % in σ'' in an experimental sand column inoculated with *Pseudomonas aeruginosa* from microbial abundance, biolfilm maturation and pore constriction within a 24 day-period.

The influence of biofilm on the polarization aside, the occurrence of iron sulfide mineral precipitates during dissimilatory sulfate reduction to H_2S by sulfate-reducing bacteria (SRB), as described in Eqs 4 to 6, likely explains a large part of the observed response in σ''. *Ntarlagiannis et al.* [2010] reported a near linear, positive correlation between σ'' and

abiotic FeS precipitation while σ' remained insensitive to this precipitation. Weller et al. [2010] reported a strong linear correlation between σ'' and metallic minerals (sand-iron and sand-magnetite mixtures) that they attributed to enhanced metal-fluid interface polarization. Likewise, it appears that precipitation of metal sulfide further increased the polarizability of the mineral/bacterial cell/metal sulfide surface that might have formed in our system. The temporal variability in σ'', after the occurrence of black precipitates in the active columns, most likely reflected periodic changes in iron sulfide mineral formation during alternating anaerobic and sub-aerobic transitions in our system. Likewise, *Personna et al.* [2008] captured an electrical response to microbial mediated FeS formation under anaerobic conditions, and subsequent FeS dissolution upon return to an aerobic state. The unexpected late time increase in σ'' in the control C2 by day 60 and C1 by day 68 was probably due to microbial contamination and an enhancement of interfacial polarization as described above. The SEM analysis performed at the end of the experiment confirmed microbial contamination for both C1 and C2 (data not shown for brevity).

5.6.3. Implications for monitoring long-term degradation processes for EtOH and other organic contaminants

The CR responses (ϕ, σ', F_{app}, σ'') were diagnostic of EtOH biodegradation processes in porous media. These mechanisms may include rapid microbial growth, development of biofilm, metal sulfide precipitation, and subsequent variation in the degree of anaerobic conditions with further input of aerobic solutions containing TEAs and nutrients, respectively. The initiation and evolution of EtOH biodegradation induced a series of sequential and subtle changes in the petrophysical properties of the geological medium

that were reflected in the temporal changes of the electrical and geochemical responses. The DD modeled parameters (m and m_n) are consistent with temporal changes in ϕ and σ'', indicating that the electrical response can largely be described by single low-frequency measurements. This encourages the use of field geophysical instrumentation that may only provide a single frequency CR measurement for monitoring of EtOH biodegradation. Our results identify the potential for using CR measurements for long-term monitoring of EtOH and other hydrocarbon contaminated sites undergoing intrinsic or induced biodegradation. Although our results are based on laboratory experiments, numerous recent studies have shown that CR techniques are deployable in the field for monitoring of bioremediation of heavy metals [*Williams et al.*, 2009; *Flores Orozco et al.*, 2011] and mapping of organic contaminants [*Kemna et al.*, 2004; *Vanhala*, 1997; *Flores Orozco et al.*, 2012].Therefore, CR measurements might help assess the effectiveness of remediation technologies and assist decision makers managing sites where EtOH has contaminated water and soils. However, field-scale CR measurements at EtOH contaminated sites are required to confirm the application of the technique in more complex environmental settings.

5.7. Conclusions

This research suggests that CR measurements have captured multiple processes occurring during ethanol biodegradation. At an early time of the experiment, the substantial decrease in σ' likely reflects the high sensitivity of σ' to microbial growth and potential biofilm development in response to intense microbial activity in the system. This σ' response is opposite to what has been observed by others during hydrocarbon

biodegradation. The variation in F_{app} during a period of stable imaginary conductivity suggests changes in porosity/tortuosity due to rapid biomass production in the pore space. At a later time of the experiment, an increase in σ'' and ϕ was recorded almost concurrently with visual observation of black precipitates in the system. The σ'' and ϕ responses agree with previous studies on CR responses to biomineralization of metal sulfide. Changes in aqueous chemistry along with SEM imaging corroborate the observed electrical responses. Our results indicate the sensitivity and accuracy of the CR method to EtOH biodegradation processes in porous media and the potential for its deployment either in the lab or field setting to identify and monitor microbial processes.

CHAPTER 6: CONCLUSIONS AND RECOMMENDATIONS FOR FUTURE WORK

6.1. Primary scientific findings and significance

This laboratory research has demonstrated the potential for using CR measurements for non-invasive detection of water and soils contaminated by ethanol. Ethanol interactions with geologic media and its end biodegradation products alter the physical and chemical properties of the subsurface and lead to distinctive geophysical responses. This research offers insight into the potential application of CR measurement as an effective tool for spatial and real time monitoring of EtOH evolution and fate in the subsurface. Thus, this research shows that the CR technique could provide a wealth of reliable information to help assess the effectiveness of remediation technologies and assist decision makers managing sites where EtOH has contaminated water and soils, in addition to other organic contaminated sites such as dense and light non aqueous phase liquid.

The results of the first research topic, which examines the electrical properties of water-EtOH interactions in mixtures, indicate the dependence and sensitivity of electrical conductivity measurements to the interactions occurring in the mixtures as EtOH concentration is varied. The measured $|\sigma|$ values were related to the changes in water-EtOH solution properties. This research demonstrates that the application of a simple L-R mixing model can be combined with electrical data to reasonably estimate EtOH concentration at ≤ 0.4 v/v EtOH in the water-EtOH mixtures.

The results of the second research topic, which examines the electrical properties of EtOH-clay interactions, show that clay polarization is significantly suppressed ($P \leq 0.001$) for both measured phase (ϕ) and imaginary conductivity (σ'') with increasing EtOH concentration. In addition, the interactions of EtOH with clay indicate strong hysteresis effects in the electrical response due to strong adsorption of EtOH on clay. The consistency between Debye Decomposition model parameters and σ'' indicates that single low-frequency CR measurements are adequate for tracking changes in EtOH-clay system. This encourages the use of field geophysical instrumentation that may only provide a single frequency CR measurement for monitoring of EtOH-clay interactions. Therefore, the results indicate the potential application of this technique for characterization and monitoring of ethanol contamination in sediments containing clays and potentially for other organic contamination in low permeability media.

The results of the third research topic, which examines the electrical properties of microbial simulated EtOH degradation processes in sand matrix, indicate distinctive electrical responses characterized by a substantial decrease in σ' and an increase in σ'' and ϕ. The σ' reflected changes at early time of microbial growth on EtOH almost immediately post-microbial inoculation while the imaginary conductivity (σ'') and phase (ϕ) anomalies reflected changes at a later time, almost concurrently with mineral precipitation in the system. The consistency of the Debye Decomposition model parameters with σ'' indicates that the observed electrical responses can be described by

single low-frequency CR measurements. Our results indicate the accuracy and sensitivity of CR technique to multiple processes occurring during EtOH biodegradation in porous media and, therefore, the opportunities of using this technique for long-term monitoring of EtOH and other hydrocarbon contaminated sites undergoing intrinsic or induced biodegradation.

In addition to demonstrating the potential application of CR measurement for spatial and real time monitoring of subsurface EtOH contamination, the observed changes in ϕ and σ'' during the second research topic appear to reflect potential chemical ion exchange and kinetics reactions occurring in the clay-water-EtOH system towards a near equilibrium state. Thus, this research provides insight into the potential application of CR technique for predicting non-equilibrium and equilibrium state of chemical reactions.

6.2. Challenges and recommendations for future work

The controlled laboratory conditions are simpler than the real field conditions. The application of the CR technique in real field conditions is more challenging as CR imaging is of much lower resolution due to larger electrode spacing and phase-out of signals with depth. The interpretations of field-scale CR data are also more challenging due to more complex and various physical, chemical and microbial factors and interactions that could influence the electrical responses. In addition, our knowledge is still very limited in terms of the exact biogeochemical processes responsible for the electrical responses although many studies have documented the potential application of geophysical methods for tracking the presence of microorganisms in the subsurface, their

interactions with the geologic media and the alterations of petrophysical properties due to microbial activity. Further research in both controlled laboratory and complex field conditions is required to advance our knowledge on the specific mechanisms that generate the electrical responses associated with EtOH presence, interactions and biodegradation processes. My recommendations for future work are as follows:

At the laboratory-scale:

1) Explore the potential of using CR for tracking EtOH in unsaturated geologic media. Some recent field studies on EtOH behavior have shown long term persistence of EtOH in the unsaturated in capillary fringe.
2) Investigate CR responses to EtOH-clay interactions for various clay types and concentrations. Subsurface EtOH contamination can occur in aquifers and low permeability geologic media with various clay types and concentrations.
3) Conduct an experiment that integrates various geophysical methods (e.g. CR, electrodic potential, NMR, GPR, acoustic wave propagation) and microbial methods (DNA identification, protein analysis for biomass approximation) and geochemical methods (IR spectroscopy for mineral identification, synchrotron radiation for chemical speciation, measurements of Eh, pH). This integrated research would offer insight into the exact changes in the system driving the geophysical responses and which methods are more useful at different stages.

At the field-scale:

1) Investigate the CR responses at existing EtOH contaminated sites in Minnesota and Kansas or other potential sites.

References

Abdel Aal, G. Z., E. A. Atekwana, and E. A. Atekwana (2010), Effect of bioclogging in porous media on complex conductivity signatures, *Journal of Geophysical Research*, *115*(null), G00G07.

Abdel Aal, G. Z., E. A. Atekwana, L. D. Slater, and E. A. Atekwana (2004), Effects of microbial processes on electrolytic and interfacial electrical properties of unconsolidated sediments, *Geophys. Res. Lett*, *31*(12), L12505.

Abdel Aal, G. Z., L. D. Slater, and E. A. Atekwana (2006), Induced-polarization measurements on unconsolidated sediments from a site of active hydrocarbon biodegradation, *Geophysics*, *71*(2), H13-H24.

Allen, J. P., E. A. Atekwana, E. A. Atekwana, J. W. Duris, D. D. Werkema, and S. Rossbach (2007), The microbial community structure in petroleum-contaminated sediments corresponds to geophysical signatures, *Applied and environmental microbiology*, *73*(9), 2860-2870.

Archie, G. (1942), The electrical resistivity log as an aid in determining some reservoir characteristics, *Trans. AIMe*, *146*(99), 54-62.

Atamas, N., and A. Atamas (2009), The investigations of water-ethanol mixture by Monte Carlo method, *World Academy of Science, Engineering and Technolog y*, *55*, 2070-3724.

Atekwana, E. A., and E. A. Atekwana (2010), Geophysical signatures of microbial activity at hydrocarbon contaminated sites: A review, *Surveys in Geophysics*, *31*(2), 247-283.

Atekwana, E. A., and L. D. Slater (2009), Biogeophysics: A new frontier in Earth science research, *Reviews of Geophysics*, *47*(4), RG4004.

Atekwana, E. A., D. D. Werkema, J. W. Duris, S. Rossbach, E. A. Atekwana, W. A. Sauck, D. P. Cassidy, J. Means, and F. D. Legall (2004c), In-situ apparent conductivity measurements and microbial population distribution at a hydrocarbon-contaminated site, *Geophysics*, *69*(1), 56-63.

Atekwana, E. A., E. A. Atekwana, D. D. Werkema, J. P. Allen, L. A. Smart, J. W. Duris, D. P. Cassidy, W. A. Sauck, and S. Rossbach (2004d), Evidence for microbial enhanced electrical conductivity in hydrocarbon-contaminated sediments, *Geophysical Research Letters*, *31*(23), L23501.

Atekwana, E. A., E. A. Atekwana, R. S. Rowe, D. D. Werkema, and F. D. Legall (2004b), The relationship of total dissolved solids measurements to bulk electrical

conductivity in an aquifer contaminated with hydrocarbon, *Journal of Applied Geophysics*, *56*(4), 281-294.

Atekwana, E. A., E. Atekwana, F. D. Legall, and R. Krishnamurthy (2004a), Field evidence for geophysical detection of subsurface zones of enhanced microbial activity, *Geophysical Research Letters*, *31*(23), L23603.

Baveye, P., P. Vandevivere, B. L. Hoyle, P. C. DeLeo, and D. S. de Lozada (1998), Environmental impact and mechanisms of the biological clogging of saturated soils and aquifer materials, *Critical Reviews in Environmental Science and Technology*, *28*(2), 123-191.

Bhat, J. I., and M. K. Shetty (2011), Evaluation of limiting molar conductance, Walden product, association constant and thermodynamic properties of sulfacetamide sodium in water+ EtOH mixtures, *Journal of Molecular Liquids*, *160*(3), 140-143.

Binley, A., and A. Kemna (2005), DC resistivity and induced polarization methods, in *Hydrogeophysics*, edited, pp. 129-156, Springer.

Binley, A., L. D. Slater, M. Fukes, and G. Cassiani (2005), Relationship between spectral induced polarization and hydraulic properties of saturated and unsaturated sandstone, *Water Resources Research*, *41*(12), W12417.

Bissada, K., W. Johns, and F. Cheng (1967), Cation-dipole interactions in clay organic complexes, *Clay Minerals*, *7*(2), 155-166.

Blaschek, R., and A. Hördt (2009), Numerical Modelling of the IP Effect at the Pore Scale, *Near Surface Geophysics*, *7*, 579-588.

Börner, F., M. Gruhne, and J. Schön (1993), Contamination indications derived from electrical properties in the low frequency range1, *Geophysical Prospecting*, *41*(1), 83-98.

Brindley, G., and R. W. Hoffmann (1962), Orientation and packing of aliphatic chain molecules on montmorillonite, *Clays and Clay Minerals*, *9*, 546-556.

Brindley, G., K. Wiewiora, and A. Wiewiora (1969), Intracrystalline swelling of montmorillonite in some water-organic mixtures:(Clay organic studies XVII), *American Mineralogist*, *54*, 1635-1644.

Brown, S. R., J. R. Sorenson, and T. I. Brown (2004), A Laboratory Study of the Complex Electrical Resistivity Response of Soils, paper presented at Symposium on the Application of Geophysics to Engineering and Environmental Problems 2004, Society of Exploration Geophysicists.

Bryant, M., L. L. Campbell, C. Reddy, and M. Crabill (1977), Growth of Desulfovibrio in lactate or ethanol media low in sulfate in association with H2-utilizing methanogenic bacteria, *Applied and environmental microbiology*, *33*(5), 1162-1169.

Cápiro, N. L., B. P. Stafford, W. G. Rixey, P. B. Bedient, and P. J. Alvarez (2007), Fuel-grade ethanol transport and impacts to groundwater in a pilot-scale aquifer tank, *Water Research*, *41*(3), 656-664.

Cápiro, N. L., M. L. Da Silva, B. P. Stafford, W. G. Rixey, and P. J. Alvarez (2008), Microbial community response to a release of neat ethanol onto residual hydrocarbons in a pilot-scale aquifer tank, *Environmental Microbiology*, *10*(9), 2236-2244.

Clausen, P., M. Signorelli, A. Schreiber, E. Hughes, C. J. Plummer, D. Fessas, A. Schiraldi, and J.-A. E. Månson (2009), Equilibrium desorption isotherms of water, ethanol, ethyl acetate, and toluene on a sodium smectite clay, *Journal of thermal analysis and calorimetry*, *98*(3), 833-841.

Cole, K. S., and R. H. Cole (1941), Dispersion and absorption in dielectrics I. Alternating current characteristics, *The Journal of Chemical Physics*, *9*, 341.

Corseuil, H. X., B. I. Kaipper, and M. Fernandes (2004), Cosolvency effect in subsurface systems contaminated with petroleum hydrocarbons and ethanol, *Water Research*, *38*(6), 1449-1456.

Corseuil, H. X., C. S. Hunt, R. C. Ferreira dos Santos, and P. J. Alvarez (1998), The influence of the gasoline oxygenate ethanol on aerobic and anaerobic BTX biodegradation, *Water Research*, *32*(7), 2065-2072.

Cosenza, P., A. Ghorbani, C. Camerlynck, F. Rejiba, R. Guérin, and A. Tabbagh (2009), Effective medium theories for modelling the relationships between electromagnetic properties and hydrological variables in geomaterials: a review, *Near Surf. Geophys*, *7*, 563-578.

Da Silva, M. L., and P. J. Alvarez (2002), Effects of ethanol versus MTBE on benzene, toluene, ethylbenzene, and xylene natural attenuation in aquifer columns, *Journal of Environmental Engineering*, *128*(9), 862-867.

Davidson, D., and R. Cole (1951), Dielectric Relaxation in Glycerol, Propylene Glycol, and n-Propanol, *The Journal of Chemical Physics*, *19*, 1484.

Davis, C. A., E. Atekwana, E. Atekwana, L. D. Slater, S. Rossbach, and M. R. Mormile (2006), Microbial growth and biofilm formation in geologic media is detected with complex conductivity measurements, *Geophysical Research Letters*, *33*(18), L18403.

Dowdy, R., and M. Mortland (1967), Alcohol-water interactions on montmorillonite surfaces. I. Ethanol, *Clays Clay Miner*, *15*, 259-271.

Drzyzga, O., R. El Mamouni, S. N. Agathos, and J. C. Gottschal (2002), Dehalogenation of chlorinated ethenes and immobilization of nickel in anaerobic sediment columns under sulfidogenic conditions, *Environmental science & technology*, *36*(12), 2630-2635.

EPA (2011), Four dimensional geophysical measurements of a controlled ethanol release in Ottawa sand. APM 253. Glaser, D. R., Werkema, D. D., Henderson, R.D., Johnson, T., Versteeg, R. J., Lane, J. W.

Flores Orozco, A., A. Kemna, C. Oberdörster, L. Zschornack, C. Leven, P. Dietrich, and H. Weiss (2012), Delineation of subsurface hydrocarbon contamination at a former hydrogenation plant using spectral induced polarization imaging, *Journal of contaminant hydrology*, *136-137*, 131-144.

Flores Orozco, A., K. H. Williams, P. E. Long, S. S. Hubbard, and A. Kemna (2011), Using complex resistivity imaging to infer biogeochemical processes associated with bioremediation of an uranium-contaminated aquifer, *Journal of Geophysical Research*, *116*(G3), G03001.

Frank, H. S., and W.-Y. Wen (1957), Ion-solvent interaction. Structural aspects of ion-solvent interaction in aqueous solutions: a suggested picture of water structure, *Discussions of the Faraday Society*, *24*, 133-140.

Franks, F. t., and D. Ives (1966), The structural properties of alcohol–water mixtures, *Quarterly Reviews, Chemical Society*, *20*(1), 1-44.

Freitas, J. G., and J. F. Barker (2011a), Oxygenated gasoline release in the unsaturated zone—Part 1: Source zone behavior, *Journal of contaminant hydrology*, *126*(3), 153-166.

Freitas, J. G., and J. F. Barker (2011b), Monitoring lateral transport of ethanol and dissolved gasoline compounds in the capillary fringe, *Ground Water Monitoring & Remediation*, *31*(3), 95-102.

Freitas, J. G., and J. F. Barker (2013), Denatured ethanol release into gasoline residuals, Part 1: Source behaviour, *Journal of contaminant hydrology*.

Freitas, J. G., B. Fletcher, R. Aravena, and J. F. Barker (2010), Methane production and isotopic fingerprinting in ethanol fuel contaminated sites, *Ground water*, *48*(6), 844-857.

Freitas, J. G., M. T. Mocanu, J. L. G. Zoby, J. W. Molson, and J. F. Barker (2011), Migration and fate of ethanol-enhanced gasoline in groundwater: A modeling analysis of a field experiment, *Journal of contaminant hydrology*, *119*(1), 25-43.

German, W., and D. Harding (1969), The adsorption of aliphatic alcohols by montmorillonite and kaolinite, *Clay Miner*, *8*, 213-227.

Gomez, D. E., and P. J. Alvarez (2009), Modeling the natural attenuation of benzene in groundwater impacted by ethanol-blended fuels: Effect of ethanol content on the lifespan and maximum length of benzene plumes, *Water Resources Research*, *45*(3), W03409.

Gomez, D. E., and P. J. Alvarez (2010), Comparing the effects of various fuel alcohols on the natural attenuation of benzene plumes using a general substrate interaction model, *Journal of contaminant hydrology*, *113*(1), 66-76.

Gomez, D. E., and P. J. Alvarez (2010), Comparing the effects of various fuel alcohols on the natural attenuation of benzene plumes using a general substrate interaction model, *Journal of contaminant hydrology*, *113*(1), 66-76.

Henderson, R., D. Werkema, R. Horton, and J. Lane (2009), Broadband Geoelectrical Signatures of Water-Ethanol Solutions in Ottawa Sand, paper presented at AGU Fall Meeting Abstracts.

Hördt, A., R. Blaschek, A. Kemna, and N. Zisser (2007), Hydraulic conductivity estimation from induced polarisation data at the field scale—the Krauthausen case history, *Journal of Applied Geophysics*, *62*(1), 33-46.

Ingram, L. O. (1989), Ethanol tolerance in bacteria, *Critical reviews in biotechnology*, *9*(4), 305-319.

IUPAC (2006), Compendium of Chemical Terminology, 2nd ed. (the "Gold Book", 1997). Web. <http://old.iupac.org/publications/compendium/S.html>.

Jones, D. P. (1997), Investigation of clay-organic reactions using complex resistivity, Colorado School of Mines.

Kemna, A., A. Binley, and L. Slater (2004), Crosshole IP imaging for engineering and environmental applications, *Geophysics*, *69*(1), 97-107.

Kemna, A., A. Binley, G. Cassiani, E. Niederleithinger, A. Revil, L. Slater, K. H. Williams, A. F. Orozco, F.-H. Haegel, and A. Hoerdt (2012), An overview of the spectral induced polarization method for near-surface applications, Near Surface Geophysics, 10(6), 453-468.

Konhauser, K. (2007), *Introduction to geomicrobiology*, Blackwell Pub.

Kowalska, M., H. Güler, and D. L. Cocke (1994), Interactions of clay minerals with organic pollutants, *Science of the total environment*, *141*(1), 223-240.

Kruschwitz, S., A. Binley, D. Lesmes, and A. Elshenawy (2010), Textural controls on low-frequency electrical spectra of porous media, *Geophysics*, *75*(4), WA113-WA123.

Lagaly, G., M. Ogawa, and I. Dékány (2006), .3 Clay Mineral Organic Interactions, *Developments in Clay Science*, *1*, 309-377.

Leroy, P., A. Revil, A. Kemna, P. Cosenza, and A. Ghorbani (2008), Complex conductivity of water-saturated packs of glass beads, *Journal of Colloid and Interface Science*, *321*(1), 103-117.

Leroy, P., and A. Revil (2009), A mechanistic model for the spectral induced polarization of clay materials, *Journal of Geophysical Research*, *114*(B10), B10202.

Lesmes, D. P., and K. M. Frye (2001), Influence of pore fluid chemistry on the complex conductivity and induced polarization responses of Berea Sandstone, *Journal of Geophysical Research*, *106*(B3), 4079-4090.

Lesmes, D. P., and S. P. Friedman (2005), Relationships between the electrical and hydrogeological properties of rocks and soils, in *Hydrogeophysics*, edited, pp. 87-128, Springer.

Lu, Y., and J. J. Pignatello (2002), Demonstration of the "conditioning effect" in soil organic matter in support of a pore deformation mechanism for sorption hysteresis, *Environmental science & technology*, *36*(21), 4553-4561.

Ma, J., Z. Xiu, A. L. Monier, I. Mamonkina, Y. Zhang, Y. He, B. P. Stafford, W. G. Rixey, and P. J. Alvarez (2011), Aesthetic Groundwater Quality Impacts from a Continuous Pilot-Scale Release of an Ethanol Blend, *Ground Water Monitoring & Remediation*, *31*(3), 47-54.

Mackay, D. M., D. Freyberg, P. Roberts, and J. Cherry (1986), A natural gradient experiment on solute transport in a sand aquifer, 1. Approach and overview of plume movement, *Water Resources Research*, *22*(13), 2017-2029.

Mackay, D. M., N. R. de Sieyes, M. D. Einarson, K. P. Feris, A. A. Pappas, I. A. Wood, L. Jacobson, G. Larry, M. N. Noske, and K. M. Scow (2006), Impact of ethanol on the natural attenuation of benzene, toluene, and o-xylene in a normally sulfate-reducing aquifer, *Environmental science & technology*, *40*(19), 6123-6130.

Mansoor, N., and L. Slater (2007), On the relationship between iron concentration and induced polarization in marsh soils, *Geophysics*, *72*(1), A1-A5.

Marshall, D. J., and T. R. Madden (1959), Induced polarization, a study of its causes, *Geophysics*, *24*(4), 790-816.

McDowell, C. J., T. Buscheck, and S. E. Powers (2003), Behavior of gasoline pools following a denatured ethanol spill, *Ground water*, *41*(6), 746-757.

McNaughton, C. H., J. D. Mosquera, A. L. Endres, and J. G. Freitas (2010), Monitoring of sequential gasoline-ethanol releases using high frequency ground penetrating radar, paper presented at Ground Penetrating Radar (GPR), 2010 13th International Conference on, IEEE.

Mizuno, K., Y. Miyashita, Y. Shindo, and H. Ogawa (1995), NMR and FT-IR studies of hydrogen bonds in ethanol-water mixtures, *The Journal of Physical Chemistry*, *99*(10), 3225-3228.

Molson, J., J. Barker, E. O. Frind, and M. Schirmer (2002), Modeling the impact of ethanol on the persistence of benzene in gasoline-contaminatedgroundwater, *Water Resources Research*, *38*(1), 1003.

Mortland, M. (1970), Clay-organic complexes and interactions, *Adv. Agron*, *22*(75), 117.

Nagpal, S., S. Chuichulcherm, A. Livingston, and L. Peeva (2000), Ethanol utilization by sulfate-reducing bacteria: An experimental and modeling study, *Biotechnology and bioengineering*, *70*(5), 533-543.

Nelson, D. K., T. M. LaPara, and P. J. Novak (2010), Effects of ethanol-based fuel contamination: Microbial community changes, production of regulated compounds, and methane generation, *Environmental science & technology*, *44*(12), 4525-4530.

Nordsiek, S., and A. Weller (2008), A new approach to fitting induced-polarization spectra, *Geophysics*, *73*(6), F235-F245.

Ntarlagiannis, D., and A. Ferguson (2009), SIP response of artificial biofilms, *Geophysics*, *74*(1), A1-A5.

Ntarlagiannis, D., K. H. Williams, L. Slater, and S. Hubbard (2005), Low-frequency electrical response to microbial induced sulfide precipitation, *Journal of Geophysical Research*, *110*(G2), G02009.

Ntarlagiannis, D., N. Yee, and L. Slater (2005), On the low-frequency electrical polarization of bacterial cells in sands, *Geophysical Research Letters*, *32*(24), L24402.

Ntarlagiannis, D., R. Doherty, and K. H. Williams (2010), Spectral induced polarization signatures of abiotic FeS precipitation, *Geophysics*, *75*(4), F127-F133.

Olhoeft, G. (1985), Low-frequency electrical properties, *Geophysics*, *50*(12), 2492-2503.

Olhoeft, G. R. (1986), Direct detection of hydrocarbon and organic chemicals with ground penetrating radar and complex resistivity.

Olhoeft, G., and T. King (1991), Mapping subsurface organic compounds noninvasively by their reactions with clays, paper presented at US Geological Survey Toxic Substance Hydrology Program, in Proceedings of technical meeting, Monterey, California.

Olphen, H. v. (1977), An introduction to clay colloid chemistry, for clay technologists, geologists, and soil scientists, *John Wiley & Sons*(2nd edition).

Parke, S. A., and G. G. Birch (1999), Solution properties of ethanol in water, *Food chemistry*, *67*(3), 241-246.

Personna, Y. R., D. Ntarlagiannis, L. Slater, N. Yee, M. O'Brien, and S. Hubbard (2008), Spectral induced polarization and electrodic potential monitoring of microbially mediated iron sulfide transformations, *J. Geophys. Res*, *113*, G02020.

Personna, Y. R., L. Slater, D. Ntarlagiannis, D. Werkema, and Z. Szabo (2013a), Electrical signatures of ethanol-liquid mixtures: implications for monitoring biofuels migration in the subsurface, *Journal of contaminant hydrology*, *144*, 99-107.

Personna, Y. R., L. Slater, D. Ntarlagiannis, D. Werkema, and Z. Szabo (2013b), Complex resistivity signatures of ethanol in sand-clay mixtures, *Journal of contaminant hydrology*, 149, 76-87.

Petek, A., D. Pecar, and V. Dolecek (2001), Volumetric properties of ethanol-water mixtures under high pressure, *Acta Chimica Slovenica*, *48*(3), 317-324.

Petong, P., R. Pottel, and U. Kaatze (2000), Water-ethanol mixtures at different compositions and temperatures. A dieletric relaxation study, *The Journal of Physical Chemistry A*, *104*(32), 7420-7428.

Poortinga, A. T., R. Bos, W. Norde, and H. J. Busscher (2002), Electric double layer interactions in bacterial adhesion to surfaces, *Surface Science Reports*, *47*(1), 1-32.

Powers, S. E., C. S. Hunt, S. E. Heermann, H. X. Corseuil, D. Rice, and P. J. Alvarez (2001b), The transport and fate of ethanol and BTEX in groundwater contaminated by gasohol, *Critical Reviews in Environmental Science and Technology*, *31*(1), 79-123.

Powers, S. E., D. Rice, B. Dooher, and P. J. Alvarez (2001a), Peer Reviewed: Will Ethanol-Blended Gasoline Affect Groundwater Quality?, *Environmental science & technology*, *35*(1), 24-30.

Prego, M., O. Cabeza, E. Carballo, and C. Franjo (2000), Measurement and interpretation of the electrical conductivity of 1-alcohols from 273 K to 333 K, *Journal of Molecular Liquids*, *89*(1), 233-238.

Prodan, C., F. Mayo, J. Claycomb, J. Miller, and M. Benedik (2004), Low-frequency, low-field dielectric spectroscopy of living cell suspensions, Journal of applied physics, 95(7), 3754-3756.

Prodan, E., C. Prodan, and J. H. Miller (2008), The dielectric response of spherical live cells in suspension: an analytic solution, Biophysical journal, 95(9), 4174-4182.

Revil, A., and M. Skold (2011), Salinity dependence of spectral induced polarization in sands and sandstones, *Geophysical Journal International*, *187*(2), 813-824.

Revil, A., and N. Florsch (2010), Determination of permeability from spectral induced polarization in granular media, *Geophysical Journal International*, *181*(3), 1480-1498.

Revil, A., E. Atekwana, C. Zhang, A. Jardani, and S. Smith (2012b), A new model for the spectral induced polarization signature of bacterial growth in porous media, *Water Resources Research*, *48*(9), W09545.

Revil, A., M. Karaoulis, T. Johnson, and A. Kemna (2012a), Review: Some low-frequency electrical methods for subsurface characterization and monitoring in hydrogeology, *Hydrogeology Journal*, 1-42.

Reynolds, J. M. (1997), An introduction to applied and environmental geophysics, Wiley & Sons, Ltd.

Roberts, J. J., and D. Wildenschild (2004), Electrical Properties of Sand–Clay Mixtures Containing Trichloroethylene and Ethanol, *Journal of Environmental and Engineering Geophysics*, *9*, 1.

Ruiz-Aguilar, G., K. O'Reilly, and P. Alvarez (2003), A Comparison of Benzene and Toluene Plume Lengths for Sites Contaminated with Regular vs. Ethanol-Amended Gasoline, *Ground Water Monitoring & Remediation*, *23*(1), 48-53.

Russell, J., and V. Farmer (1964), Infrared spectroscopic study of the dehydration of montmorillonite and saponite, *Clay Minerals Bulletin*, *5*(32), 443-464.

Sadowski, R. M. (1988), Clay-organic interactions, Colorado School of Mines.

Schmutz, M., A. Revil, P. Vaudelet, M. Batzle, P. F. Viñao, and D. Werkema (2010), Influence of oil saturation upon spectral induced polarization of oil-bearing sands, *Geophysical Journal International*, *183*(1), 211-224.

Schott, J., O. S. Pokrovsky, and E. H. Oelkers (2009), The link between mineral dissolution/precipitation kinetics and solution chemistry, *Reviews in mineralogy and geochemistry*, *70*(1), 207-258.

Schultze-Lam, S., D. Fortin, B. Davis, and T. Beveridge (1996), Mineralization of bacterial surfaces, *Chemical Geology*, *132*(1), 171-181.

Schwarz, G. (1962), A theory of the low-frequency dielectric dispersion of colloidal particles in electrolyte solution1, 2, *The Journal of Physical Chemistry*, *66*(12), 2636-2642.

Sinoti, A. L. L., J. d. S. Politi, and L. C. G. Freitas (1996), Monte Carlo Simulation of Water-Pyridine Mixtures, *J. Braz. Chem. Soc*, *7*, 133.

Slater, L. (2007), Near surface electrical characterization of hydraulic conductivity: From petrophysical properties to aquifer geometries—A review, *Surveys in Geophysics*, *28*(2-3), 169-197.

Slater, L. D., and D. Lesmes (2002), IP interpretation in environmental investigations, *Geophysics*, *67*(1), 77-88.

Slater, L. D., J. Choi, and Y. Wu (2005), Electrical properties of iron-sand columns: Implications for induced polarization investigation and performance monitoring of iron-wall barriers, *Geophysics*, *70*(4), G87-G94.

Slater, L., and A. Binley (2006), Synthetic and field-based electrical imaging of a zerovalent iron barrier: Implications for monitoring long-term barrier performance, *Geophysics*, *71*(5), B129-B137.

Slater, L., and D. Glaser (2003), Controls on induced polarization in sandy unconsolidated sediments and application to aquifer characterization, *Geophysics*, *68*(5), 1547-1558.

Slater, L., and E. Atekwana (2013), Geophysical Signatures of Subsurface Microbial Processes, *Eos, Transactions American Geophysical Union*, *94*(8), 77-78.

Slater, L., D. Ntarlagiannis, and D. Wishart (2006), On the relationship between induced polarization and surface area in metal-sand and clay-sand mixtures, *Geophysics*, *71*(2), A1-A5.

Slater, L., D. Ntarlagiannis, Y. R. Personna, and S. Hubbard (2007), Pore-scale spectral induced polarization signatures associated with FeS biomineral transformations, *Geophys. Res. Lett*, *34*(21), L21404.

Sogade, J. A., F. Scira-Scappuzzo, Y. Vichabian, W. Shi, W. Rodi, D. P. Lesmes, and F. D. Morgan (2006), Induced-polarization detection and mapping of contaminant plumes, *Geophysics*, *71*(3), B75-B84.

Spalding, R. F., M. A. Toso, M. E. Exner, G. Hattan, T. M. Higgins, A. C. Sekely, and S. D. Jensen (2011), Long-Term Groundwater Monitoring Results at Large, Sudden Denatured Ethanol Releases, *Ground Water Monitoring & Remediation*, *31*(3), 69-81.

Sposito, G., N. T. Skipper, R. Sutton, S.-h. Park, A. K. Soper, and J. A. Greathouse (1999), Surface geochemistry of the clay minerals, *Proceedings of the National Academy of Sciences*, *96*(7), 3358-3364.

Stafford, B. P., and W. G. Rixey (2011), Distribution of Fuel-Grade Ethanol near a Dynamic Water Table, *Ground Water Monitoring & Remediation*, *31*(3), 55-60.

Stafford, B. P., N. L. Cápiro, P. J. Alvarez, and W. G. Rixey (2009), Pore Water Characteristics Following a Release of Neat Ethanol onto Pre-existing NAPL, *Ground Water Monitoring & Remediation*, *29*(3), 93-104.

Steefel, C. I., and K. Maher (2009), Fluid-rock interaction: A reactive transport approach, *Reviews in mineralogy and geochemistry*, *70*(1), 485-532.

Sumner, J. S. (1976), *Principles of induced polarization for geophysical exploration*, Elsevier.

Theng, B. K. (1974), The Chemistry of Clay-Organic Reactions, *John Willey & Sons Inc.* .

Thullner, M., J. Zeyer, and W. Kinzelbach (2002), Influence of microbial growth on hydraulic properties of pore networks, *Transport in Porous Media*, *49*(1), 99-122.

Titov, K., A. Kemna, A. Tarasov, and H. Vereecken (2004), Induced polarization of unsaturated sands determined through time domain measurements, *Vadose Zone Journal*, *3*(4), 1160-1168.

Titov, K., V. Komarov, V. Tarasov, and A. Levitski (2002), Theoretical and experimental study of time domain-induced polarization in water-saturated sands, *Journal of Applied Geophysics*, *50*(4), 417-433.

Ulrich, C., and L. Slater (2004), Induced polarization measurements on unsaturated, unconsolidated sands, *Geophysics*, *69*(3), 762-771.

Ustra, A., L. Slater, D. Ntarlagiannis, and V. Elis (2012), Spectral Induced Polarization (SIP) signatures of clayey soils containing toluene, *Near Surface Geophysics*, *10*(6), 503-515.

Vacquier, V., C. R. Holmes, P. R. Kintzinger, and M. Lavergne (1957), Prospecting for ground water by induced electrical polarization, *Geophysics*, *22*(3), 660-687.

Vandevivere, P., and P. Baveye (1992), Sampling method for the observation of microorganisms in unconsolidated porous media via scanning electron microscopy, *Soil Science*, *153*(6), 482-485.

Vanhala, H. (1997), Mapping Oil-Contaminated Sand and Till with the Spectral Induced Polarization (SIP) Method, *Geophysical Prospecting*, *45*(2), 303-326.

Vaudelet, P., A. Revil, M. Schmutz, M. Franceschi, and P. Bégassat (2011a), Changes in induced polarization associated with the sorption of sodium, lead, and zinc on silica sands, *Journal of Colloid and Interface Science*, *360*(2), 739-752.

Vaudelet, P., A. Revil, M. Schmutz, M. Franceschi, and P. Bégassat (2011b), Induced polarization signatures of cations exhibiting differential sorption behaviors in saturated sands, *Water Resources Research*, *47*(2), W02526.

Vinegar, H., and M. Waxman (1984), Induced polarization of shaly sands, *Geophysics*, *49*(8), 1267-1287.

Waxman, M. H., and L. J. M. Smits (1968), Electrical conductivities in oil-bearing shaly sands, *Society of Petroleum Engineers Journal*, *8*(2), 107-122.

Weaver, J. W. (2009), Composition and Behavior of Fuel Ethanol, US Environmental Protection Agency, Office of Research and Development.

Weller, A., and L. Slater (2012), Salinity dependence of complex conductivity of unconsolidated and consolidated materials: Comparisons with electrical double layer models, *Geophysics*, *77*(5), D185-D198.

Weller, A., L. Slater, S. Nordsiek, and D. Ntarlagiannis (2010), On the estimation of specific surface per unit pore volume from induced polarization: A robust empirical relation fits multiple data sets, *Geophysics*, *75*(4), WA105-WA112.

Werkema Jr, D. D., E. A. Atekwana, A. L. Endres, W. A. Sauck, and D. P. Cassidy (2003), Investigating the geoelectrical response of hydrocarbon contamination undergoing biodegradation, *Geophysical Research Letters*, *30*(12), 1647.

Widdel, F. (1988), Microbiology and ecology of sulfate-and sulfur-reducing bacteria, *Biology of Anaerobic Microorganisms.*, 469-585.

Wiggins, P. M. (1997), Hydrophobic hydration, hydrophobic forces and protein folding, *Physica A: Statistical Mechanics and its Applications*, *238*(1), 113-128.

Williams, K. H., A. Kemna, M. J. Wilkins, J. Druhan, E. Arntzen, A. L. N'Guessan, P. E. Long, S. S. Hubbard, and J. F. Banfield (2009), Geophysical monitoring of coupled microbial and geochemical processes during stimulated subsurface bioremediation, *Environmental science & technology*, *43*(17), 6717-6723.

Williams, K. H., D. Ntarlagiannis, L. D. Slater, A. Dohnalkova, S. S. Hubbard, and J. F. Banfield (2005), Geophysical imaging of stimulated microbial biomineralization, *Environmental science & technology*, *39*(19), 7592-7600.

Wu, Y., L. D. Slater, and N. Korte (2005), Effect of precipitation on low frequency electrical properties of zerovalent iron columns, *Environmental science & technology*, *39*(23), 9197-9204.

Wu, Y., L. D. Slater, and N. Korte (2006), Low frequency electrical properties of corroded iron barrier cores, *Environmental science & technology*, *40*(7), 2254-2261.

Yariv, S., and H. Cross (2002), *Organo-clay complexes and interactions*, Marcel Dekker Inc.

Zakri, T., J.-P. Laurent, and M. Vauclin (1998), Theoretical evidence forLichtenecker's mixture formulae'based on the effective medium theory, *Journal of Physics D: Applied Physics*, *31*(13), 1589.

Zhang, C., L. Slater, and C. Prodan (2013), Complex dielectric properties of sulfate-reducing bacteria suspensions, *Geomicrobiology Journal*, *30*, 490-496.

Zisser, N., A. Kemna, and G. Nover (2010), Relationship between low-frequency electrical properties and hydraulic permeability of low-permeability sandstones, *Geophysics*, *75*(3), E131-E141.

Zonge, K., J. Wynn, and S. Urquhart (2005), Resistivity, induced polarization and complex resistivity, *Society of Exploration Geophysics*, 265-300

Vita

1996	B. S., Agricultural Science and Natural Resources Management/ The State University of Haiti, Honor
1996-1998	Environmental Specialist, Haiti Department of Environment (HDE)
1999	M.S., Aquaculture and Aquatic Ecosystem Management/University of Liege, Belgium, Honor.
2000-2005	Environmental consulting, various institutions : HDE, United Nations Development Program, United Nations Environment Program-Global Environment Facility, OXFAM Great Britain
2004-2005	National Focal Point/Cartagena Protocol on Biosafety, HDE
2005-2007	Fulbright Scholar, attended Rutgers University, Newark, New Jersey
2006-2007	Graduate Research Assistant, Rutgers University, Newark, New Jersey
2007	M.S. Environmental Sciences/ Rutgers University, Newark, New Jersey
2007	Peer-reviewed article: Slater, L., D. Ntarlagiannis, Y. R. Personna, and S. Hubbard (2007), Pore-scale spectral induced polarization signatures associated with FeS biomineral transformations, *Geophys. Res. Lett*, *34*(21), L21404.
2008	Peer-reviewed article: Personna, Y. R., D. Ntarlagiannis, L. Slater, N. Yee, M. O'Brien, and S. Hubbard (2008), Spectral induced polarization and electrodic potential monitoring of microbially mediated iron sulfide transformations, *J. Geophys. Res*, *113*, G02020.
2008-2010	Environmental consulting, various institutions : US Agency for International Development, Interamerican Development Bank
2010-2012	US E.P.A. Student contract for research on subsurface biofuel contamination
2010-2013	PhD Student, Rutgers University, Newark, New Jersey
2010-2013	Graduate Research Assistant, Rutgers University, Newark, New Jersey
2012-2013	Dissertation Fellow, Rutgers University, Newark, New Jersey
2013	Peer-reviewed article: Personna, Y. R., L. Slater, D. Ntarlagiannis, D. Werkema, and Z. Szabo (2013), Electrical signatures of ethanol-liquid mixtures: implications for monitoring biofuels migration in the subsurface, *Journal of contaminant hydrology*, *144*, 99-107.
2013	Peer-reviewed article: Personna, Y. R., L. Slater, D. Ntarlagiannis, D. Werkema, and Z. Szabo (2013), Complex resistivity signatures of ethanol in sand-clay mixtures, *Journal of contaminant hydrology*, *149*, 76-87.